# DESIGN AND IMPLEMENTATION OF A LOW EMITTANCE HIGH POWER THERMIONIC DC ELECTRON GUN

A THESIS SUBMITTED TO
THE GRADUATE SCHOOL OF NATURAL AND APPLIED SCIENCES
OF
MIDDLE EAST TECHNICAL UNIVERSITY

BY

MUSTAFA MURAT SEZER

IN PARTIAL FULFILLMENT OF THE REQUIREMENTS
FOR
THE DEGREE OF MASTER OF SCIENCE
IN
PHYSICS

FEBRUARY 2021

Approval of the thesis:

**DESIGN AND IMPLEMENTATION OF A LOW EMITTANCE HIGH POWER THERMIONIC DC ELECTRON GUN**

submitted by **MUSTAFA MURAT SEZER** in partial fulfillment of the requirements for the degree of **Master of Science in Physics Department, Middle East Technical University** by,

Prof. Dr. Halil Kalıpçılar
Dean, Graduate School of **Natural and Applied Sciences** _____

Prof. Dr. Altuğ Özpineci
Head of Department, **Physics** _____

Prof. Dr. Ali Murat Güler
Supervisor, **Physics, METU** _____

**Examining Committee Members:**

Prof. Dr. Ömer Yavaş
Physics Engineering, Ankara University _____

Prof. Dr. Ali Murat Güler
Physics, METU _____

Prof. Dr. Orhan Çakır
Physics, Ankara University _____

Prof. Dr. Bayram Tekin
Physics, METU _____

Assist. Prof. Dr. Deniz Yılmaz
Physics Engineering, Ankara University _____

Date: 08.02.2021

**I hereby declare that all information in this document has been obtained and presented in accordance with academic rules and ethical conduct. I also declare that, as required by these rules and conduct, I have fully cited and referenced all material and results that are not original to this work.**

Name, Surname: Mustafa Murat Sezer

Signature :

# ABSTRACT

## DESIGN AND IMPLEMENTATION OF A LOW EMITTANCE HIGH POWER THERMIONIC DC ELECTRON GUN

Sezer, Mustafa Murat
M.S., Department of Physics
Supervisor: Prof. Dr. Ali Murat Güler

February 2021, 121 pages

In this thesis, a thermionic electron gun generating low emittance and the high power electron beam is designed. The thermionic cathode made of a $LaB_6$ single crystal is chosen as a thermionic emitter because of its properties ensuring high electron beam current in lower temperatures which provide lower emittance. The main goal of the gun design is to achieve a high DC beam current and low emittance. Computer Simulation Technology (CST) and MATLAB are used to design the gun and optimize electrode shapes and corresponding fields. In addition, control and regulation of electron beam current are carried out by a focusing and control electrode in an electron gun at CST. From no current to full current, this current control is provided in every voltage step without increasing the beam's emittance value. The electron gun is kept under a high voltage DC source which varies between -60kV to -100 kV and DC beam current up to 75 mA. The simulation and test results are presented.

Keywords: DC electron gun, electron beam, focusing and control electrode, low emittance, thermionic cathode

# ÖZ

## DÜŞÜK YAYINIMLI YÜKSEK GÜÇLÜ TERMİYONİK DC ELEKTRON TABANCASI TASARIMI VE UYGULAMASI

Sezer, Mustafa Murat
Yüksek Lisans, Fizik Bölümü
Tez Yöneticisi: Prof. Dr. Ali Murat Güler

Şubat 2021 , 121 sayfa

Bu tez çalışmasında, düşük yayınım ve yüksek güçte elektron demeti üretebilen termiyonik DC elektron tabancası tasarlanmıştır. $LaB_6$ tekli kristal malzemesinden yapılan termiyonik katot, düşük yayınım sağlayan düşük sıcaklıklarda yüksek elektron demet akımı çıkarabilmesi nedeniyle termiyonik kaynak olarak seçilmiştir. Elektron tabancası Computer Simulation Technology (CST) adlı programda modellenmiş ve simüle edilmiştir. Yüksek DC elektron demet akımı ve düşük yayınım elde edebilmek için, elektrot şekillerinin ve bu şekillerden kaynaklı oluşan ilgili alanların optimizasyonu ise MATLAB programında yapılmıştır. Ek olarak, elektron demeti akımının kontrolü ve regülasyonu, CST de tasarlanan elektron tabancası içinde bulunan odaklama ve kontrol elektrodu adlı yapı ile sağlanmaktadır. Sistemde akım bulunmadığı durumdan sistemin tüm akımının sağladığı duruma kadar, bu akım kontrolü, demetin yayınım değerini arttırmadan her voltaj adımında sağlanmaktadır. Elektron tabancası, -60kV ile -100 kV arasında değişebilen yüksek gerilimli DC güç kaynağı altında tutulmaktadır ve maksimum DC demet akımı 75 mA değerindedir. Simülasyon ve test sonuçları tez içerisinde verilmiştir.

Anahtar Kelimeler: DC elektron tabancası, elektron demeti, odaklayıcı ve kontrol elektrodu, düşük yayınım, termiyonik katot

*To My Family...*

## ACKNOWLEDGMENTS

First and foremost, praises and thanks to the God, the Almighty, for His showers of blessings throughout my thesis work to complete this study successfully.

I must express my very profound gratitude to my parents Hülya Sezer, Nuri Sezer and to my sister İpek Sezer Yalçın for providing me with unfailing support and continuous encouragement throughout my years of study and through the process of researching and writing this thesis.

I would like to express my deep gratitude to Prof. Dr. Ali Murat Güler, my supervisor, for his patient guidance, enthusiastic encouragement and useful critiques of this thesis.

Besides my advisor, I would like to thank the rest of my thesis committee: Prof. Dr. Ömer Yavaş, Prof. Dr. Orhan Çakır, Prof. Dr. Bayram Tekin and Assist. Prof. Dr. Deniz Yılmaz, for their encouragement and insightful comments.

I am grateful to ASELSAN Electronic Industries for giving me opportunity to improve my research capabilities and for providing me every king of hardware, software and financial support.

I am also grateful to Turkish Accelerator and Radiation Laboratory (TARLA) for providing all kinds of support and service to this work.

I would like to extend my special appreciation to my precious friends Salih Geduk, Murat Hacıosmanoğlu, Ferhat Emre Kaya, Ali Gezer, Muhammed Yusuf Candan, İbrahim Tayyip İşler, Beheşti Sarıhan, Taha Zoray and Sinan Oğuz for their support, patience and valuable advice throughout my graduate study.

I would also thank my colleagues in ASELSAN and all the people who have supported me to complete this thesis directly or indirectly.

## TABLE OF CONTENTS

ABSTRACT . . . . . v

ÖZ . . . . . vi

ACKNOWLEDGMENTS . . . . . ix

TABLE OF CONTENTS . . . . . x

LIST OF TABLES . . . . . xiv

LIST OF FIGURES . . . . . xv

LIST OF ABBREVIATIONS . . . . . xxi

CHAPTERS

1 INTRODUCTION . . . . . 1

1.1 Problem Definition of the Designing Electron Gun . . . . . 1

1.2 Thesis Outline . . . . . 2

2 LITERATURE RESEARCH . . . . . 5

2.1 Types of Electron Guns . . . . . 5

2.1.1 DC Guns . . . . . 5

2.1.2 RF Guns . . . . . 6

2.2 Components of Electron Gun . . . . . 8

2.3 Beam Parameters . . . . . 11

2.3.1 Beam Divergence Angle . . . . . 11

2.3.2 Perveance . . . . . 11
2.3.3 Time Structure . . . . . 12
2.3.4 Beam Current . . . . . 12
2.3.5 Beam Size . . . . . 13
2.3.6 Beam Brightness and Energy Spread . . . . . 14
2.3.7 Emittance . . . . . 15
2.3.7.1 Ellipse of Emittance . . . . . 16
2.3.7.2 R.M.S Emittance Calculation . . . . . 18
2.3.7.3 Normalized Emittance . . . . . 18
3 THEORY OF OPERATION . . . . . 21
3.1 Electron Emission Types . . . . . 21
3.1.1 Maxwell-Boltzmann and Fermi-Dirac Statistics . . . . . 21
3.1.2 Fields of Cathode Surface . . . . . 23
3.1.3 Thermionic Emission Operation . . . . . 25
3.1.3.1 Current Density of Thermionic Emission . . . . . 27
3.1.3.2 Cathode Types According to the Material Used in Thermionic Emission . . . . . 28
3.1.3.3 Cathode Selection for Thermionic Emission Operation . 30
3.1.4 Field Emission Method . . . . . 31
3.1.5 Photo Emission Method . . . . . 32
3.1.6 Emittance of the Three Emission Method and Discussion of Them . . . . . 34
3.2 General Structure . . . . . 34
3.3 Space Charge Effect . . . . . 37

3.3.1 Space Charge . . . . . 37
3.3.2 Space Charge Fields . . . . . 38
3.3.3 Space Charge Forces . . . . . 39
3.4 Space Charge Limited Current – Child and Langmiur's Law . . . . . 40
3.4.1 Child and Langmiur's Law . . . . . 40
3.5 Pre-Design Work . . . . . 44
3.5.1 Voltage-Emittance Relation . . . . . 44
3.5.2 Voltage-Current Relation . . . . . 44
3.5.3 Current-Emittance Relation . . . . . 45
4 DESIGN AND SIMULATION . . . . . 47
4.1 Gun Assembly . . . . . 47
4.2 Design of Focusing and Control Electrode . . . . . 49
4.2.1 Computer Technology Simulation Particle Studio . . . . . 52
4.2.1.1 Solver Modules . . . . . 53
4.2.2 First Design- Linear Focusing and Control Electrode Geometry 54
4.2.3 Second Design-Quadratic Parabola Focusing and Control Electrode . . . . . 67
4.3 Anode Design . . . . . 69
4.4 Parameter Sweep Results . . . . . 70
4.5 Beam Current Regulation . . . . . 79
5 2D ELECTRIC FIELD OPTIMIZATION AND DESIGN OF ELECTRON GUN IN MATLAB . . . . . 81
5.1 Optimized Field Shapes and Analytical Calculations of Potentials . . 81

5.1.1 What Should Be The Shape of Electric Field and Equipotential Lines? . . . . . 81

5.1.2 Numerical Solution for Laplace's Equation Using Finite Difference Method . . . . . 83

5.2 Obtaining Desired Geometry for Proper Potential Lines and Implementing It in Matlab . . . . . 87

5.3 Comparison of MATLAB Results with CST . . . . . 88

6 IMPLEMENTATION OF DESIGNED ELECTRON GUN AND TEST RESULTS . . . . . 105

6.1 Test Setup and Procedure . . . . . 106

6.2 Test Results . . . . . 111

7 CONCLUSIONS . . . . . 115

REFERENCES . . . . . 117

## LIST OF TABLES

TABLES

Table 2.1 A Comparison of DC and RF Guns . . . . . 8

Table 2.2 Calculation of R.M.S Emittance and Twiss Parameters for 100 keV beam . . . . . 20

Table 3.1 Comparison of Cathode Types . . . . . 30

Table 4.1 Emittance and Current Values By Changing the Focusing Electrode Angle . . . . . 56

Table 4.2 Emittance and Current Values By Changing of Cathode Distance to Electrode Aperture ($Z_{cath}$) . . . . . 71

Table 4.3 Emittance and Current Values By Changing of Electrode Tip Radius $r_i$ 73

Table 4.4 Effects of Parameters on Beam Current and Beam Emittance . . . . 77

Table 5.1 Results of CST Simulation . . . . . 102

Table 7.1 Comparison of Simulation and Experiment Results . . . . . 116

## LIST OF FIGURES

FIGURES

Figure 2.1 a) shows a cross-sectional view of a diode DC gun b) shows a cross-sectional view of a triode DC gun [5] . . . . . 6

Figure 2.2 Pillbox Cavity or Resonant Cavity Representation [7] . . . . . 7

Figure 2.3 Electron Gun . . . . . 9

Figure 2.4 a) the picture shows the experiment performed under only Xe (Xenon) gas at a pressure of lower than 1 mbar b) the picture shows the experiment performed under Xe and Ar (Argon) gas at a pressure of higher than 5 mbar [10] . . . . . 10

Figure 2.5 Beam Divergence Angle . . . . . 11

Figure 2.6 a) represents the definition of the pulse current b) represents pulse currents for given period c) representation of average current with $T_p$ pulse duration d) representation of continuous beam current [14] . . 13

Figure 2.7 2D projection of beam (a) before going through a nonlinear system (b) after going through a nonlinear system. The volume of beam (shown in blue) is conserved thanks to liouville's theorem however the area of the elliptical circle increases [19] . . . . . 16

Figure 2.8 Calculation of important parameters for emittance with ellipse geometry . . . . . 17

Figure 2.9 Calculation for Emittance Parameters, black color represents $1\epsilon$ Red represents $2\epsilon$ and purple represents $3\epsilon$ of the beam . . . . . 19

Figure 3.1 Comparasion of M-B and F-D Distribution [22] . . . . . 22

Figure 3.2 Representation of creating image charge [23] . . . . . 23

Figure 3.3 Potentials around the Cathode Surface [23] . . . . . 24

Figure 3.4 Total Potentials [23] . . . . . 24

Figure 3.5 Distributions of fields [23] . . . . . 25

Figure 3.6 Thermionic Emission Operation [23] . . . . . 26

Figure 3.7 Fermi Dirac Distribution [23] . . . . . 27

Figure 3.8 Field Emission Method [30] . . . . . 31

Figure 3.9 Steps of Photo Emission Method [22] . . . . . 32

Figure 3.10 Electrons Motion in Electric Field . . . . . 35

Figure 3.11 The Lorentz force (F) acts on electrons in the magnetic field (B), changing their direction of motion (v) [33] . . . . . 36

Figure 3.12 Coulomb repulsion and magnetic attraction between two particles of equal charge, at rest and travelling [34] . . . . . 38

Figure 3.13 Electromagnetic Forces on a charged particle [34] . . . . . 38

Figure 3.14 Force due to an azimuthal magnetic field $B_\theta$ [34] . . . . . 40

Figure 3.15 Schematic view of one-dimensional electron gun [36] . . . . . 41

Figure 3.16 Representation of the electric fields expected to be applied (Red Colored) . . . . . 45

Figure 4.1 Proposed Gun Assembly . . . . . 48

Figure 4.2 Effect of the voltage on the Wehnelt Cylinder to focus, (a) The voltage applied to the Wehnelt cylinder is low, the focusing ability is low, (b) the medium level voltage, the focusing ability has improved, (c) the applied voltage is at the upper level, in the plane perpendicular to the direction of the beam. [38] . . . . . 50

Figure 4.3 Different regions of Electron Gun [39] . . . . . 51

Figure 4.4 Fully Parametric Focusing and Control Electrode Structure . . . 54

Figure 4.5 Linear Geometry View . . . . . 55

Figure 4.6 Beam Emittance (red colored) and Current (blue colored) values by changing of focusing electrode angle . . . . . 57

Figure 4.7 Showing of changing electric field in front of the cathode and focusing electrode with 0 focusing angle . . . . . 59

Figure 4.8 Showing of changing electric field in front of the cathode and focusing electrode with 10 focusing angle . . . . . 59

Figure 4.9 Showing of changing electric field in front of the cathode and focusing electrode with 20 focusing angle . . . . . 59

Figure 4.10 Showing of changing electric field in front of the cathode and focusing electrode with 30 focusing angle . . . . . 60

Figure 4.11 Showing of changing electric field in front of the cathode and focusing electrode with 40 focusing angle . . . . . 60

Figure 4.12 Showing of changing electric field in front of the cathode and focusing electrode with 50 focusing angle . . . . . 60

Figure 4.13 Showing of changing electric field in front of the cathode and focusing electrode with 60 focusing angle . . . . . 61

Figure 4.14 Showing of changing electric field in front of the cathode and focusing electrode with 70 focusing angle . . . . . 61

Figure 4.15 1D results of electric field in front of the cathode and focusing electrode with respect to changing focusing electrode angle . . . . . 63

Figure 4.16 Display of Beam Trajectory with 0 focusing angle . . . . . 63

Figure 4.17 Display of beam trajectory with 5 focusing angle . . . . . 64

Figure 4.18 Display of beam trajectory with 10 focusing angle . . . . . 64

Figure 4.19 Display of beam trajectory with 20 focusing angle . . . . . 64

Figure 4.20 Display of beam trajectory with 30 focusing angle . . . . . 65

Figure 4.21 Display of beam trajectory with 40 focusing angle . . . . . 65

Figure 4.22 Display of beam trajectory with 50 focusing angle . . . . . 65

Figure 4.23 Display of beam trajectory with 60 focusing angle . . . . . 66

Figure 4.24 Display of beam trajectory with 70 focusing angle . . . . . 66

Figure 4.25 Parametrized CST model of focusing and control electrode and anode . . . . . 68

Figure 4.26 Structure of Anode Design [43] . . . . . 69

Figure 4.27 Beam current versus cathode distance to electrode aperture distance . . . . . 72

Figure 4.28 Beam current versus cathode distance to electrode aperture distance . . . . . 72

Figure 4.29 Beam emittance versus electrode tip radius result . . . . . 74

Figure 4.30 Beam current versus electrode tip radius result . . . . . 74

Figure 4.31 Beam emittance versus electrode parabola parameter a . . . . . 76

Figure 4.32 Beam current versus electrode parabola parameter a . . . . . 76

Figure 4.33 Displaying Non-uniform electric field in front of the cathode in parametrized CST model . . . . . 78

Figure 4.34 Beam current regulation results in CST . . . . . 80

Figure 5.1 View of electric field lines (blue) and equipotential lines (green) [44] . . . . . 82

Figure 5.2 Using most common grid types . . . . . 84

Figure 5.3 View of grids and their gap distance [48] . . . . . 85

Figure 5.4 The solution of Laplace's Equation on grids [46] . . . . . 86

Figure 5.5 Designed geometry in MATLAB . . . . . 88

Figure 5.6 The potential curves for -60 kV from MATLAB . . . . . 89

Figure 5.7 The potential curves for -60KV from CST . . . . . 90

Figure 5.8 Electric Field in front of the Cathode for -60 kV from MATLAB 91

Figure 5.9 Electric Field in front of the Cathode for -60 kV from CST . . . 92

Figure 5.10 Potential curves for -100 kV from MATLAB . . . . . 93

Figure 5.11 Potential curves for -100 kV from CST . . . . . 94

Figure 5.12 Electric field in front of the cathode for -100 kV from MATLAB 95

Figure 5.13 Electric field in front of the cathode for -100 kV from CST . . . 96

Figure 5.14 Potential Lines with Electric Field Results in MATLAB . . . . . 97

Figure 5.15 Emittance value for -60 kV in CST . . . . . 98

Figure 5.16 Current value for -60 kV in CST . . . . . 98

Figure 5.17 Emittance value for -100 kV in CST . . . . . 99

Figure 5.18 Current value for -100 kV in CST . . . . . 100

Figure 5.19 Electric field strength for -60 kV in CST . . . . . 101

Figure 5.20 Electric field strength for -100 kV in CST . . . . . 101

Figure 5.21 a) View of optimized design of the electron gun in CST b) the cross-sectional view of optimized design of the electron gun in CST . . 103

Figure 6.1 Picture of manufactured anode (left) and focusing electrode (Right) 105

Figure 6.2 System block diagram . . . . . 106

Figure 6.3 Performance characteristics of $LaB_6$ cathode [52] . . . . . 107

Figure 6.4 Photo of the cathode used in the test . . . . . 108

Figure 6.5 Photo of ceramic structure and focusing electrode placement . . 109

Figure 6.6 Photo of the test set-up at Turkish Accelerator and Radiation Laboratory (TARLA) [50] [51] . . . . . 110

Figure 6.7 Measured current value of the beam, 1V = 10 mA . . . . . 111

Figure 6.8 Photo of copper table before test . . . . . 112

Figure 6.9 Photo of copper table after test. The beam size is measured as 2mm . . . . . 113

Figure 6.10 Calculation of angle of beam spread . . . . . 114

## LIST OF ABBREVIATIONS

| | |
|---|---|
| 1D | 1 Dimensional |
| 2D | 2 Dimensional |
| 3D | 3 Dimensional |
| DC | Direct Current |
| RF | Radio Frequency |
| CST | Computer Simulation Technology |
| W | Tungsten |
| LaB6 | Lanthanum Hexaboride |
| GaAs | Gallium Arsenide |
| CS2Te | Cesium Telluride |
| GaN | Gallium Nitride |
| K | Perveance |
| $\epsilon$ | Emittance |
| $\sigma$ | Beam Size |
| B | Beam Brightness |
| e | Electron |
| eV | Electron Volt |
| M-B | Maxwell-Boltzman Distribution |
| F-D | Fermi-Dirac Distribution |
| DOS | Distribution of Occupied States |
| E | Electric Field |
| B | Magnetic Field |
| J | Current Density |
| $\phi$ | Work Function |

| | |
|---|---|
| $v$ | Velocity |
| PIC | Particle In Cell |
| $Z_{cath}$ | Cathode Distance to Electrode Aperture |
| $x_i$ | Radius of Electode Aperture |
| $r_i$ | Electrode Tip Radius |
| $\alpha$ | Focusing and Control Electrode Angle |
| $x_o$ | Distance of the End of the Curve from the Z-Axis |
| $R_o$ | The Upper Electrode Tip Radius |
| $R_c$ | Radius of the Focusing Electrode |
| $R_a$ | Radius of the Anode Circle |
| $R$ | Distance of the Anode-Cathode Centripetal Circles |
| $\Phi$ | Scalar Potential |
| kV | kiloVolt |

# CHAPTER 1

# INTRODUCTION

Particle Accelerators are machines that accelerate atomic or subatomic particles for a purpose. Particle accelerators in today's technology accelerate, direct and focus charged particles by electromagnetic forces. This technology finds dozens of application areas in many civil and military sectors and plays critical roles.

Electron guns are being used widely in pre-accelerator of many applications. It provides proper accelerator fields that affect beam dynamics in the rest of the system. They are used in scientific instruments, electron devices, and industrial facilities. They are regularly used for various metallurgical applications such as melting, welding, coating, annealing, heat treatment, surface hardening, alloy formation, and atomic, molecular, and surface physics. [1] [2]

## 1.1 Problem Definition of the Designing Electron Gun

Although there are numerous design requirements depending on the application, the main challenge for this work is to achieve building high power low emittance DC electron gun. The higher the power values of the electron gun, the higher the emittance value. The aim of this study is to increase the power values of the electron gun while decreasing its emittance value. The following describe the design properties of the gun:

- Highly focusable that is capable of producing low emittance beam smaller than $1\ mm * mrad$
- Producing a DC beam with 2 electrode focusing electrode and anode

- Having low beam divergence angle in order not to get scattering beam
- Variable acceleration voltage, beam current and high mean power

Even though the electron gun is a small part of the whole system, it plays an important role in the performance of electron optics of the entire system. [3] [4] It provides proper accelerator fields that affect the beam dynamics in the rest of the system. In this study, an electron gun model that is designed as parametrically is proposed. The contribution of each individual model parameter to the electromagnetic fields, emittance, and current is thoroughly analyzed. The simulation results, done via Computer Simulation Technology (CST) and MATLAB, are presented.

The main motivation of this thesis is to decrease the transverse electric fields in front of the cathode and increase the electric field strength in the longitudinal direction along the way to the anode in an electron gun. It is aimed to solve the above mentioned difficult situations with the electron gun to be designed.

## 1.2 Thesis Outline

The structure of this thesis is as follows. In the first part of this thesis, it is mentioned which type of electron guns are used. According to the application, the suitability of DC and RF electron guns is specified and the differences are explained. Next, the components in an electron gun are introduced and each component is explained. Then, the beam parameters are explained and the effects of each parameter on the electron gun are explained in detail. In addition, it is emphasized which parameters are important in this study. After that, the general working principles of the electron gun are mentioned in detail. Each electron emission method is described in detail and it is specified which electron emission method is suitable for this study. The properties of the cathode to be selected according to the appropriate electron emission method are shown and compared with different cathode types. Then, the space charge that affects the design criteria and the performance of the electron gun is discussed and explained in detail. In the last part of the first part of the thesis, the relations of important parameters before design are mentioned. Since the design will be made

according to these relations, it is explained in detail what these parameters are and what they affect.

In the second part of the thesis, design and simulation studies are carried out and it is verified which geometry will provide the required parameter values. First of all, the proposed gun assembly model to be used in this study is presented. Second, the design of the focusing and controlling electrode, which is the most important design part of the electron gun, is explained in detail. Then, the design of the second electrode, the anode, is explained in detail. Before moving on to the simulation results and designs, the simulation program used is mentioned. Thirdly, linear geometry, which is the first design of the electron gun, is mentioned and design details are shared. Simulation is done in CST and results are shared. According to the results, linear geometry is not a suitable geometry in terms of providing the required parameters in this study. The second design, focusing, and control electrode with a quadratic parabola curve is proposed. The main advantage of this design is that it has a parabolic curve. Because, thanks to the parabolic curve, the electric fields approached the desired situation. The proposed geometry is a fully parametric geometry.

In the last part of the thesis, the electric field optimization of the electron gun is made. The optimization process is done with MATLAB. The geometry obtained in CST is transferred to MATLAB as a boundary condition. An adequate result is obtained in terms of design requirements. Finally, this geometry is produced and experimentally verified.

# CHAPTER 2

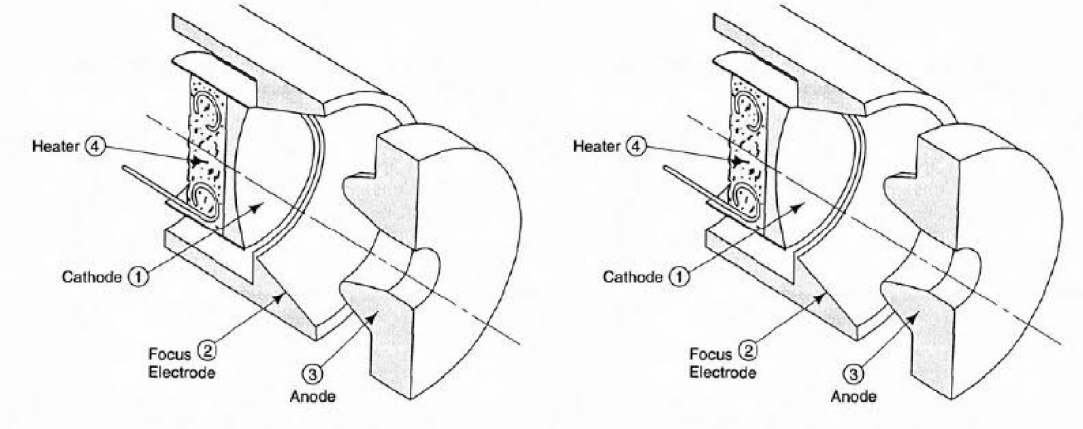
# LITERATURE RESEARCH

## 2.1 Types of Electron Guns

Depending on the type of electric field generation, an electron gun can be designed in two ways which are DC or RF. Both of them are being used in various applications. One of the most common uses of electron guns is in cathode ray tubes. They are commonly used in computer and television monitors.

### 2.1.1 DC Guns

DC electron guns are one of the main sources for many applications. The electron beam can be obtained by applying a DC voltage. DC electron guns have two working modes which are continuous and pulsed. In continuous mode, the beam can be emitted constantly. In pulsed mode, the beam will be emitted when the DC power supply is on the state. A DC electron gun can be modeled in two ways. The first one is a diode electron gun and the second one is a triode electron gun. A diode gun consists of a cathode, an anode, a focusing electrode, and a heater. A triode gun composed of a cathode, an anode, a focus electrode, a heater, and a control grid. The cathode potential is at a negative voltage; whereas anode potential is at the ground. Electrons are extracted from the cathode by these voltage differences and not only accelerated but also focused on the beam hole in the anode. To be able to control beam current over a large range without changing cathode-anode voltage, a control grid is placed between them in triode guns. Generally, the needed grid voltage in order to control beam current is 2.5-5% of the cathode-anode voltage. [5] Their cross-sectional view is shown in Figure 2.1.




(a) (b)

Figure 2.1: a) shows a cross-sectional view of a diode DC gun b) shows a cross-sectional view of a triode DC gun [5]

In order to get electrons from cathodes in a DC electron gun, there are three major methods: Thermionic, photoelectric, and electric field emissions. In a thermionic DC electron gun, a tungsten (W) and Lanthanum hexaboride ($LaB_6$) are used as cathodes. These cathodes are heated in order to create an electron beam. In photoelectric DC electron guns, GaAs, $Cs_2Te$, GaN, etc. can be used as the cathode. In these cathodes, electrons are generated by sending light to the surface of the cathode material. In electric field emission, DC guns same cathodes are used with thermionic DC electron gun. The level of applied electric fields should be $10^7 - 10^8$ V/cm. At these levels, the surface of the thermionic cathode achieves a critical level and electrons can tunnel through the barrier. [6]

### 2.1.2 RF Guns

The generation of electron beam based on RF gun is one of the important ways of designing an electron gun. RF guns are widely used in numerous applications because high-quality electron beams can be obtained with these guns. Two main RF guns are used nowadays which are thermionic and photo-cathode RF guns. The main difference between them is the type of cathode material. [6] To be able to get electrons from the cathode, thermionic cathodes should be heated. Mostly, $LaB_6$ and Tungsten

material is being used as thermionic cathodes. Their material properties will be explained in detail Section 3.1. [6] A pillbox cavity, or it can be called a resonant cavity as well, can be given as an example design for RF thermionic electron guns shown in Figure 2.2. If RF fields in the cavity are in phase with the accelerating phase, electrons will be accelerated from the cathode to the exit-hole on the opposite side of the cathode.[7] If the design is made properly, electron beams will already be gone out from the cavity before the fields change themselves into the decelerating phase. This will occur in every RF cycle period when the RF power supply is connected correctly to the electron gun. Problems will come true for thermionic RF electron guns when the emission of the electron beams is in the out accelerating phase of radio-frequency fields and during every period of it. That results in an electron beam not only a big momentum spread but also a big time-spread. [7]

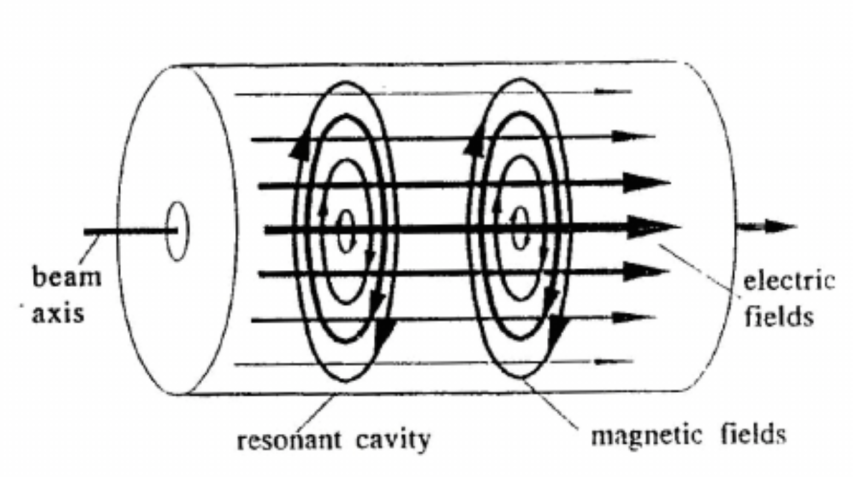



Figure 2.2: Pillbox Cavity or Resonant Cavity Representation [7]

For photocathode RF guns, a laser can be used in order to get electrons from the cathode. These cathodes are also called photoemitters. $LaB_6$, $Cs_2Sb$, and $CsK_2Sb$ materials are being used for photocathodes commonly. In most cases, the laser pulses have shorter than the RF period. Because of that, emission from cathode happens over only a very short period of time. Therefore, photocathode RF guns generate a much shorter electron beam with respect to thermionic RF electron guns at the same RF frequency. [6]

The high current density can be obtained from photo emitter cathodes. This results in

a much higher charge per beam for photocathode RF guns than thermionic RF guns due to the short time interval for emitting electrons in photocathode RF guns. The focusing effect of RF fields in photocathode RF guns has a very much less impact on electron beam than thermionic RF guns gives lower emittances. [8] Owing to high current density in photocathode RF guns, the beam does not need to be compressed to get high peak currents. Hereby, in photocathode RF guns longer beams can be produced than thermionic RF guns because, it must be compressed to a very short beam to get high peak currents. [6]

In Table 2.1. a comparison of DC and RF guns are shown. [8]

Table 2.1: A Comparison of DC and RF Guns

| | **DC Guns** | **RF Guns** |
|---|---|---|
| Maximum Electric Field Gradient Obtained | $8MV/m$ | $20MV/m$ |
| Typical Output Energies (MeV) | 0.08-0.4 | 2-3 |
| Peak Current | Less Peak Current | Higher Peak Current |
| Lifetime of Cathode | More Cathode Lifetime | Less Cathode Lifetime |
| Brightness of the Beam | Providing less bright beam | Delivering more bright beam |

## 2.2 Components of Electron Gun

The electron gun produces and accelerates electrons to a desired energy and and forms them into a beam which continues in its own way with the correct parameters. An electron gun is also responsible for controlling beam current. It should give the desired current value to the system. Due to these, the electron gun is the most important part of the system. An electron gun consists of five main parts:

- Cathode
- Control Electrode
- Anode
- Vacuum
- Accelerating Voltage

- Ceramic Structure

A schematic view of an electron gun is shown in Figure 2.3.

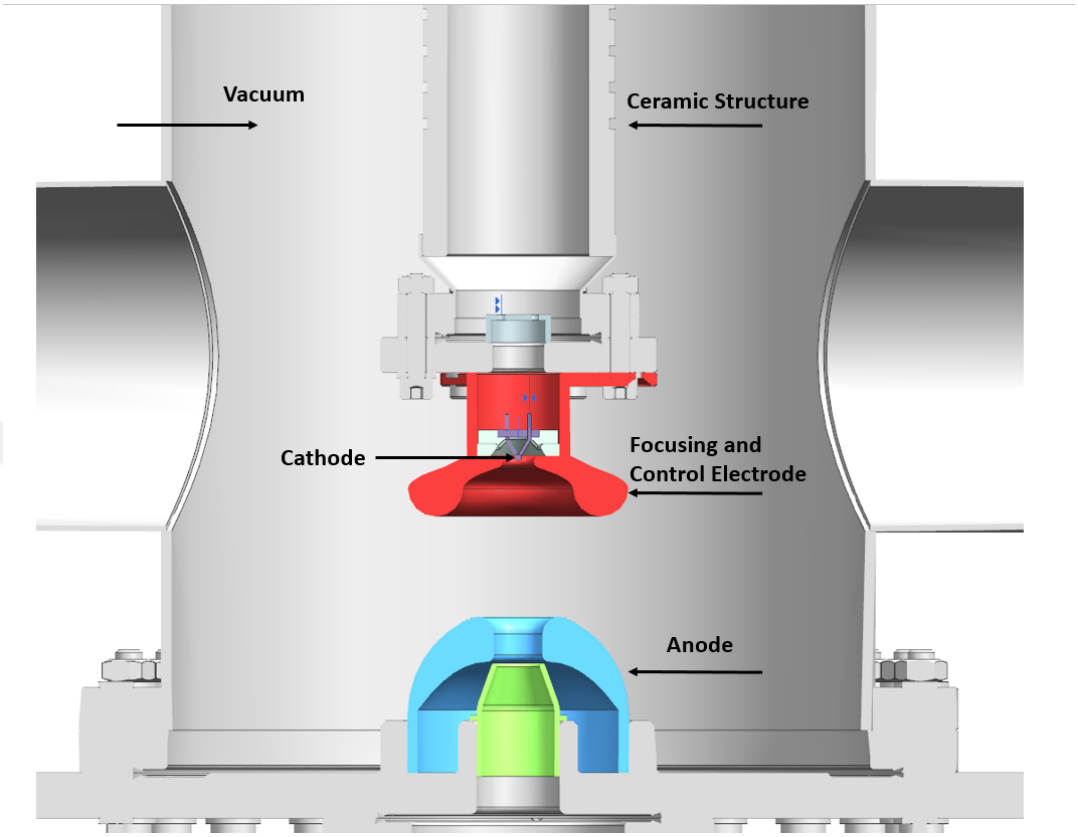



Figure 2.3: Electron Gun

The cathode is the most important part of the electron gun. It is the part that allows electrons to come out in bunches. Electrons are attached to the cathode material. Energy must be supplied from the outside to release electrons from the cathode. There are some methods to give this energy. This will be discussed in Section 3.1.1.

The control electrode is positioned between the cathode and the anode to provide a transverse focus for the beam. By applying a bias voltage between the control electrode and cathode, the beam current can be controlled in the desired range.

The anode is another important part of the electron gun. By grounded anode, electrons start to accelerate towards it and further focus the beam after the control electrode.

The accelerator voltage is very important in terms of enabling electrons to accelerate

on a linear electric field and reach the required energy. By connecting the positive terminal of the power supply to the anode and the negative terminal to the cathode, the accelerating voltage is created. The higher the accelerating voltage, the better the beam quality.

The vacuum is the elementary part of the electron gun system. The emitted electrons from the cathode can only accelerate in a vacuum. If the electrons emanating from the source are kept in a normal environment instead of a vacuum while moving in a beam, they will lose a significant part of their energy by colliding with the molecules they encounter. This will cause them not only to loose their energy but also cause the beam to deteriorate which means the electron beam will not be focused and accelerated. Therefore, it is important to work in a vacuum at a certain pressure value. The vacuum environment where the source should be kept is very important in order to use the system efficiently. The vacuum value is $10^{-7}$ to $10^{-9}$ mbar generally. [9] In Figure 2.4, an image of the beam is given for two different situations.

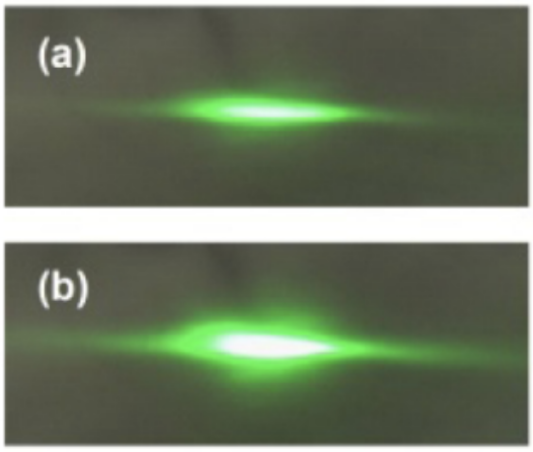



Figure 2.4: a) the picture shows the experiment performed under only Xe (Xenon) gas at a pressure of lower than 1 mbar b) the picture shows the experiment performed under Xe and Ar (Argon) gas at a pressure of higher than 5 mbar [10]

As can be seen from Figure 2.4, the beam travels more collectively and steadily in a vacuum, low-pressure environment. Another advantage of being a vacuum is that it provides insulation between anode and cathode. A vacuum prevents any short circuit caused by high voltage better than a normal environment. This allows the distance between anode and cathode to be shortened. As a result, it increases the current value

and decreases the emittance.

## 2.3 Beam Parameters

### 2.3.1 Beam Divergence Angle

After the electrons are released from the cathode, they move towards the anode with the help of the focusing electrode. After passing through the hole present in the anode, they tend to disperse. The angular increase in diameter due to the dispersion tendency it shows after the anode from the moment it emerges from the cathode is called the beam divergence. [11]

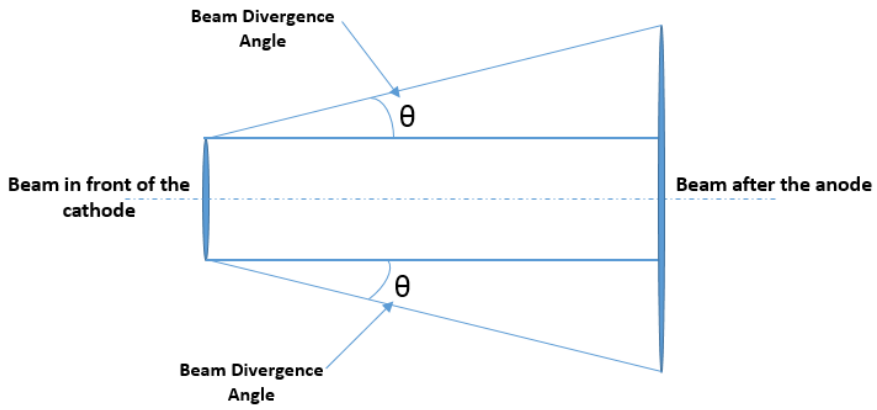



Figure 2.5: Beam Divergence Angle

### 2.3.2 Perveance

Perveance determines the effect of independent charges on the beam motion. Although its mathematical formula depends on current and voltage, also it only depends on the geometry of the electron source. The Low perveance of a beam means less irregularity of that beam, high means more distortion in the beam. For this reason, low perveance should be preferred for a more stable beam. Its mathematical expression is

as follows [12]:

$$K = \left(\frac{I}{V^{3/2}}\right)\left(\frac{1}{4\pi\epsilon_0(2q/m)^{1/2}}\right) \tag{2.1}$$

where K is the beam perveance, I is the beam current, V is the applied acceleration voltage.

### 2.3.3 Time Structure

The time structure is a parameter that can change according to the desired gun type which is mentioned in Section 2.1. The time structure of a continuous flow beam is different from the time structure of the bunched beam.. If the particles are accelerated by RF fields, a bunched beam is produced, on the other hand, if a continuous beam flow is desired instead of bunched, this can only be generated with DC fields. The pulsed beam consists of a limited number of bunches or in a continuous flow of particles in a limited time period. [13]

### 2.3.4 Beam Current

Beam current, also called beam intensity, is one of the basic parameter of the current. The time interval required to measure the charge of bunched beams can be shorter than the time duration of the bunch or the beam pulse, or longer than both. [14]

In Figure 2.6. a general time structure of beams is shown. Electrostatic accelerators can produce pulsed beams if they can turn the accelerator voltage in short time intervals on and off. The pulse current, $I_p$ is the average current value defined during the pulse time. $I_p$ can be given as:

$$I_p = \widehat{I}\frac{\tau_\mu}{T_{mu}} = \frac{q}{T_\mu} \tag{2.2}$$

where $\tau_\mu$ is the span of the bunch and $T_\mu$ is the time between consecutive bunches.

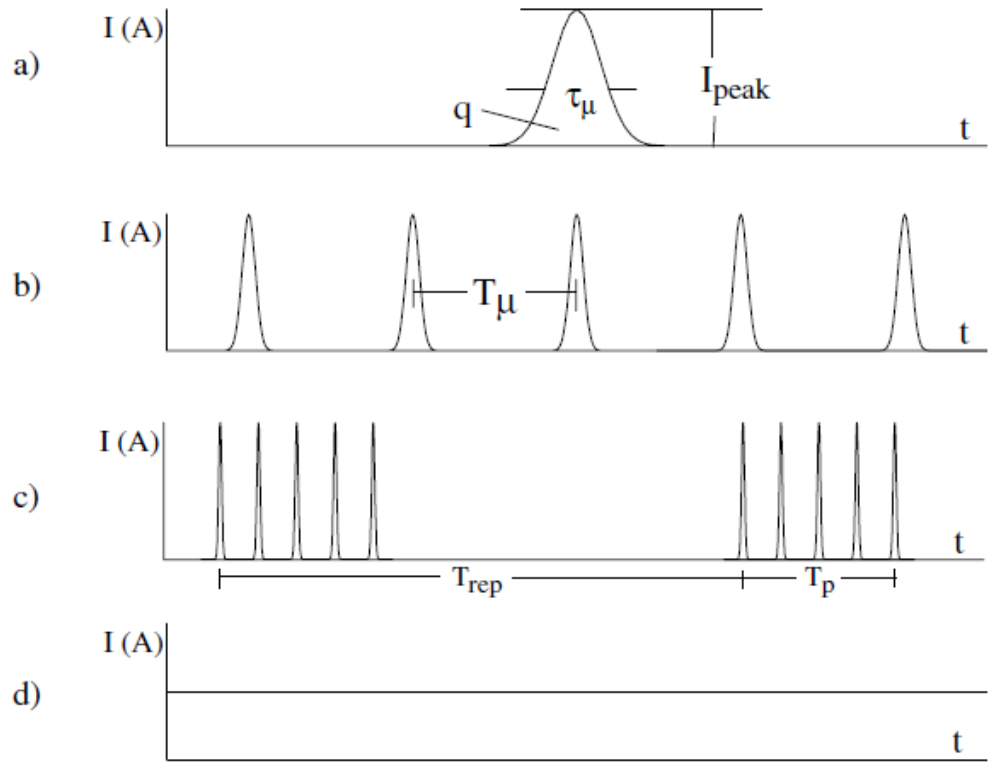



Figure 2.6: a) represents the definition of the pulse current b) represents pulse currents for given period c) representation of average current with $T_p$ pulse duration d) representation of continuous beam current [14]

Finally, the average beam current then is averaged over a complete cycle of the accelerator.

$$< I >= I_p \frac{T_p}{T_\Gamma} = \frac{q}{T_\Gamma} \frac{T_p}{T_{mu}} = \frac{n_\mu q}{T_{rep}} \tag{2.3}$$

where $n_\mu$ is the number of bunches per applied pulse and q is the total charge passing through in a beamline per unit time.

### 2.3.5 Beam Size

The beam diameter is the width perpendicular to the beam path and is a critical parameter in electromagnetic lens designs in the beam line. The beam size is also related to beam emittance. It is usually shown by $\sigma$. This generally indicates standard deviation

and it is equal to the square root of the mean value of the beam distribution. [15] [16]

$$\sigma =< x^2 >^{\frac{1}{2}} \tag{2.4}$$

This also relates to emittance value of the beam which will be mentioned in the emittance section. Its formula can be written as follows statistically [15]:

$$\epsilon = 2\sigma_x 2\sigma_{vx} \tag{2.5}$$

where $\epsilon$ is the beam emittance, $\sigma_x$ is the beam size, and $\sigma_{vx}$ is the standard deviation of the angle made by the particles with respect to the x-axis. If the beam size and the standard deviation of the angle of the beam are known, the emittance can be found using this formula theoretically.

### 2.3.6 Beam Brightness and Energy Spread

The electron source determines the quality of the beam brightness. Its mathematical expression is as follows:

$$B = \frac{BeamCurrent}{BeamArea \times BeamDivergence} = \frac{Emissivity(J)}{\sqrt{Temperature/mass}} = \frac{J_e}{\left(\sqrt{\frac{kT}{\gamma m_0 c^2}}\right)^2} \tag{2.6}$$

B is a constant parameter for electron gun systems. It changes the divergence angle of the source. The more B value, the more electrons can be extracted from the source at a certain size. Therefore, more information can be obtained from the sample that is the target. However, if the target is sensitive, the more B value can damage it. The B value of the sources is shown in Table 3.1.

The energy spread value of the electron beam generally varies between 0.3 and 3 eV. This value depends on the electron source used. In this study, $LaB_6$ electron source is used and its energy spread value is 1 eV. The energy spread is dependent on the brightness of the electron beam. High brightness can be achieved simultaneously with

a high energy spread. The energy spread is also related to the stability of accelerating voltage. The more the instability on the voltage causes the higher the energy spread of the beam. It is not much important for imaging application, but it is important for spectroscopy. It can be measured via an electron spectrometer. [17]

### 2.3.7 Emittance

Emittance is one of the elementary beam parameters for electron guns. It determines the quality of the electron beam. It defines and gives information about the beam size. Simply, it is the area or volume in the phase space of the beam. [18] It states the distribution in the linear motion of the beam. The greater the emittance, the more dispersed beam. Therefore it is not a desired condition for the beam design.The scattered beam cannot go through the desired beam path and it loses its energy very quickly. Therefore, the emittance value at the design stage should be kept at a low level.

Momentum and position are two phase space variables. These variables for a particle are $x$, $p_x$, $y$ , $p_y$ , $z$, $p_z$ and time as an independent variable. These variables are valid for each spatial direction. [15]

Emittance is a measure of the transverse velocity of the particles that form the package. With the focusing function in the accelerator, the width of the beam can be changed, but if the beam size is reduced too much, the transverse velocities will increase, so the phase space field will remain constant. This phenomenon is known in accelerator physics as the Liouville theorem and is independent of the direction of the coordinate. Liouville's theorem in its most general form: [19]

$$\epsilon_u = \oint u_i^{'} du_i \tag{2.7}$$

Here $u = x, y, z$ as mentioned above and the conservation of the emittance value under conservative forces is valid for all coordinates. Usually, in continuous beams such as DC electron guns or long pulse DC electron guns, the longitudinal direction of the beam is not taking care of distribution. Only, transverse distributions ($x$,$p_x$) and

($y$,$p_y$) of the beam are used in place of using full phase-space distribution for the sake of simplicity. In addition, this distribution can be changed by nonlinear forces acting on the particles. In most accelerators, this volume size and shape of the transverse distribution are important features for electron beams since most accelerator devices have an acceptance window in the phase space in which they can work. In Figure 2.7, one can see the effect of nonlinear forces on the beam. [19]

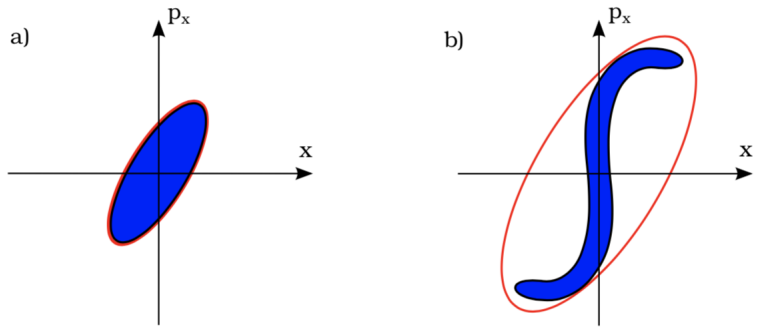



Figure 2.7: 2D projection of beam (a) before going through a nonlinear system (b) after going through a nonlinear system. The volume of beam (shown in blue) is conserved thanks to liouville's theorem however the area of the elliptical circle increases [19]

In this work, we are interested in the beam which is before going through the nonlinear optical system, and then we calculate the emittance of the surrounded volume (Figure 2.7a).

#### 2.3.7.1 Ellipse of Emittance

In order to model the DC electron gun beam envelope in $x, p_x(x^{'})$ phase space, a proper shape is required. Typically, in most electron guns have Gaussian distributions in both directions since contours of the two-dimensional Gaussian distributions are ellipses. Therefore, in the 2D phase space using an ellipse to design the beam model is an obvious solution for electron guns. Equation 2.8 for an ellipse is as follows: [15]

$$\gamma x^2 + 2\alpha x x^{'} + \beta x^{'2} = \epsilon \tag{2.8}$$

where the scaling

$$\beta\gamma - \alpha^2 = 1 \tag{2.9}$$

is selected. Here $\epsilon$ is the emittance value of the beam for two-dimensional transverse direction distribution, and $\alpha$, $\beta$ and $\gamma$ are the twiss parameters or Courant-Snyder parameters which define the beam tilt, shape, and size. The ellipse is as follows in Equation 2.10:

$$A = \epsilon * \pi = R_1 * R_2 * \pi \tag{2.10}$$

The major and minor radius of the ellipse is shown as $R_1$ and $R_2$ respectively. From Equation 2.10., ellipse dimension can be calculated in order to get the emittance value of the beam. In Figure 2.8, the calculation of important parameters for the emittance is shown.

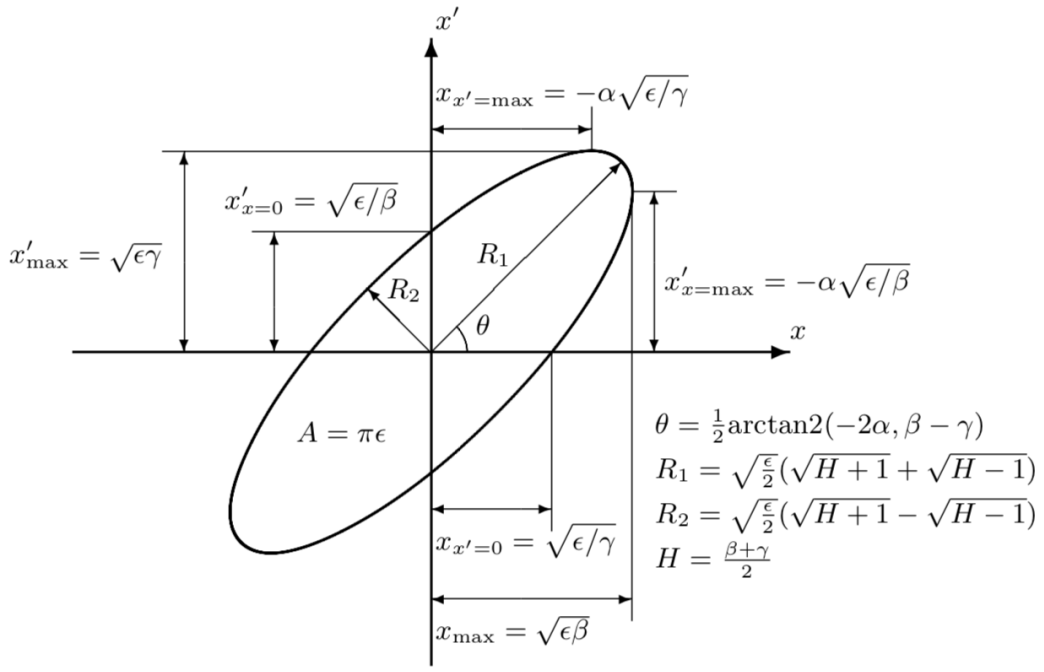



Figure 2.8: Calculation of important parameters for emittance with ellipse geometry

[19]

#### 2.3.7.2 R.M.S Emittance Calculation

In order to produce a proper ellipse, a statistical definition which is known as r.m.s emittance is being used. Its equation is as follows: [16] [19]

$$\epsilon_{rms} = \sqrt{< x'^2 >< x^2 > - < xx' >^2} \tag{2.11}$$

Their expectation values are defined as:

$$< x^2 >= \frac{\int\int x^2 I(x,x^{'})dxdx^{'}}{\int\int I(x,x^{'})dxdx^{'}} \tag{2.12}$$

$$< x^{'2} >= \frac{\int\int x'^2 I(x,x^{'})dxdx^{'}}{\int\int I(x,x^{'})dxdx^{'}} \tag{2.13}$$

$$< xx^{'} >= \frac{\int\int xx^{'} I(x,x^{'})dxdx^{'}}{\int\int I(x,x^{'})dxdx^{'}} \tag{2.14}$$

$I(x,x^{'})dxdx^{'}$ is the magnitude of the beam current. In a similar way, twiss parameters can be found from Equation 2.15:

$$\alpha = -\frac{< xx^{'} >}{\epsilon}, \quad \beta = \frac{< x^2 >}{\epsilon} \quad and \quad \gamma = \frac{< x^{'2} >}{\epsilon} \tag{2.15}$$

#### 2.3.7.3 Normalized Emittance

The normalized emittance is called geometric emittance. The longitudinal beam velocity has an impact on transverse emittance during acceleration. When the beam is accelerated, its momentum in the z direction will be increased. Therefore, $x^{'} = p_x/p_z$ will be decreased. To be able to prevent this effect, velocity should be normalized to the speed of light $c$. It is given in Equation 2.16: [19]

$$x_n^{'} = \frac{p_x}{p_{z1}}\frac{v_{z1}}{c} = \frac{v_x}{c} = \frac{p_x}{p_{z2}}\frac{v_{z2}}{c} \tag{2.16}$$

For non-relativistic speeds. By using the above equation and unnormalized emittance, normalized emittance can be calculated which is shown in Equation 2.17:

$$\epsilon_n = \frac{v_z}{c} \tag{2.17}$$

Figure 2.9 gives the horizontal phase space of a 100 keV energy particle and the calculated parameters for this distribution. The twiss parameters calculated and the emittance bands covering the phase space are given in Figure 2.8. The area shown in black ($1\epsilon$ ) is the area covering 95 % of the beam. The area shown in red is $2\epsilon$ and the area shown in purple is $3\epsilon$ of the beam. As can be seen, the RMS emittance includes a part of $1\epsilon_x$ particles. Twiss parameters are calculated using the Equation 2.15. They are given in Table 2.2.

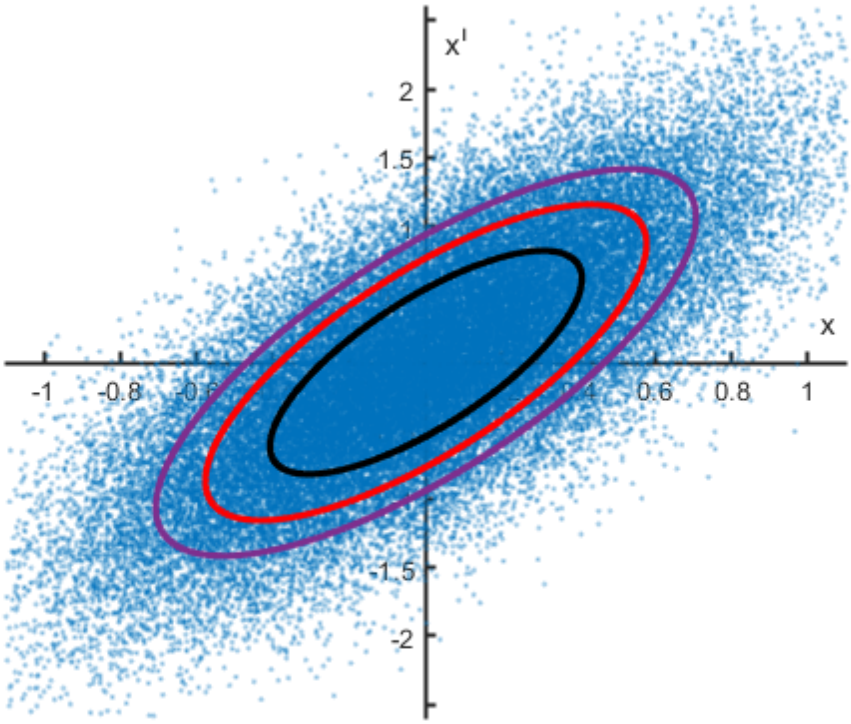



Figure 2.9: Calculation for Emittance Parameters, black color represents $1\epsilon$ Red represents $2\epsilon$ and purple represents $3\epsilon$ of the beam

Table 2.2: Calculation of R.M.S Emittance and Twiss Parameters for 100 keV beam

| | |
|---|---|
| $E_0$ | $100(keV)$ |
| $<x^2>$ | $0.1667(mm)$ |
| $\beta_x$ | $0.7559(m/rad)$ |
| $\alpha_x$ | $-1.1339$ |
| $\gamma_x$ | $3.0237$ |
| $\epsilon_{x,rms}$ | $0.2205(mm * mrad)$ |

The emittance value of the beam is determined by adding the emittance values of one or more of the beam and dividing it by the total number of packages in the beam. In reality, the emittance measurements are obtained by the average of the spectra of many packages, such as the beam size. Therefore, the already measured emittance is the average of the emittance values of many packages, not just one package that makes up the beam. At this point, it should be noted that in cases of instability, the emittance may differ from package to package.

All of these parameters can change many requirements in the system. Therefore, these parameters must be calculated and determined accurately. Since changing one parameter will affect the other, their interaction with each other is important. For example, the greater the distance and anode diameter between cathode-anode, the less current and perveance value of the beam will be. This will make it easier to achieve the desired situation.

# CHAPTER 3

# THEORY OF OPERATION

## 3.1 Electron Emission Types

Electron guns can be classified according to their application areas based on the emission method. There are three basic methods to achieve electron emission. [20]

- Thermionic Emission Method
- Photo Emission Method
- Field Emission Method

Before explaining the emission methods, it is necessary to define the Maxwell-Boltzmann and Fermi-Dirac statistics. Additionally, the electric field on the cathode surface for the escape of electrons will be discussed. Then these three methods will be explained.

### 3.1.1 Maxwell-Boltzmann and Fermi-Dirac Statistics

In general, elementary particles can be classified according to their spins. Particles with integer spin are called bosons and obey classical Maxwell-Boltzmann statistics, while particles with half-integer spin are called fermions and follow Fermi-Dirac statistics. The property of these statistics is that it calculates the probability of a particle occupying a given energy state based on the distribution of N particles in k-energy intervals for the two-particle types [21]:

1. Particles such as photons that can share the same energy state regardless of the

number, obey the Maxwell-Boltzmann (M-B) distribution and its energy distribution of occupied states given by,

$$f_{MB} = e^{\frac{-E}{k_B T}} \tag{3.1}$$

2. Particles such as electrons that cannot share the same energy state and have only one particle per energy state, follow Fermi-Dirac distribution, and its energy Distribution of Occupied States (DOS) is given by the Fermi-Dirac (F-D) function [22],

$$f_{FD} = \frac{1}{1 + e^{\frac{E - E_f}{k_B * T}}} \tag{3.2}$$

A comparison of their distribution is shown in Figure 3.1. They have almost the same high-energy tails. During thermionic emission, the cathode is heated to high temperatures. This promotes emissions and increases the high energy tail of the distribution. Therefore, Maxwell-Boltzmann statistics can be applicable and valid in this case. On the other hand, it will be explained below, in photoelectric and field emission, electrons are excited below the fermi energy level not only the tail of the distribution. Thus, Fermi-Dirac statistics are used in this process.

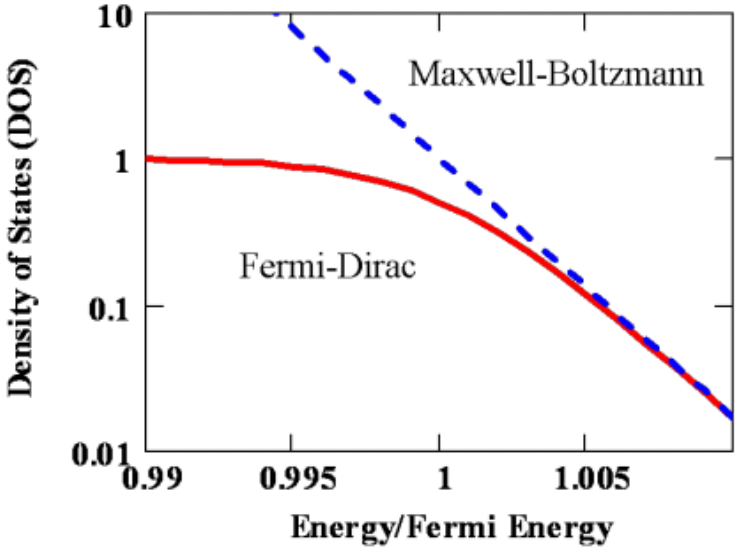



Figure 3.1: Comparasion of M-B and F-D Distribution [22]

### 3.1.2 Fields of Cathode Surface

The fields and potentials that are formed very close to the cathode surface have a significant effect on electron emission. After an electron is released, its image charge will change the potential near the material surface. [23] Its representation is shown in Figure 3.2.

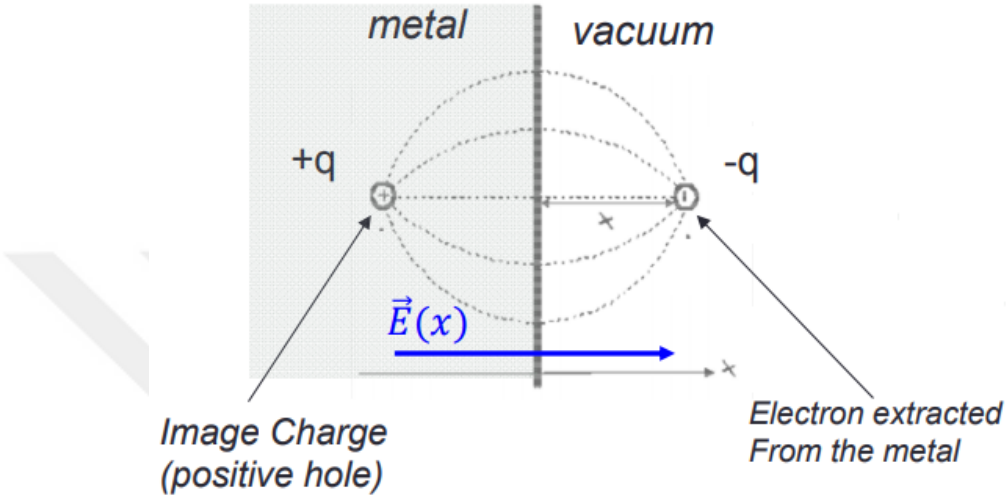



Figure 3.2: Representation of creating image charge [23]

Its electric field and potential in Figure 3.2 is given by Equations 3.3 and 3.4.

$$E(x) = \frac{q}{4\pi\epsilon_0(2x)^2} \tag{3.3}$$

$$V_{CI}(x) = \frac{-q}{16\pi\epsilon_0}\frac{1}{x} \tag{3.4}$$

Its effect on potentials near the metal surface is shown in Figure 3.3.

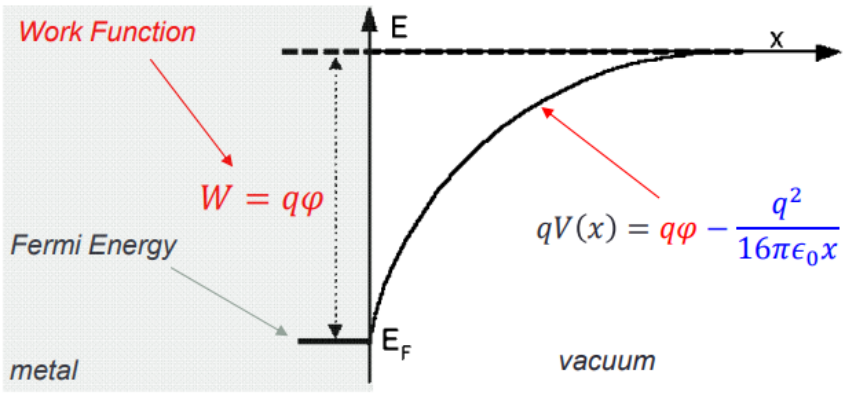



Figure 3.3: Potentials around the Cathode Surface [23]

Using Equations 3.3 and 3.4, the total electric potential energy for an electron as a function of distance from the cathode to the anode is given by Equation 3.5. [22]

$$e\Phi = e\phi_{work} - \frac{e^2}{16\pi\epsilon_0 x} - eE_0 x \tag{3.5}$$

and its distribution is shown in Figure 3.4:

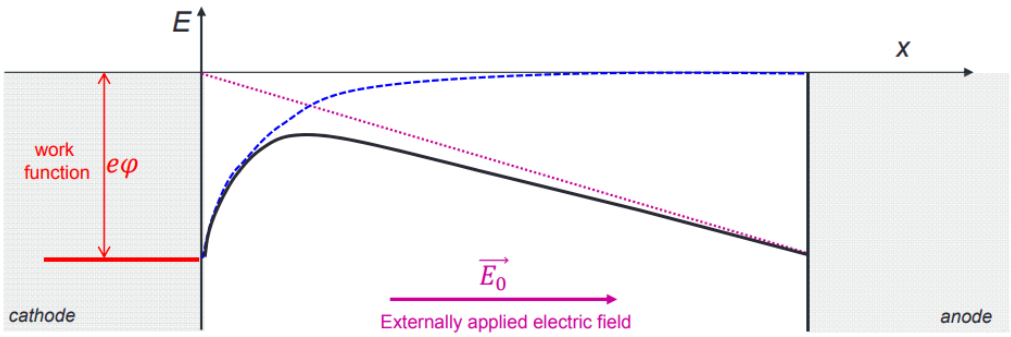



Figure 3.4: Total Potentials [23]

The potential energy is the sum of the work function, $\phi_{work}$, the image charge potential, and applied electric field $E_0$.

Electric fields and the energy density of the comparison of the occupied state around the cathode surface-vacuum boundary is shown in Figure 3.5.

Electrons with higher energy than work function can exit from the cathode or electrons with lower energy than work function can tunnel through the barrier. For

thermionic and photoemission methods, electrons that are emitted must have larger energies than the barrier, whereas, in the field emission method, they can tunnel the barrier. [22]

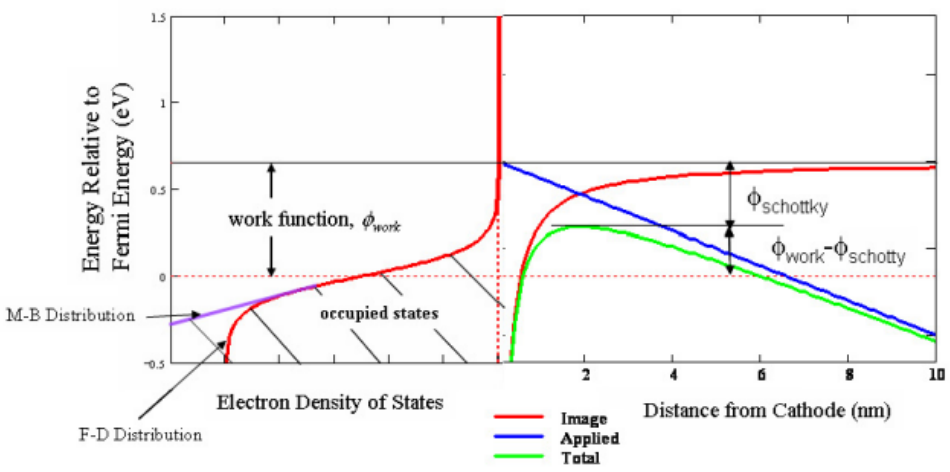



Figure 3.5: Distributions of fields [23]

With the applied electric field effect, there is a decrease in the effect of the barrier and this is called Schottky effect. It plays an important role in all emission methods, especially in field emission method. [22]

### 3.1.3 Thermionic Emission Operation

The electron extraction method by heating the material to high temperatures is called the thermionic emission method. As the material heats up, this temperature increase is transferred to the electrons partially ($E \sim kT_e$) which can populate excited states above the Fermi level due to the thermal vibration that occurs on it. The heated electrons reach such an energy level $E$ that is larger than the work function of the material $W$, so they can no longer stand on material anymore. Therefore, they are thrown out of the material. The work function of a metal depends on [24]:

- The properties of the metal
- The purity of the metal
- The nature of the metal surface

The cathode is the most important part of the electron source. It is the part that allows electrons to come out in a beam. Electrons are bound to the cathode material. External energy must be supplied to ensure that it is released from the cathode.

The energy given by the thermionic method depends on the temperature. Each material has a threshold energy (Fermi Level) value that must be given to get the electron. In order to give this value, the cathode is heated in the thermionic method to gain sufficient kinetic energy in order to emit an electron from the surface. Its equation is as follows [22]:

$$\frac{mv_x^2}{2} > e\phi_{work} \quad \Rightarrow \quad v_x > \sqrt{\frac{2e\phi_{work}}{m}} \tag{3.6}$$

An illustration of thermionic emission is given in Figure 3.6.

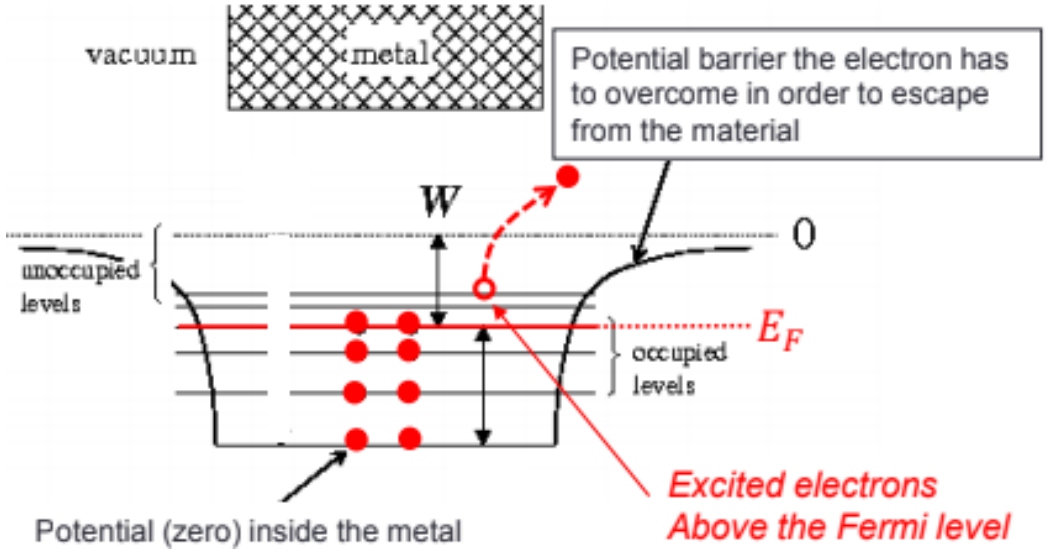



Figure 3.6: Thermionic Emission Operation [23]

Fermi-Dirac distribution for thermionic emission is shown in Figure 3.7. Electrons that have high energy are thermally emitted from the cathode surface. The more it is heated, the more energetic electrons will have, so it will be easier for them to come out. As can be seen from Figure 3.7, the part shown in brown has extracted more electrons because it has a higher temperature, but since the temperature of the part shown in red is less, the electron density has decreased.

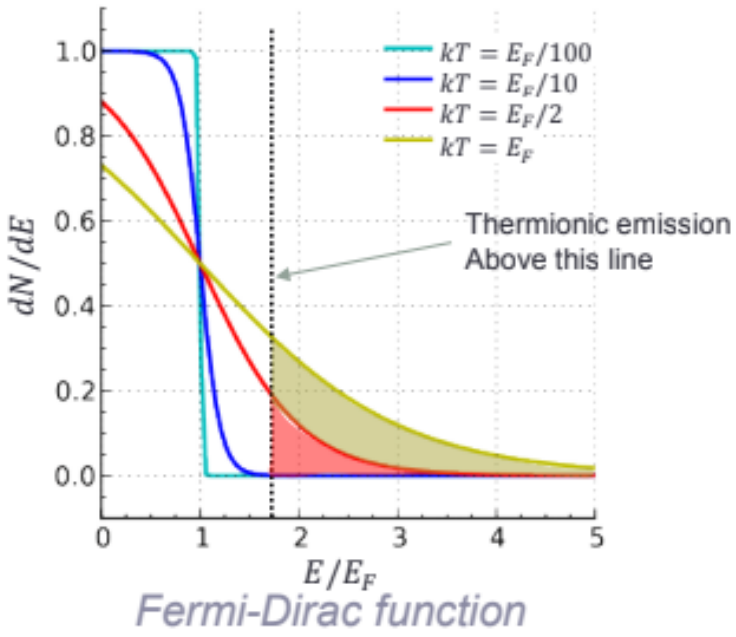



Figure 3.7: Fermi Dirac Distribution [23]

#### 3.1.3.1 Current Density of Thermionic Emission

As explained above, electrons follow the F-D distribution, but high energy electrons can also follow the classical M-B distribution as can be seen from Figure 3.1(High energy tails of the F-D distribution, larger than 1.005 $E_F$).

$$f_{MB} = e^{\frac{-E}{k_B T}} \tag{3.7}$$

The current density equation arises [25]:

$$j_{thermionic} = n_0 e \int_{v_x > \sqrt{\frac{2e\phi_{work}}{m}}} v_x f_{MB} dv = n_0 e \int_{v_x > \sqrt{\frac{2e\phi_{work}}{m}}} v_x e^{-\frac{m(v_x^2 + v_y^2 + v_z^2)}{2k_B T}} dv \tag{3.8}$$

Taking integrals in Equation 3.8 gives current density:

$$j_{thermionic} = 2n_0 e \left(\frac{2k_B T}{m}\right)^2 e^{-\frac{\phi_{work}}{k_B T}} \tag{3.9}$$

By grouping regarding constants in Equation 3.9, Richardson-Dushman (R-D) equation can be obtained [25] [22]:

$$j_{thermionic} = A(1-r)T^2 e^{-\frac{\phi_{work}}{k_B T}} \tag{3.10}$$

where A is 120 $A/cm^2/degK^2$ and (1-r) accounts for the reflection of electrons at the metal surface. In this study, r is taken as 0, and Equation 3.10 becomes [12]:

$$J(\frac{A}{m^2}) = 1.2 * 10^{-6} * T^2 * e^{\frac{-E_{threshold}}{k*T}} \tag{3.11}$$

As can be seen from Equation 3.11, the thermionic emission current density depends on the temperature and the threshold energy of the cathode material. The following interpretation can be made here: If a high current density is desired, a cathode material with low threshold energy and capable of operating at high temperatures should be selected.

#### 3.1.3.2 Cathode Types According to the Material Used in Thermionic Emission

The cathode to be used for the electron particle production system is the most important element that determines the properties of the metal sample to be produced. It is desirable that the electron beam emitted from the electron source should have high flux and low dispersion. The beam produced is accelerated under the electric field thanks to the high voltage potential applied between the cathode and anode. The most common types of cathodes [24]:

- Oxide Coated Cathodes: They are known as types of cathode that are not directly heated. Generally, the alkaline metal oxide is coated on nickel cathode material to increase emission and the surface is heated from behind. The oldest known material is barium oxide. The monoatomic (very thin) layer of barium at the barium oxide cathode has a very small work function.The modern oxide cathodes are produced as mixtures of Barium oxide, Strontium oxide, and Calcium oxide. Another oxide standard is a mixture of barium oxide, calcium

oxide, and aluminum oxide in a ratio of 5: 3: 2. Oxide cathodes operate between 800-1000 ° C. [26]

- Boride Cathodes: They are formed by coating the cathode surfaces with materials such as Lanthanum hexaboride ($LaB_6$) and Cerium hexaboride ($CeB_6$). Hexaborides reduce the work function of the surface to about 2.5 eV. Boride cathodes emit 10 times more than tungsten cathodes and have 10-15 times longer lifetime. These cathodes are widely used in electron microscopes, microwave tubes, electron beam welding machines, and electron guns. The working temperatures are around 1500 ° C. [27]

- Thorium Cathodes: They are cathodes formed by adding a small amount of thorium to a tungsten filament. Tungsten is heated up to 2400 ° C and the emission is enriched by moving thorium atoms to the filament surface. Thorium filaments can have a very long lifetime and are highly resistant against back bombardment that may occur at a high voltage (thorium is continuously absorbed from the surface and creates a new surface). These cathodes are used in high-power tubes of almost all radio transmitters. Because Thorium is radioactive, Zirconium Dioxide is an alternative to Thorium Dioxide. [28]

- Dispenser Cathodes: Dispenser cathodes consist of alloys in the continuous metal phase, in which tightly-bonded, heat-resistant metals are homogeneously interspersed with the radiating metals. The emitting metal is covered with a permeable matrix layer, and the emitting layer works like a reservoir. When the permeable matrix layer is used thermionically, it stands out as a low work function. Oxide coated, pure metal, and thorium tungsten cathode groups are outside this group. On the other hand, oxide-coated cathodes form the basis of this type of cathode. The Tungsten layer forms the permeable emission surface and the Barium mixed emission layer is located as a reservoir behind the permeable layer. There is a heating cabin just behind the emission layer. These cathodes, whose operating temperature is around 2000 ° C, have a longer life than others. [29]

The comparison of the thermionic emitting cathode types can be seen in Table 3.1.

Table 3.1: Comparison of Cathode Types

| **Parameters** | **Tungsten (W)** | **Lanthanum Hexaboride ($LaB_6$)** | **Cold Field Diffusion Source** |
|---|---|---|---|
| Operating Temperature (K) | 2800 | 1900 | 300 |
| Work Function (eV) | 4.5 | 2.4 | 4.5 |
| Brightness ($A/cm^2sr^{-1}$) | $10^5$ | $10^6$ | $10^8$ |
| Lifetime (h) | 40-100 | 200-1000 | >1000 |
| Source Size | 30-100 $\mu$m | 5-50 $\mu$m | <5nm |
| Energy Spread (eV) | 1-3 | 1-2 | 0.3 |

#### 3.1.3.3 Cathode Selection for Thermionic Emission Operation

In this study, thermionic cathode is chosen as a electron source because it can generate a DC beam with a high beam current. For example, Tungsten is one of the most preferred cathode types in this respect. Tungsten can operate at very high temperatures, but its threshold energy (4.5 eV) is also high. Therefore, Lanthanum (III) oxide with threshold energy lower than tungsten and operating at higher temperatures; has started to be preferred more than tungsten. Finally, Lanthanum hexaboride ($LaB_6$), which has been developed recently to replace Lanthanum (III) oxide, has begun to be used more than others as a cathode. The reason is that it can operate at high temperatures with a low threshold energy (2.4 eV) and has a longer lifetime. This is the main reason why ($LaB_6$) is preferred as cathode material within the scope of the thesis.

Another reason for choosing the Lanthanum hexaboride ($LaB_6$) cathode is the low emittance value at the cathode output. As stated above, the threshold energy of LaB6 is 2.4 eV. This will enable us to activate the cathode at a lower temperature. "Emittance" changes in direct proportion to temperature. The reason for this the more electrons are heated, the more energy they will receive, and the more they will push each other at the cathode exit, the more they will spread. Therefore, in order to keep the emittance value low, it is important that the cathode can operate at low temperatures and has low threshold energy. In addition, the cathode diameter is an important factor in choosing the cathode. In order to provide the desired current, electric field, and emittance values, it is sufficient that the cathode diameter is 0.5-4 mm according to the simulation results which will be demonstrated below. This requirement has also been taken into account in the selected cathode.

### 3.1.4 Field Emission Method

The energy given by the field emission method depends on the applied electric field.The required electric field strength should be at least $10^9\ V/m$ or more. It has been observed that when the electric field on the cathode surface reaches a critical level, the diode current on it suddenly increases. [22] In other words, the potential barrier is broken with the applied electric field. Through this broken barrier, electrons can easily get out of the material and go their own way. An illustration of this method is given in Figure 3.8:

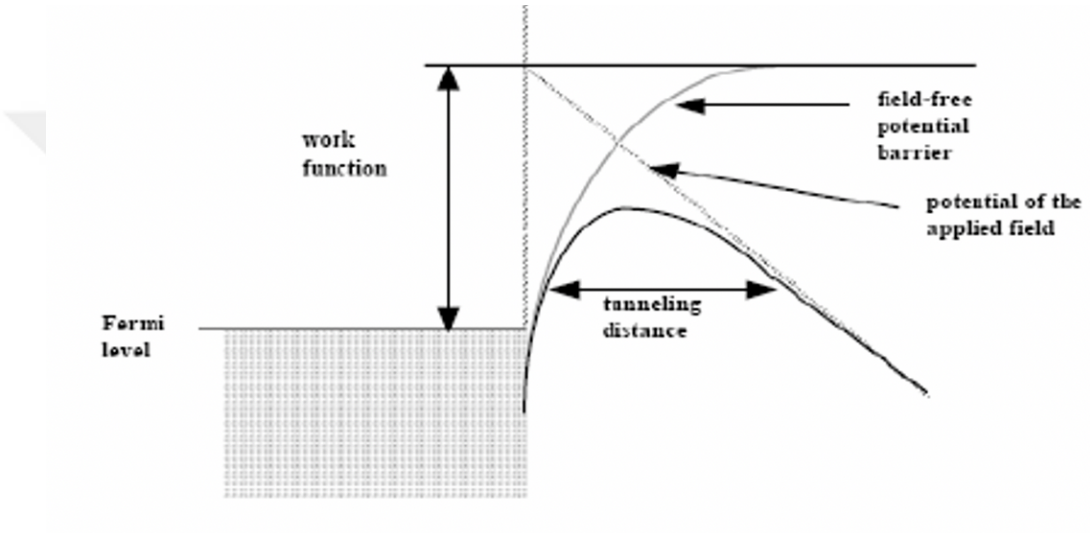



Figure 3.8: Field Emission Method [30]

As can be seen from Figure 3.8, it is a cold cathode emission. No metal heating is needed to extract electrons from the cathode surface. A strong electric field helps in removing electrons from the surface. The current density of the field emission method is given in Equation 3.12 [31]:

$$J[\frac{A}{m^2}] = \frac{k_1 E^2}{\phi} e^{-\frac{k_2 \phi^{3/2}}{E}} \tag{3.12}$$

where constants $k_1$ and $k_2$ are $1.4 \times 10^{-6}(SI)$ , $6.87 \times 10^7(SI)$ respectively. $\phi$ is the work function of the material and E is the applied field externally.

As can be interpreted from Equation 3.12. As the electric field increases the current

density is also increases of the beam.

### 3.1.5 Photo Emission Method

The energy given by the photoelectric method depends on the energy of the incoming photons. Photons falling on the cathode surface create free electrons. Photon energies below the threshold energy cannot remove any electron from the surface of the cathode. Photon energies above the threshold energy, on the other hand, emit an electron beam as much as the energy in the wavelength they come from, regardless of their density [22].

It can be summarized its operation in three steps and shown in Figure 3.9:

- Photon absorption by the electron
- Electron movement to the surface
- Exiting through the barrier

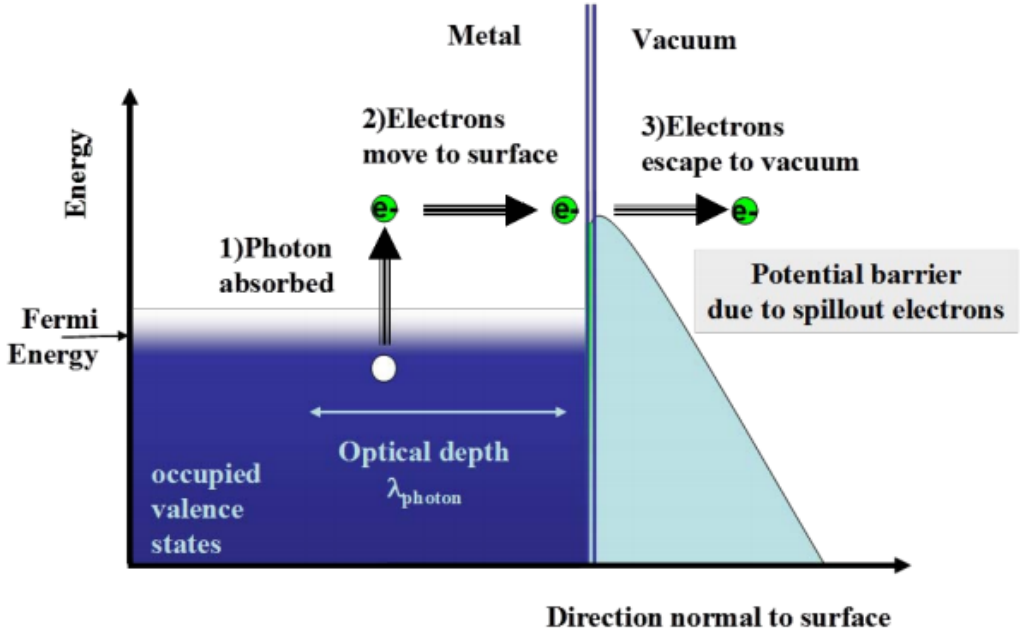



Figure 3.9: Steps of Photo Emission Method [22]

The energy of photons occurring on the surface depends on the frequency of the light and is expressed as [32]:

$$W = hf \tag{3.13}$$

where h, Planck constant, is $6.626 \times 10^{-34} Joule - Second$ and $f$ is the frequency and its unit is Hertz.

The energy of the photon first tears the electron from the atom and the remaining energy remains as kinetic energy to the photoelectron. Mathematical expressions of them are given below [32]:

$$hf = E_k + \phi \tag{3.14}$$

Here $\phi$ is the work function and corresponds to the energy required to remove the electron. The work function is a characteristic feature of the metal on which light is shined; therefore, it is a different and special value for each metal. It is expressed as follows:

$$\phi = hf_0 \tag{3.15}$$

where $f_0$ is the threshold frequency. It corresponds to the frequency threshold that must be exceeded. In this case:

$$E_k = h(f - f_0) \tag{3.16}$$

The threshold frequency is actually the energy that corresponds to the work function. If $f < f_0$ then $hf < hf_0$, so the work is not enough, the electron cannot be extracted [32].

### 3.1.6 Emittance of the Three Emission Method and Discussion of Them

Each emission method has a specific emittance calculation and different emittance values. Therefore, their mathematical expressions are different from each other. For thermionic emission, cathode emittance is given in Equation 3.17 [22]:

$$\epsilon_{thermionic} = \sigma_x \sqrt{\frac{k_B T}{mc^2}} \tag{3.17}$$

where $\sigma_x$ rms of the beam is given by the transverse beam distribution. As can be interpreted from the equation, the emittance value depends on the temperature and the beam size of the beam. $\sigma_x$ can vary depending on using particular transverse distribution. Its unit is microns/mm and generally 0.3 microns/mm for a cathode temperature of 2500 [22].

For photo emission cathode emittance is given as follows [22]:

$$\epsilon_{photo} = \sigma_x \sqrt{\frac{\hbar\omega - \phi_{eff}}{3mc^2}} \tag{3.18}$$

It depends on the beam size of the beam and potential. Its range is between $0.5$ to $1$ micron/mm depending upon the wavelength of the incoming photon.

For the field emission method, the cathode emittance depends on the applied external electric field. As the external electric field increases, the emittance value of the cathode increases. It can vary from 0.5 to 2 microns/mm for fields at $10^9 V/m$ to $10^{10} V/m$. Thus, it has a greater emittance value for the same source size than the other two emission methods [22].

## 3.2 General Structure

The working principle of electron guns is based on many basic principles of physics. For example, in order to remove electrons from the cathode, first of all, the electrons inside are heated by heating the cathode with the help of a filament. Thus, the electrons that receive enough energy leave the cathode and become a beam. This heating

process depends on the material choice of the cathode that has been discussed in Section 3.1.3.3. The Fermi energy levels of the material determine how much the metal heated. Equations like Richardson-Dushman also help calculating how many electrons will come out and the current density as mentioned in Section 3.1.3.1.

Since the released electrons are charged, they are affected by two fundamental fields. These fields are electric and magnetic fields. Inside the electric field, electrons move towards positive voltage, i.e. towards the anode. During the acceleration process, electrons gain energy. The amount of this energy is largely dependent on the high voltage applied between the cathode and anode. [18] For example, an electron accelerating by seeing 150 kV reaches 63% of the speed of light. Therefore, if the energy of the electron is to be determined, it is essential that the accelerator voltage must be known. A simple outline of the motion due to the electric field is shown in Figure 3.10.

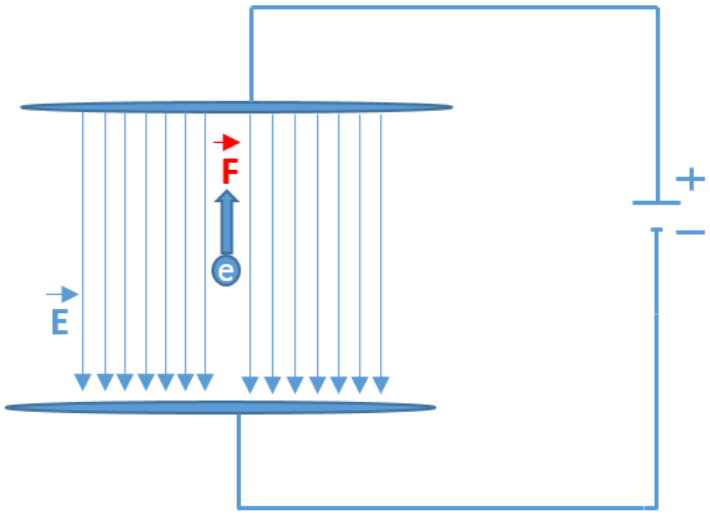



Figure 3.10: Electrons Motion in Electric Field

The second fundamental field in which electrons are affected is the magnetic field. The force acting on electrons in this field is the Lorentz force. This force causes electrons change their motion direction. Thanks to this force, electrons move perpendicular to both the field direction and the direction of travel. During this change, the speed of electrons does not alter. Therefore, the energy of electrons does not increase

in routing works. [18] This results in the following conclusion: The electric field must be used to accelerate the electron beam and the magnetic field to direct it. The motion pattern of magnetic field source electrons is shown in Figure 3.11.

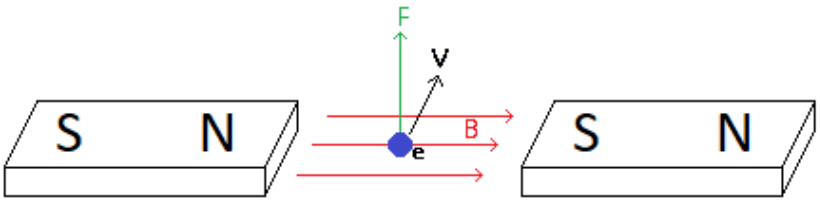



Figure 3.11: The Lorentz force (F) acts on electrons in the magnetic field (B), changing their direction of motion (v) [33]

Generally, Newton and Lorentz formulas are sufficient to describe motion. They are given as follows [2]:

$$\frac{dP}{dt} = F, \quad F = q * (E + v \times B) \tag{3.19}$$

However, this situation is different for accelerators. There is a certain route on the accelerator road, magnets or other things. Therefore, the Hamiltonian equation is required to describe the motion of the beam. Deriving the beam motion equation is found with the help of Hamiltonian. The Hamiltonian is an equation that represents the total energy of the beam. [11] It is shown in Equation 3.20:

$$H_{new} = -p_z = -\sqrt{\frac{(E - q\phi)^2}{c^2} - (p_x - qA_x)^2 - (p_y - qA_y)^2 - m^2c^2} - qA_z \tag{3.20}$$

From this equation it can be deduced that if E and B are static, that is, independent of time, the Hamiltonian equation of the beam will also be time-independent. Therefore, its total energy will be constant. It can be an intended condition depending on the

circumstances. A modeling is generally done with these equations and compared with simulation.

## 3.3 Space Charge Effect

One of the main problems in an electron guns is the space charge effect. The maximum beam current is limited by the space charge under given accelerating voltage. Emitted electrons from the cathode cannot go instantly to the anode. It takes time for traveling. In this time interval, these electrons build a cloud around the cathode surface, and this cloud keeps itself during the operation since new electrons are being produced continually from the cathode while others are gone to the anode. This is the cloud of electrons that generates a negative space charge. Therefore, the electron gun performance highly depends on space charges that will be discussed in the following section. [34]

### 3.3.1 Space Charge

Consider two electrons that share the same electric charge -e as can be seen in Figure 3.12. When they are stationary, they will repel each other due to the Coulomb force. However, when they start to move with a velocity $v = \beta * c$, they act like two parallel currents that attract each other due to their magnetic field effect. The right diagram indicates that as the speed of particles increases, the repulsive effect decreases. Special relativity suggests that when they reach the speed of light, their forces will be equal to each other and thus cancel. [34]

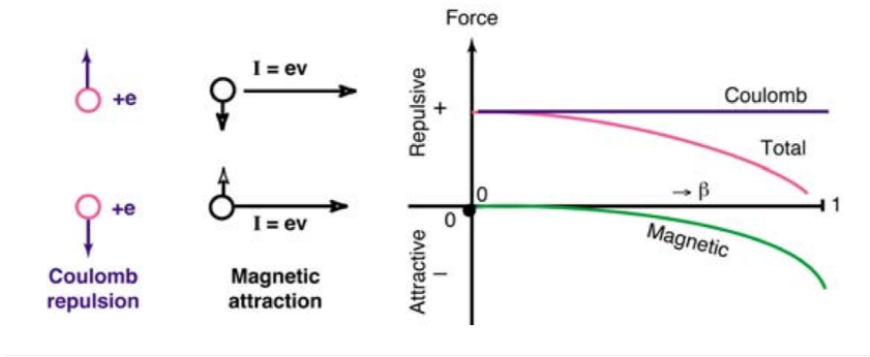



Figure 3.12: Coulomb repulsion and magnetic attraction between two particles of equal charge, at rest and travelling [34]

Now take into account many electrons that form an unbunched cloud traveling with a circular cross-section as can be seen in Figure 3.13. The Coulomb force thrust the particle that is indicated with the circle to the aside. The force in the beam center is zero and gets larger to the edge. [34]

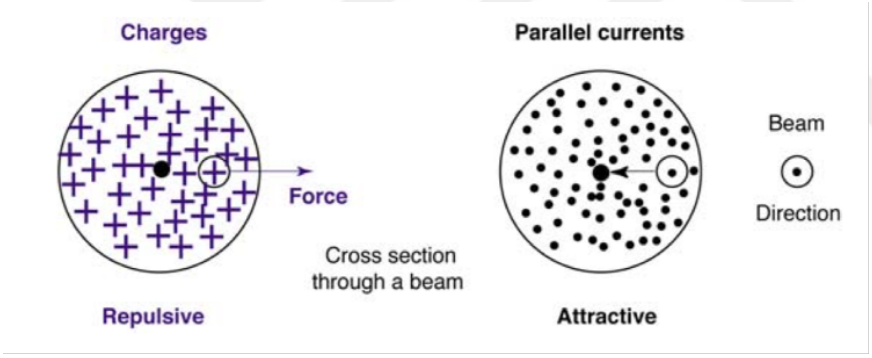



Figure 3.13: Electromagnetic Forces on a charged particle [34]

### 3.3.2 Space Charge Fields

In this thesis, the continuous beam will be studied. Therefore, for space-charge fields, this beam is considered with having cylindrical symmetry that travels at a constant velocity $v = \beta * c$. [35] The charge density of the beam is

$$\rho(x, y, z) = \rho(r) \tag{3.21}$$

where $r = \sqrt{x^2 + y^2}$. Thanks to cylindrical symmetry, the electric field has only radial component $E_r$. By using Gauss Law over a cylinder centered on the electron beam gives

$$E_r(r) = \frac{1}{\epsilon_0 r} \int_0^r \rho(r^{'}) r^{'} dr^{'} \tag{3.22}$$

The current density of the electron beam is

$$J(x, y, z) = J(r) * u_z \tag{3.23}$$

where $u_z$ is the unit vector of the beam direction. If the longitudinal speed of the particles in the beam is the same, $v_z = \beta_z * c * u_z$, it gives,

$$J(r) = \rho(r) * \beta_z * c * u_z \tag{3.24}$$

The magnetic field has also only azimuthal component $B_\theta$. By using Ampere's Law over a cylinder centered on the electron beam gives

$$B_\theta(r) = \frac{\mu_0}{r} \int_0^r J(r^{'}) r^{'} dr^{'} \tag{3.25}$$

$$= \frac{\mu_0 \beta_z c}{r} \int_0^r \rho(r^{'}) r^{'} dr^{'} \tag{3.26}$$

By combining Equations 3.22 and 3.26, the following equation is obtained for space charge self-fields (Taking $c = \frac{1}{\sqrt{\epsilon_0 * \mu_0}}$)[35] :

$$B_\theta(r) = \frac{\beta_z}{c} E_r(r) \tag{3.27}$$

### 3.3.3 Space Charge Forces

Due to space charge fields, a force will be generated in Figure 3.14 on the particle as shown in Section 3.3.1. It can be expressed by [12]:

$$F = q * (E + v \times B) \tag{3.28}$$

Considering the cylindrical geometry Equation 3.28 can be simplified to

$$F_r = e * (E_r - \beta_z * c * B_\theta) \tag{3.29}$$

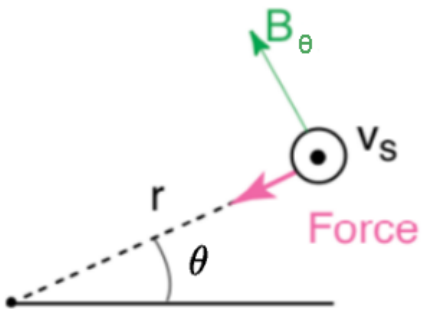



Figure 3.14: Force due to an azimuthal magnetic field $B_\theta$ [34]

If one inserts $B_\theta$ in Equation 3.29, the following equation can be obtained:

$$F_r = q * E_r(1 - \beta^2) = \frac{qE_r}{\gamma^2} \tag{3.30}$$

Due to these space charges, electric force defocuses the beam, whereas magnetic force focuses which are the important cases for the design criteria. [35] [34]

## 3.4 Space Charge Limited Current – Child and Langmiur's Law

### 3.4.1 Child and Langmiur's Law

In order to calculate maximum current density in the electron gun, a simple analytical solution was derived by Child and Langmuir in 1911. [36] A simple schematic is given in Figure 3.15. The expression is written in steady-state.

One can start with following boundary conditions

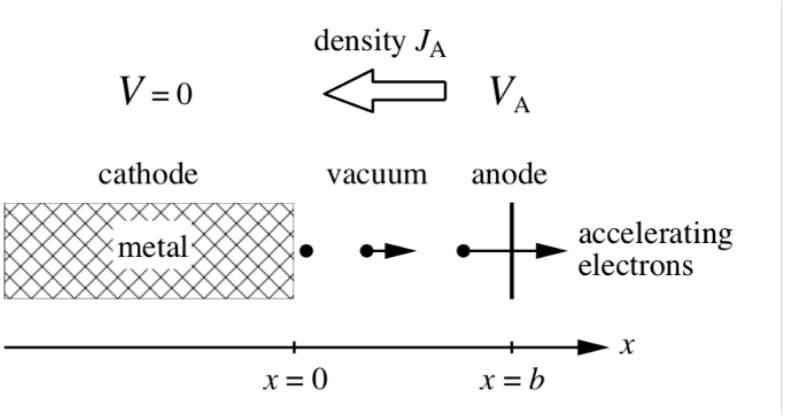



Figure 3.15: Schematic view of one-dimensional electron gun [36]

$$\Phi(0) = 0 \tag{3.31}$$

$$\Phi(b) = V_A \tag{3.32}$$

where $\Phi$ is the voltage, $V_A$ is the acceleration voltage and $b$ is the distance from cathode to anode. In a vacuum, the magnitude of the electric field is

$$E(x) = \frac{-V_A}{b} \tag{3.33}$$

For steady-state calculation, the magnitude of the current density $(J)$ is uniform in x

$$J(x) = J_A \tag{3.34}$$

And the condition of Child-Langmuir is described in such a way that the beam current is limited when the electric field at the emitting cathode is zero,

$$E(0) = 0 \tag{3.35}$$

That means the contribution of the electric field at the cathode side by the space-charge completely cancels out the applied field. [37]

One can apply the energy conservation and gets:

$$\frac{1}{2}m[v(x)]^2 - e\Phi(x) = constant = 0 \tag{3.36}$$

where $m$ and $v$ are the mass and velocity of electrons respectively, and $e$ is the charge. Due to steady-state condition, the energy is constant in the gap. In addition, velocity and potential are zero together at $x = 0$. Poisson's equation can be written also as follows [37]:

$$\nabla^2\Phi(x) = \frac{-\rho(x)}{\epsilon} \tag{3.37}$$

where $\epsilon$ is the permittivity of free space and $\rho$ is the charge density. Now, $J$ can be written in terms of $\rho$ and $v$ and note that $J(x)$ is constant in steady-state,

$$J(x) = \rho(x) * v(x) = -J_A \tag{3.38}$$

By combining Equations 3.36, 3.37 and 3.38, one can get the following differential equation:

$$\frac{d^2}{dx^2}\Phi(x) = \frac{J_A}{\epsilon}\sqrt{\frac{m}{2e\Phi(x)}} \tag{3.39}$$

which can be written as:

$$\left(\frac{d\Phi}{dx}\right)^2 = \frac{4J_A}{\epsilon}\sqrt{\frac{2m\Phi(x)}{e}} + C \tag{3.40}$$

$$= \frac{4J_A}{\epsilon}\sqrt{\frac{2m\Phi(x)}{e}} + \left(\frac{d\Phi}{dx}|_{x=0}\right)^2 \tag{3.41}$$

Since, $d\Phi/dx$ is just $E(x)$, and the boundary condition $E(0) = 0$ is considered, Equation 3.41 can be written as:

$$\frac{d\Phi}{dx} = \sqrt{\frac{4J_A}{\epsilon}\sqrt{\frac{2m\Phi(x)}{e}}} \tag{3.42}$$

And by combining $\Phi$ terms and by integrating it, the following equation is obtained:

$$\int_{\Phi(0)}^{\Phi(x)} \frac{d\Phi}{\Phi^{\frac{1}{4}}} = \int_0^x \sqrt{\frac{4J_A}{\epsilon}\sqrt{\frac{2m}{e}}}dx \tag{3.43}$$

and $\Phi(x)$:

$$\Phi(x) = \left(\frac{3z}{2}\right)^{\frac{4}{3}} \left(\frac{J_A}{\epsilon}\right)^{\frac{2}{3}} \left(\frac{m}{2e}\right)^{\frac{1}{3}} \tag{3.44}$$

In order to get limiting current density, Equation 3.44 is solved at $x = b$, and the following equation is obtained which is the maximum steady-state current density through the gap between cathode and anode, known as Child and Langmiur's Law [37] [36] [12].

$$J_A = \frac{4\epsilon}{9}\sqrt{\frac{2e}{m}}\frac{V_A^{\frac{3}{2}}}{b^2} \tag{3.45}$$

The space charge effects have an important impact on designing electron guns in practice, so it is important to understand how various systems are influenced by these designs. Equation 3.45 shows that:

- Space charges limit the current that can be extracted from the cathode
- Current density is proportional with an applied electric field, so the stronger the accelerating electric field, the more current can be drawn. How to create a strong electric field will be explained in Chapter 4.
- There is a limit on the strength of the accelerating electric fields in order not to cause an electric arc between anode and cathode due to high electric fields. Therefore, the gap distance cannot be made too small.

Child and Langmiur's law is a very useful for predicting current limits in many cases, but it makes some significant assumptions like electrons are initially at rest, one-dimensional system, and steady-state operation taking into account.

## 3.5 Pre-Design Work

The purpose of this thesis is to explain how to design and implement a low emittance high power DC electron gun. Before explaining this, it is necessary to understand the relationship between some parameters in the electron gun. These parameters are voltage, current, and emittance. The relations of these parameters with each other vary according to the desired design criteria. In addition, all these parameters are related to the applied electric field. The desired design can be made with a suitable electric field, and a suitable electric field is related to the correct design of the system's geometry. Accordingly, the selected geometries will be explained in the next section.

### 3.5.1 Voltage-Emittance Relation

There is an inverse proportion between the applied voltage and emittance in electron gun systems. If the accelerator voltage applied in the system is high, the electric field at a constant distance will be high as well. With the high electric field, the speed of the electrons that are emitting from the cathode will increase. Due to the high velocity of the electrons, they will come out of the anode before the coulomb force takes effect. Since the Coulomb force cannot act in a short time, the electric field in the transverse direction will not increase, so the electrons will not be able to push themselves and therefore will move forward without dispersing. Thus, the emittance value of the beam will decrease. If the applied voltage is low, the electrons will not be able to accelerate much due to the low electric field and they will repel each other by showing the effect of the Coulomb force. Hence, the emittance value of the beam will increase.

### 3.5.2 Voltage-Current Relation

Voltage and current are directly proportional to each other in electron gun systems. As the applied voltage increases, the electric field will also increase; hence, the beam current will increase. However, due to the space charge effect, the current will be limited no matter how much the voltage increases that was covered before.

### 3.5.3 Current-Emittance Relation

This relation determines how the design is optimized . There is an exchange between current and emittance depending on the applied electric field. The beam current will increase as the applied electric field increases. Hence, the number of electrons in the system will increase. Therefore, electrons will begin to repel each other by showing the effect of the Coulomb force. Due to the increase in the force in the transverse direction, the emittance value will increase. This is not a desirable case for this study. The aim of this study is to draw more beam current when the emittance value is low.

Considering all these relations, a field should be designed with an appropriate geometry, such that the electric fields of the electrons in the transverse direction should be minimum and the fields in the longitudinal direction should be maximum. Thus, design with a low emittance will be possible without reducing the current drawn by the cathode. Chapter 4 discusses how to design this geometry and the electric field.

Figure 3.16 explains the pre-design work principle. All motivation is suppressing transverse components of electric fields due to Coulomb forces of the electrons and increasing longitudinal components of electric fields to accelerate electrons sufficiently. If this condition is fulfilled, high current and low emittance can be achieved.

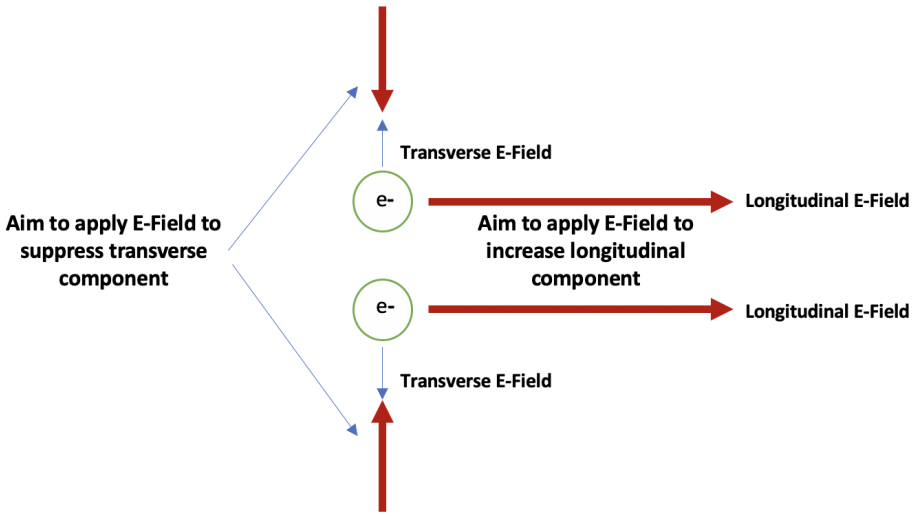



Figure 3.16: Representation of the electric fields expected to be applied (Red Colored)

# CHAPTER 4

# DESIGN AND SIMULATION

## 4.1 Gun Assembly

The proposed electron gun assembly together with its power supply connections is shown in Figure 4.1. The cathode is placed on the opening of the focusing and control electrode structure as illustrated in Figure 4.1. A high voltage power supply is connected between the cathode and anode with a ground potential on the anode in order to generate accelerating fields. To heat the cathode and thus release electrons, the filament power supply is also connected to the cathode. Focusing and control electrode is fed from the series connection of two power supplies. One of them is a high voltage power supply and the other is focusing and control electrode power supply. With the existence of focusing and control electrode power supply, beam current can be adjusted to any desired values as the power supply voltage changes. After exceeding a certain voltage value, the beam current can be ceased as well.

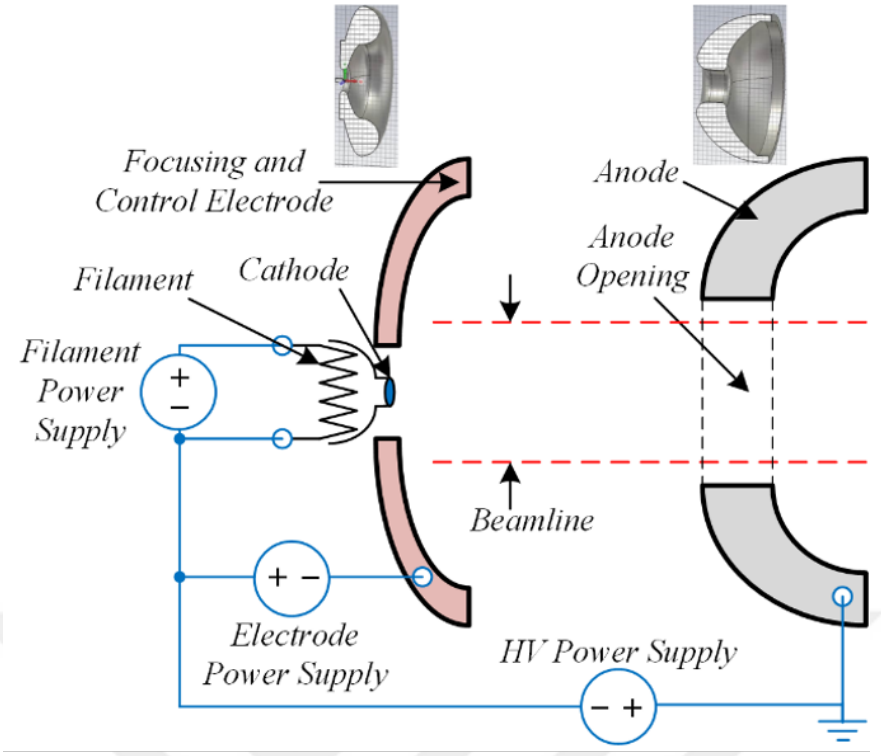



Figure 4.1: Proposed Gun Assembly

In order to satisfy the design requirements in this study, an electron gun composed of cathode, anode, and focusing electrode have been proposed, as can be seen in Figure 4.1. The cathode is responsible for the emission of electrons to the system. The cathode is made of a single crystal with a low work function and heated to higher temperatures for producing electrons. The design of the focusing and control electrode geometry is very important in this electron gun. All parameters that have been covered in Chapter 2 depending on the design of this geometry. The main purpose of this geometry is to obtain the maximum current and the lowest emittance value by providing the appropriate electric field between the anode and cathode. It also regulates the beam current by adjusting its voltage with respect to cathode voltage. Finally, an anode inserted into the structure to generate accelerating electric fields. With the help of a small opening drilled on the anode, the emitted electrons are turned out to be a beam form.

## 4.2 Design of Focusing and Control Electrode

Electrode shape should be designed to generate the desired electric fields. The following criteria must be fulfilled to generated electric field in our study [12]:

- A strong electric field must be created in front of the cathode for more electrons thus getting more current
- Stronger the accelerating fields, lower the emittance. However, the accelerating field must show a slightly focusing effect, otherwise, the beam will bunch in front of the anode and it will scatter resulting in a higher emittance
- There is a limit on the strength of the accelerating electric fields in order not to cause an electric arc between anode and cathode due to high electric fields.

Electrons exit the filament at wide angles and move forward. This leads the beam spreads. Focusing and control electrode enables the dispersed beam to focus and move forward in a more stable structure. These structures, called Wehnelt cylinders, are used as both electrostatic lenses and control grids. This structure has the same voltage as the cathode voltage which is equal to the accelerating voltage. This voltage creates an electrostatic field between the cathode and anode. This electrostatic field between them allows the beam to focus on a given point. If it is desired to focus the beam in an early place, the accelerating voltage that is given to the focusing electrode and cathode is increased. In Figure 4.2, the effect of the applied voltage to the focusing and the control electrode on focusing ability is stated.

The current strength of the beam is also adjusted via this focusing and control electrode. If a high current is required, the voltage of this electrode is low with respect to the cathode voltage; if a low current is desired or the beam is to be cut, this applied negative voltage should be increased. In this study, the geometry is designed in such way that one can obatain the highest current and the lowest emittance at low focusing and control voltage.

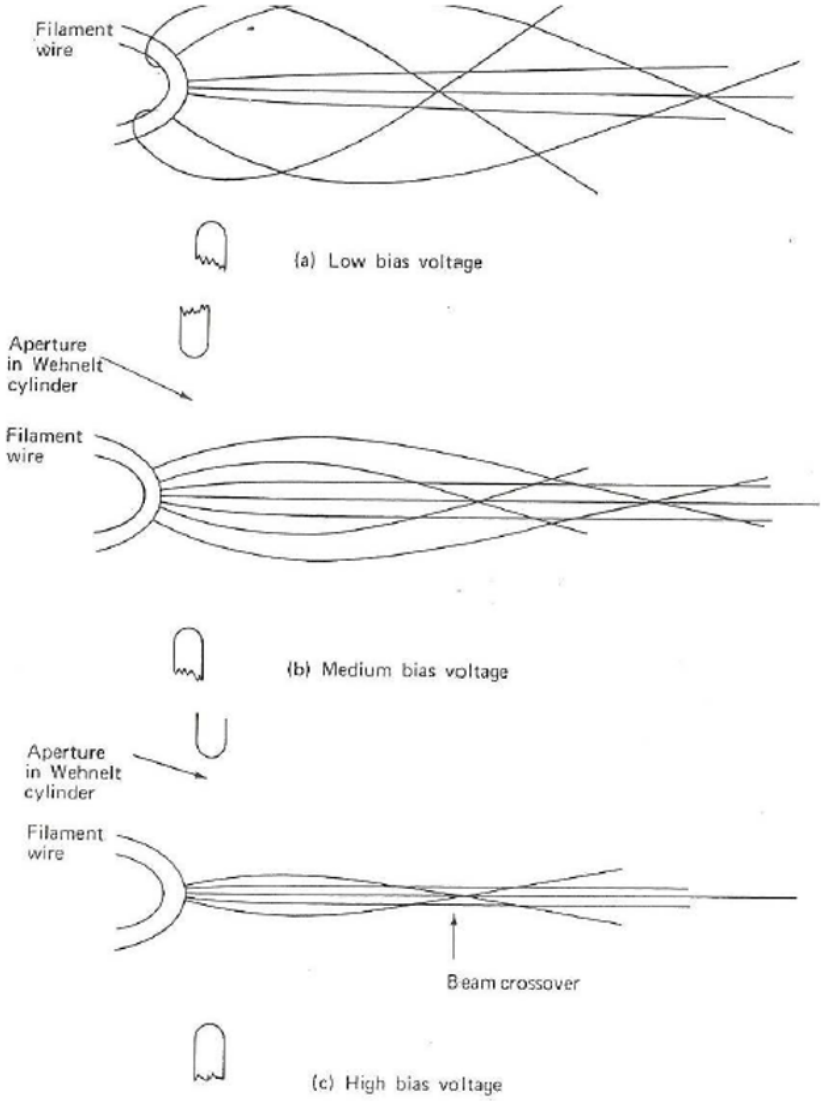



Figure 4.2: Effect of the voltage on the Wehnelt Cylinder to focus, (a) The voltage applied to the Wehnelt cylinder is low, the focusing ability is low, (b) the medium level voltage, the focusing ability has improved, (c) the applied voltage is at the upper level, in the plane perpendicular to the direction of the beam. [38]

As can be seen from Figure 4.2, the more voltage is applied to the focusing (wehnelt) electrode, the more field strength will increase, so the focusing function will occur earlier. However, since the focusing will be less at low applying accelerating voltage, the emittance value will increase. The beam will crossover at high applying accelerating voltage, so it will start to dissipate before reaching the anode and the emittance value will increase also. For this reason, such a geometry should be chosen for focusing and control electrode that will meet the requirements by minimizing these effects. After determining the geometry of the focusing and control electrode geometry, the anode geometry must be determined properly in order for the beam to pass through the anode appropriately.

There are three main regions for beam's motion through electrode geometries which are shown in Figure 4.3. [39]

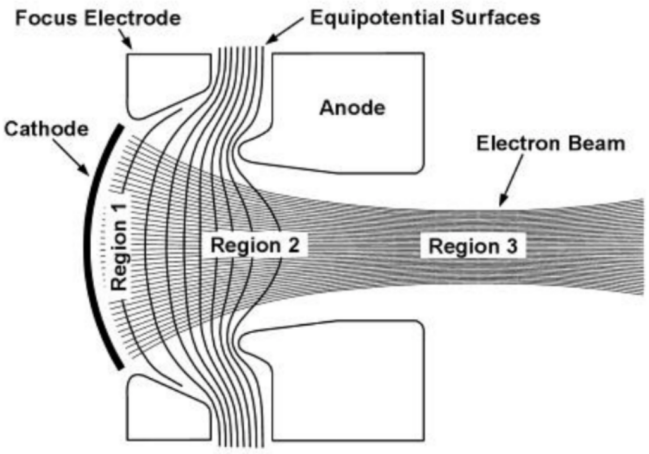



Figure 4.3: Different regions of Electron Gun [39]

The first region of the Electron Gun is the cathode region where electrons emerge. The second region is the zone where the electrons travel between the focusing structure and the anode. The third region is the region where electrons continue after the anode. The most important region in the electron guns is the second region. Since the characteristic of the beam is determined in this region. The geometry of these electrodes is actually the geometry of the equipotential surfaces of the electrostatic potential function inside the gun, represented as $\phi(r, z)$. To find the optimum geometry of the electrodes, it will be sufficient to find the appropriate potential function

that meets the desired conditions. Due to the symmetrical structure of thermionic guns, the electric fields in these structures are in an axially symmetrical form. Thus, it is seen that the known potential function on the gun symmetry axis is sufficient to calculate the potential function $\phi(r, z)$ at any point [40]. The potential function makes it possible to calculate the equipotential surfaces. Thus, the electron gun design problem is reduced to the problem of computing the one-dimensional function $\phi(0, z)$.

To optimize the accelerating field and equipotential lines, a fully parametric focusing and control electrode model is proposed as given in Figure 4.4 in the scope of this thesis. The design of the electron gun was made using the Computer Simulation Technology Particle Studio program.

### 4.2.1 Computer Technology Simulation Particle Studio

CST Studio Suite is a simulation program that includes a wide range of applications and enables the simulation of complex tools and devices. Often these complex devices are difficult to unravel and understand. In particular, it is very difficult analytically to predict this state for particles and situations whose behavior is transient. The complex electron or wave interaction responsible for a power generation or amplification process can be made via simulation. It is an important task to predict the performance of these devices before operation. CST can be used to design charged-particle devices, including Particle Tracking Solvent, Cell Particle (PIC) Solvent, and Wakefield Solvent because there are various tools to solve them. These can be used for beamline components, magnets, cavities, and absorbers. Particle dynamics simulations are essential for many devices. One of the main ones is vacuum electronic devices. In addition, with CST, magnetrons, gyrotrons, klystrons, and traveling wave tube amplifiers can be easily designed and simulated. High-power microwaves can be designed, taking into account thermal and mechanical effects, thanks to multi-physics simulation as well [41] [42]. In summary, Particle Sources, Accelerator Components, Electron Tubes, and Wake Field Simulations can be done with the CST particle studio and their solvers are explained below.

#### 4.2.1.1 Solver Modules

- **The Stationary Particle Tracking Solver**: It can mainly provide to track of charged particles such as electron through the electrostatic, magnetostatic, and eigenmode fields. Various emission models are available, including secondary emission[41].
- **The Wake Field Solver**: It can calculate the fields that are created by charged particles passing through 3D geometries such as; cavities, etc. in the time domain. It also provides information about the loss and kicks factor by integrating the total effect of accelerator elements [41].
- **The Particle in Cell (PIC) Solver**: It ensures a self-consisted method for transient simulation of particle dynamics. It is a solver that can calculate space charge and self-magnetic fields of particles. It also handles the when emitting particles through static or HF electromagnetic fields. High power MW tubes can be simulated with this solver [41].
- **The Electrostatic Solver**: It is the solver that is used in this study. It provides estimation of the accelerating fields for static guns mainly [41].
- **The Magnetostatics Solver**: Many types of magnets like dipoles, solenoids, etc. can be simulated with this solver. It calculates the fields of them[41].
- **Stationary Current Solver**: The current flow of any shaped coils can be calculated thanks to this solver in magnetostatics computations [41].
- **Eigenmode Solver**: It provides to track particles through the resonant fields in cavities[41].

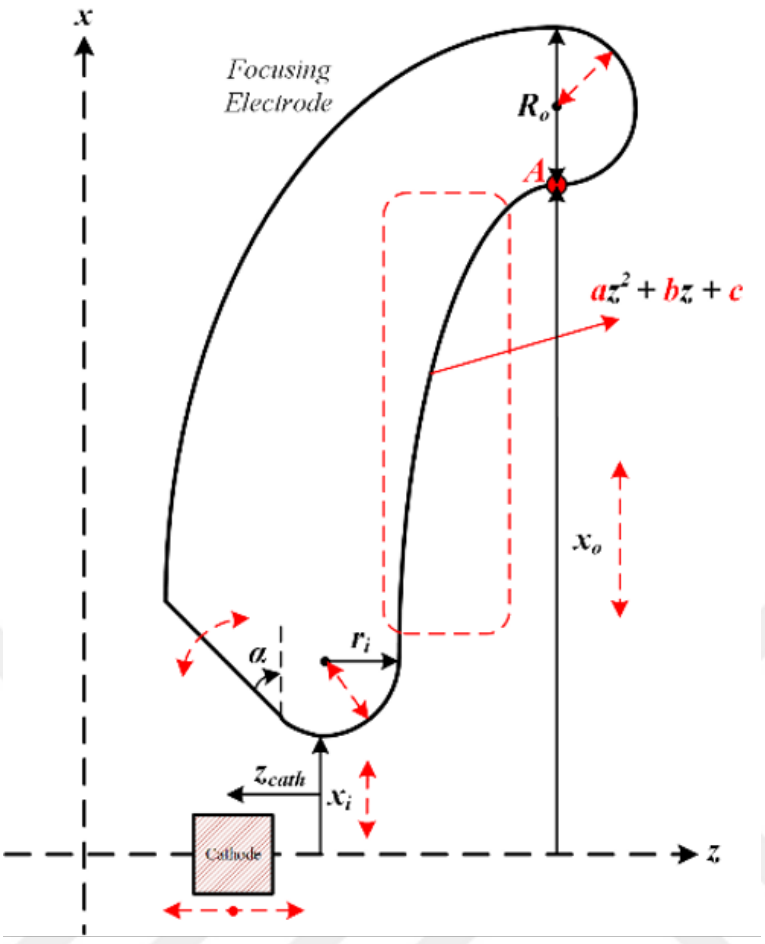



Figure 4.4: Fully Parametric Focusing and Control Electrode Structure

### 4.2.2 First Design- Linear Focusing and Control Electrode Geometry

The first design for the focusing and control electrode is done with a linear geometry and an angle with respect to the x-axis. The Computer Simulation Technology (CST) program was used to design this geometry and its view is shown in Figure 4.5.

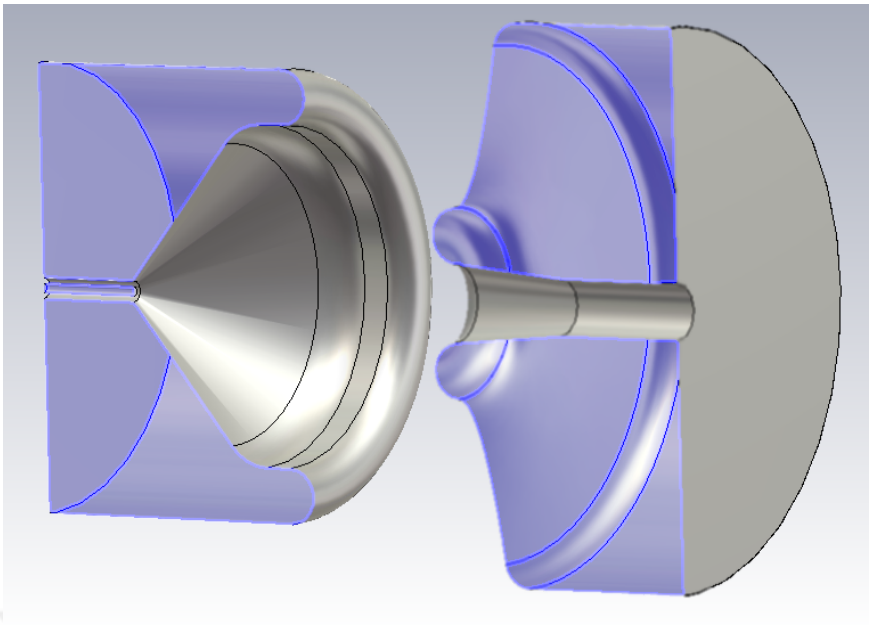


Figure 4.5: Linear Geometry View

As can be interpreted from this geometry, there is a linear relation in focusing electrode structure instead of a quadratic relation. While increasing the angle with respect to the x-axis, it is seen that the beam is over-focused. This makes the emittance value lower, but the magnitude of the electric field in front of the cathode has decreased due to this focusing effect. Therefore, the maximum current that can be drawn from the cathode gets smaller.

Table 4.1. shows the variation of current and emittance values for 90 kV according to the angle of the focusing electrode.

Table 4.1: Emittance and Current Values By Changing the Focusing Electrode Angle

| Focusing Electrode Angle (Degree) | Current (mA) | Emittance (mm*mrad) |
|---|---|---|
| 0 | 92 | 0.65 |
| 5 | 75.7 | 0.89 |
| 10 | 310 | 1.04 |
| 15 | 185 | 0.89 |
| 20 | 112 | 0.84 |
| 25 | 61.6 | 0.72 |
| 30 | 30.8 | 0.64 |
| 35 | 13.4 | 0.54 |
| 40 | 5.6 | 0.4 |
| 45 | 1.8 | 0.28 |
| 50 | 0.4 | 0.16 |
| 55 | $8.57 \times 10^{-2}$ | $7.62 \times 10^{-2}$ |
| 60 | $8.53 \times 10^{-3}$ | $2.61 \times 10^{-2}$ |
| 65 | $5.69 \times 10^{-4}$ | $1.64 \times 10^{-2}$ |
| 70 | 0 | 0 |

The Figure 4.6. also shows the change of them.

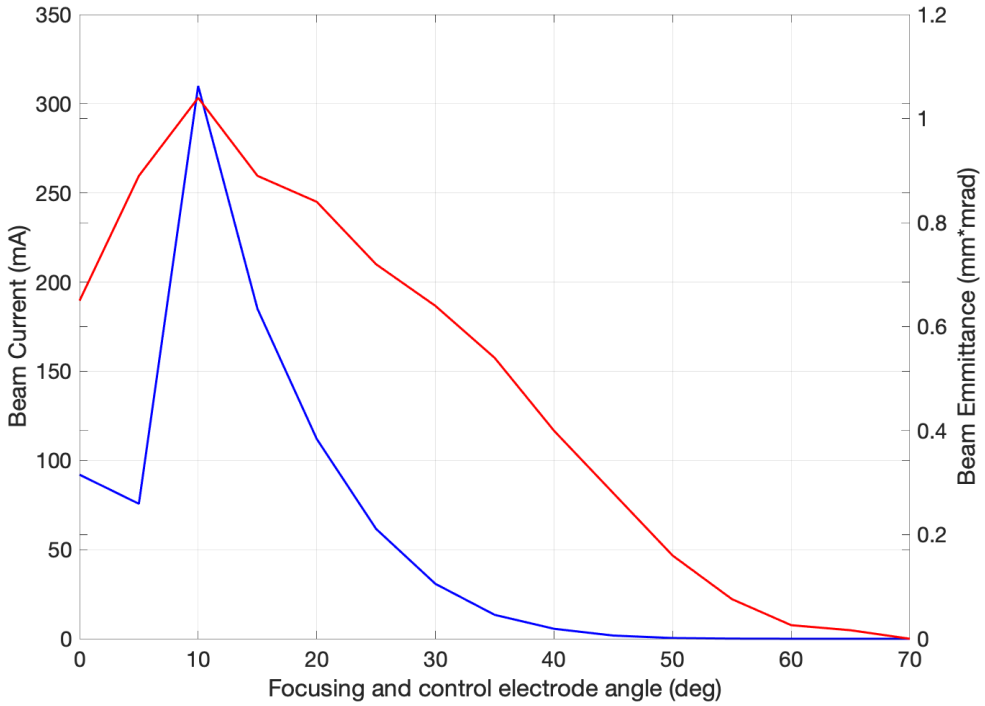



Figure 4.6: Beam Emittance (red colored) and Current (blue colored) values by changing of focusing electrode angle

As can be deduced from Figure 4.6, as the angle of the focusing electrode increases, the electrons emerge less from the source and this decreases the current value. Accordingly, the emittance value decreases. At small angles, even if the current value is high and the emittance value is low, other parameters are not as required. For example, the beam diameter is too large. In addition, the beam divergence angle is also large and as can be seen from the beam trajectories (Figure 4.16-4.17), the beam entering the anode will start to hit the edges. This is also unwanted situation. It will damage the anode. One solution may be raising the anode gap, but changing the anode gap will affect the current and emittance parameters badly since the electric field in front of the cathode will be disrupted.

The reason why the current and the emittance value decrease as the angle increases is change in electric fields in front of the cathode.. The change of the electric field for each angle value is shown in Figures 4.7 to Figure 4.14.

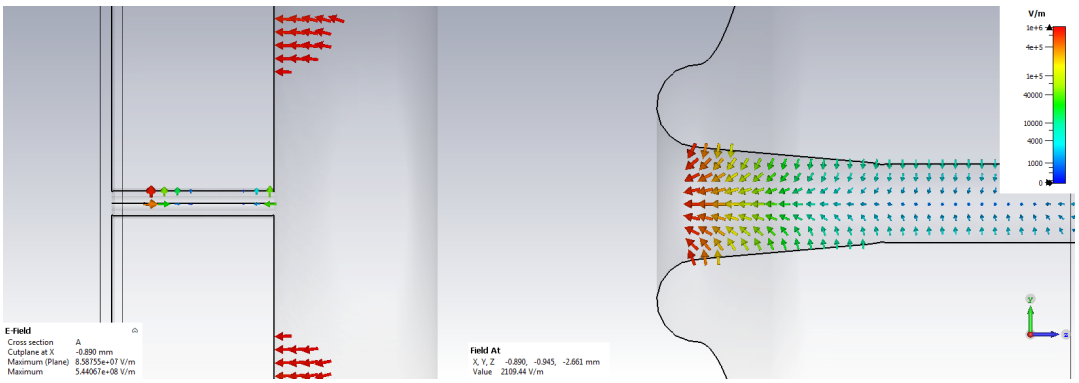



Figure 4.7: Showing of changing electric field in front of the cathode and focusing electrode with 0 focusing angle

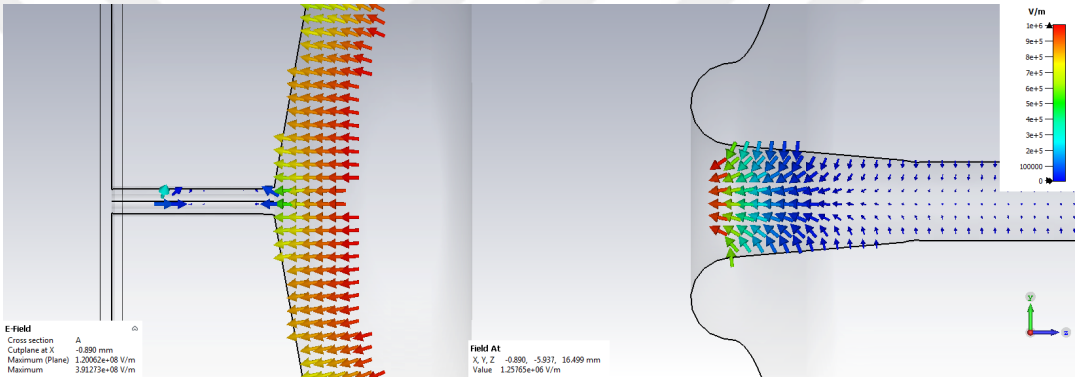



Figure 4.8: Showing of changing electric field in front of the cathode and focusing electrode with 10 focusing angle

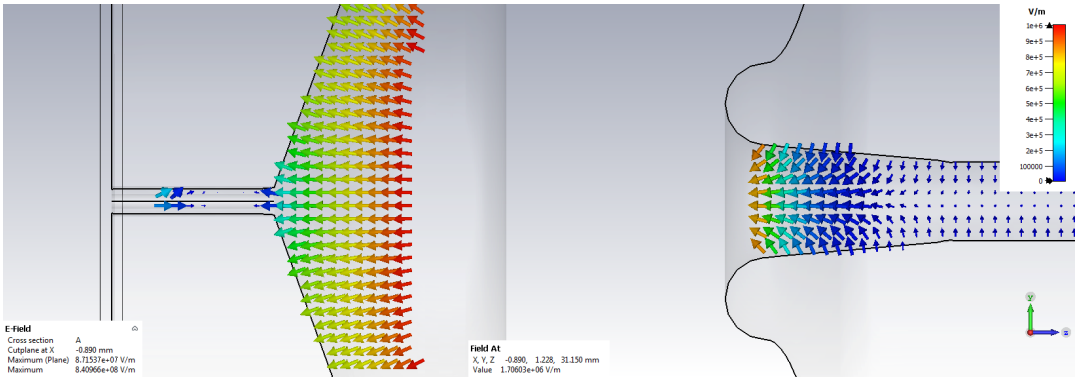



Figure 4.9: Showing of changing electric field in front of the cathode and focusing electrode with 20 focusing angle

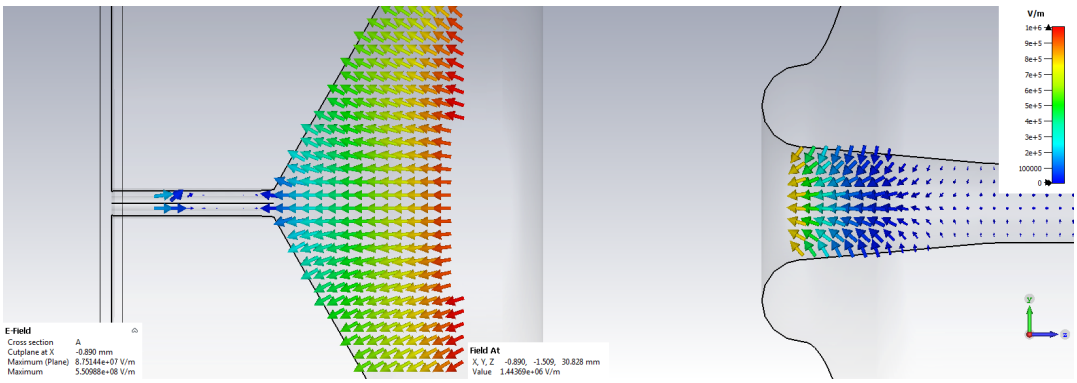



Figure 4.10: Showing of changing electric field in front of the cathode and focusing electrode with 30 focusing angle

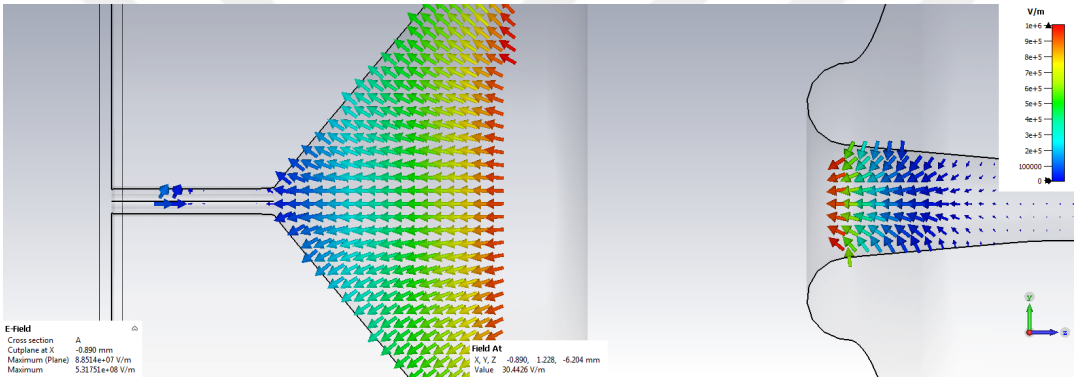



Figure 4.11: Showing of changing electric field in front of the cathode and focusing electrode with 40 focusing angle

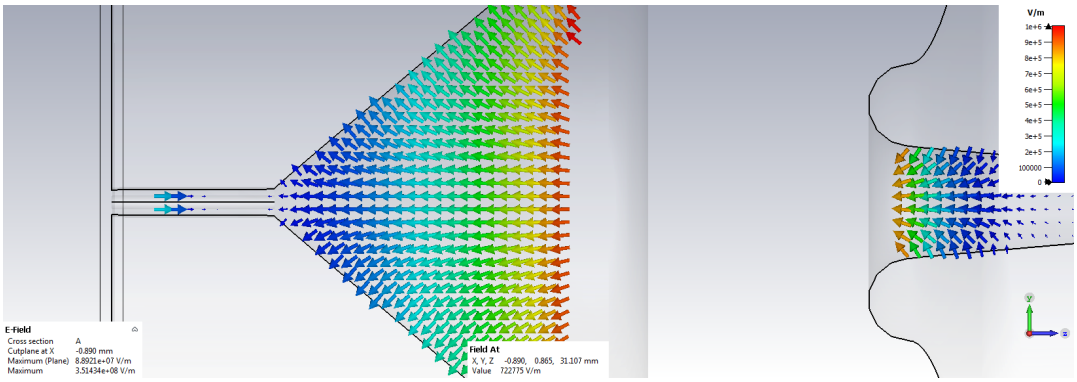



Figure 4.12: Showing of changing electric field in front of the cathode and focusing electrode with 50 focusing angle

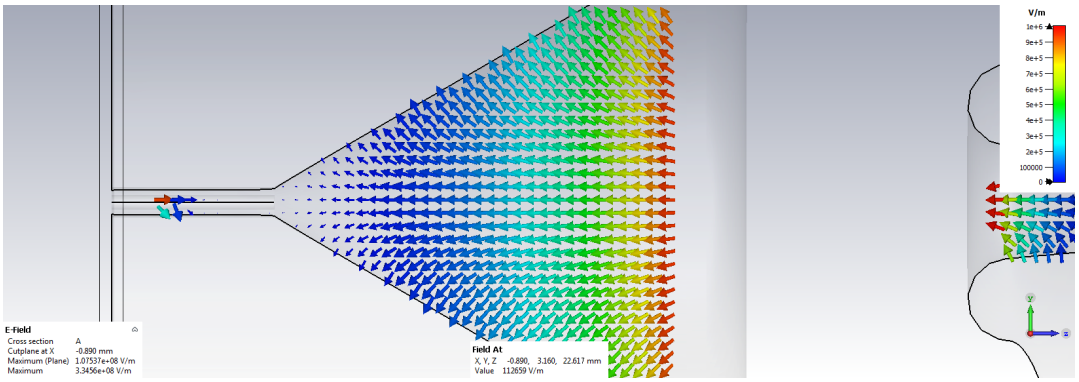



Figure 4.13: Showing of changing electric field in front of the cathode and focusing electrode with 60 focusing angle

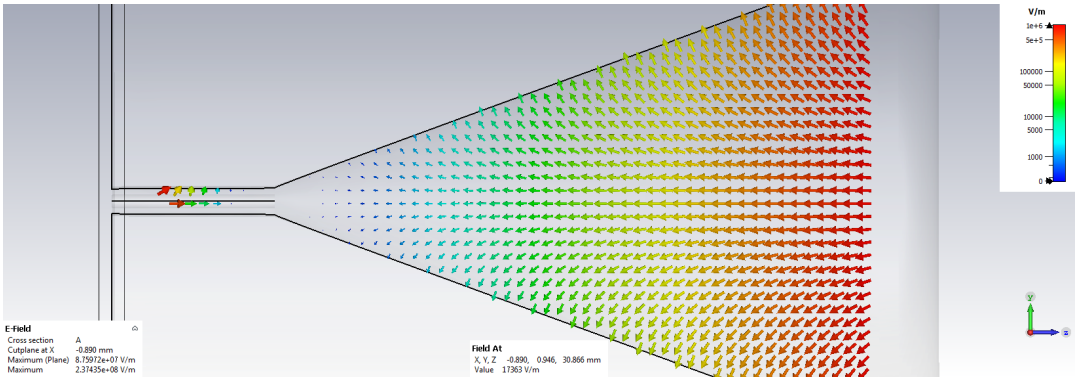



Figure 4.14: Showing of changing electric field in front of the cathode and focusing electrode with 70 focusing angle

Electric fields above 1 MV are not taken into account in the graphs. As can be seen from Figures 4.7 to Figure 4.14, as the angle increases, the magnitude of the electric field in front of the cathode decreases. This reduces the current value.

The electric field strength for some angle values is also shown in Figure 4.15.

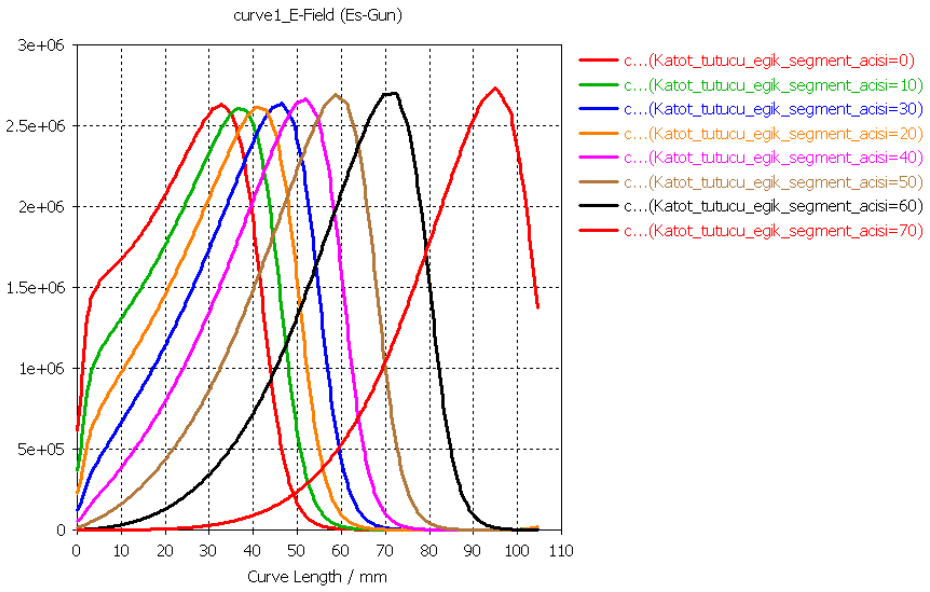



Figure 4.15: 1D results of electric field in front of the cathode and focusing electrode with respect to changing focusing electrode angle

Accordingly, the beam trajectory is shown from Figures 4.16 to Figure 4.24:

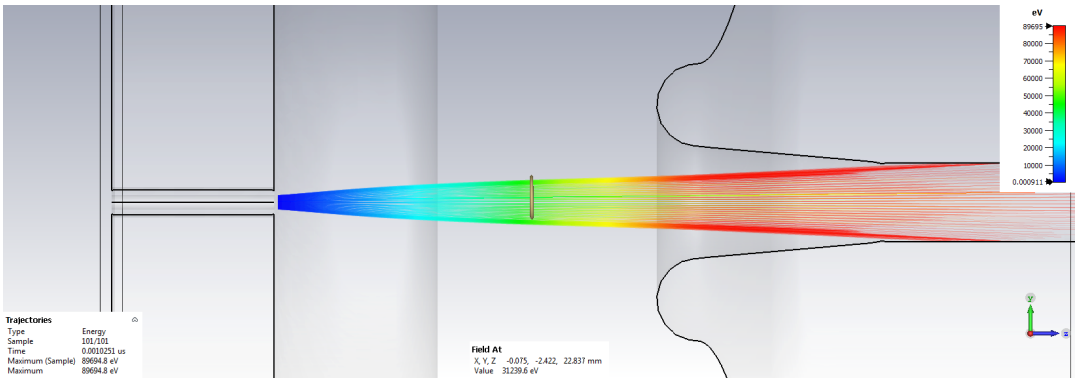



Figure 4.16: Display of Beam Trajectory with 0 focusing angle

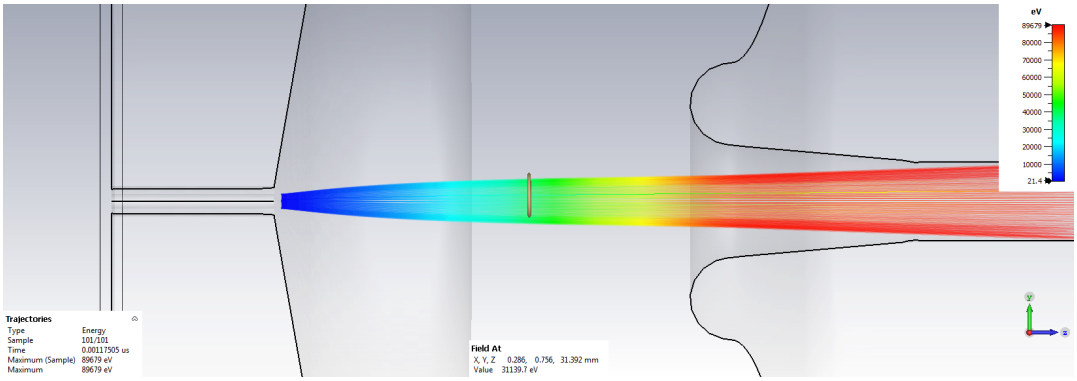



Figure 4.17: Display of beam trajectory with 5 focusing angle

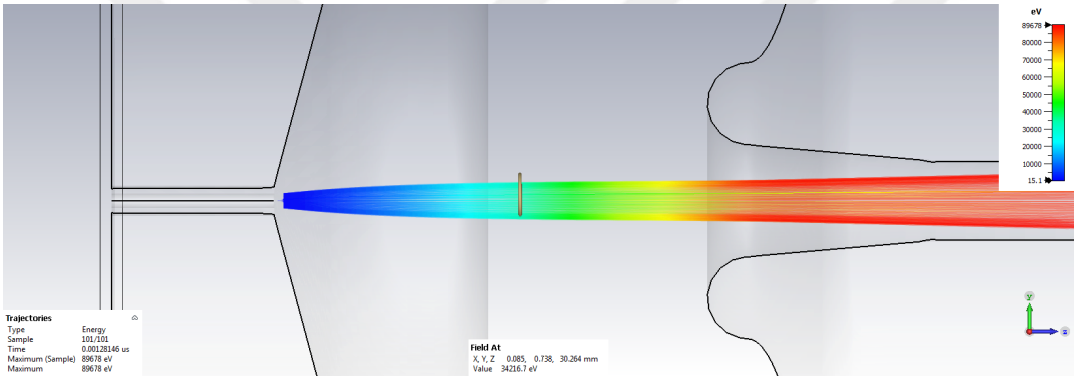



Figure 4.18: Display of beam trajectory with 10 focusing angle

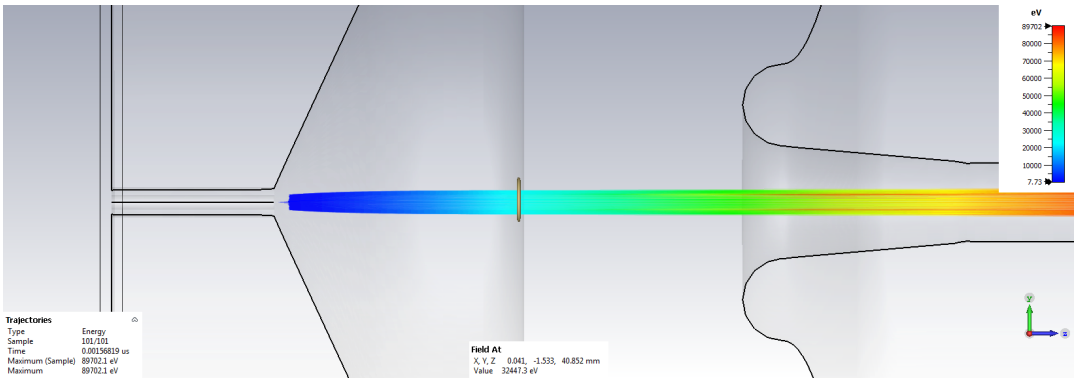



Figure 4.19: Display of beam trajectory with 20 focusing angle

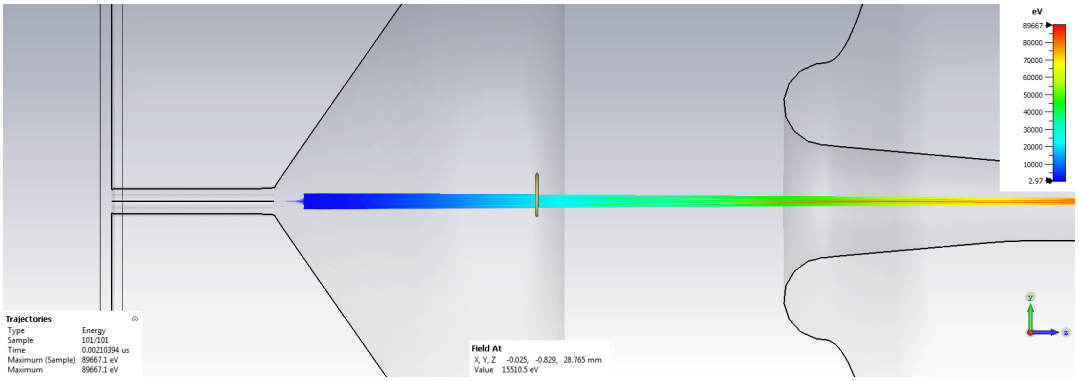



Figure 4.20: Display of beam trajectory with 30 focusing angle

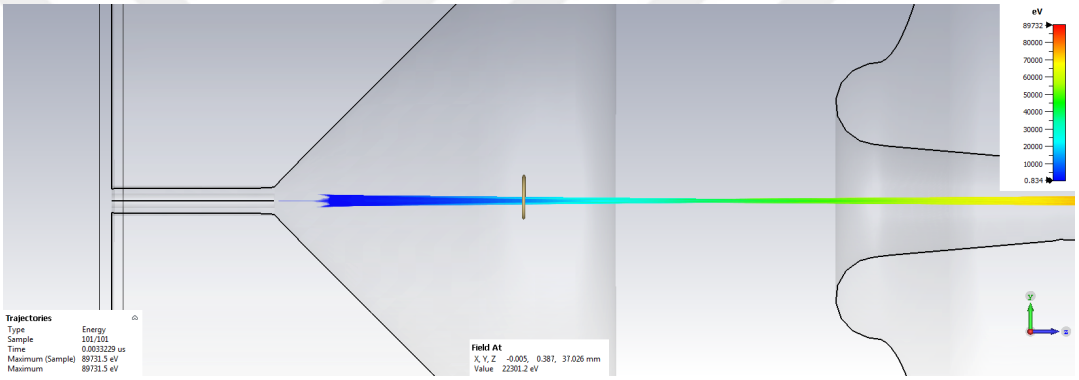



Figure 4.21: Display of beam trajectory with 40 focusing angle

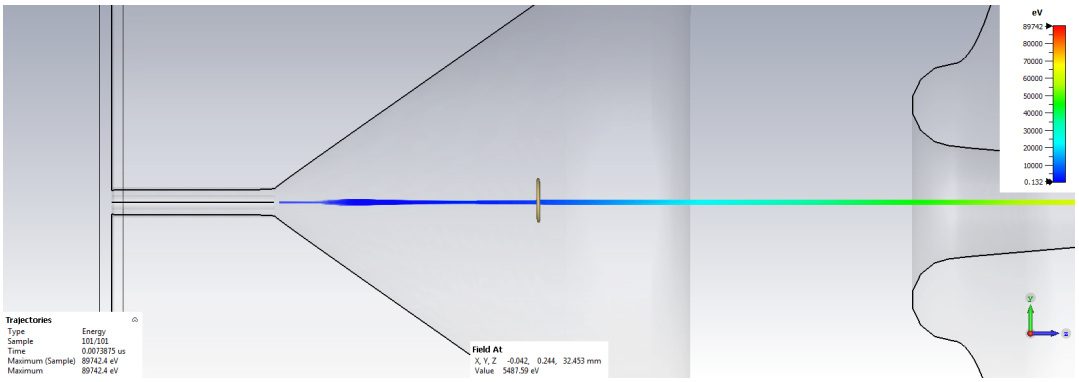



Figure 4.22: Display of beam trajectory with 50 focusing angle

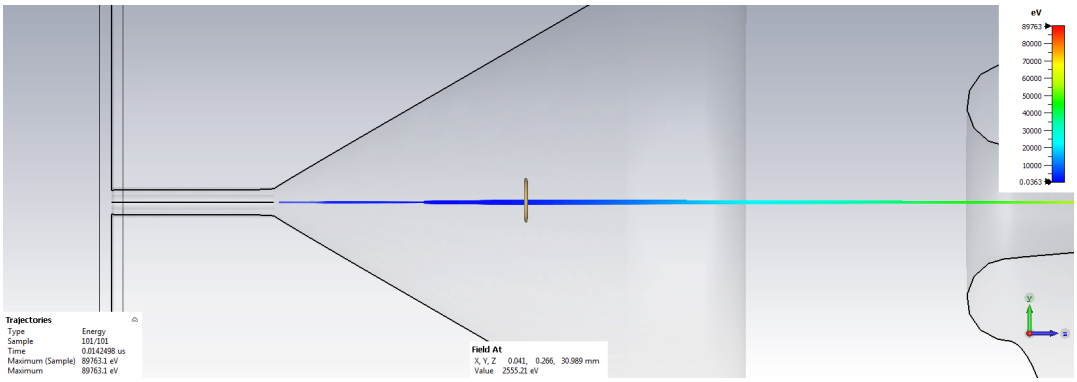



Figure 4.23: Display of beam trajectory with 60 focusing angle

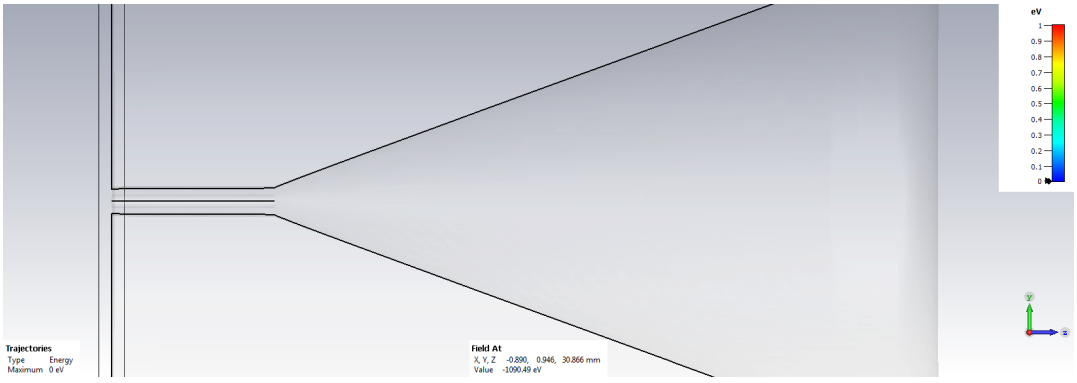



Figure 4.24: Display of beam trajectory with 70 focusing angle

It can be seen from the above figures that as the focusing angle increases, the electric field in front of the cathode becomes insufficient for the electrons to come out. The same result is valid for trajectories as well. As the angle increases, the energy of the beam decreases.

Electric fields have to rise vertically from the surface due to boundary conditions. Therefore, as the angle increases, the electric field formed in front of the cathode supresses the beam by removing fewer electrons. Thus, the current value decreases. This makes emittance value lower, but the magnitude of the electric field in front of the cathode decreases as well. Therefore, the maximum current that can be drawn from the cathode gets smaller. To overcome the exchange between emittance and maximum current in linear geometry, it must be replaced with a curve that has a decreasing tangent. A quadratic parabola is shown to be very close to the optimal shape for the focusing electrode curve [40] which is the second design of this study.

### 4.2.3 Second Design-Quadratic Parabola Focusing and Control Electrode

The second design for the focusing and control electrode is obtained by a quadratic parabola instead of using linear geometry. In linear geometry, as the angle of the focusing electrode increases, the intensity of the field preventing the exit of the beam in front of the cathode increases. This reduces the beam current, however it decreases the emittance value. Such geometry should be designed that the beam should be suppressed without decreasing the beam current and it should decrease the emittance value of the beam. This is possible with the quadratic parabola geometry [40].

The designed quadratic parabola geometry is shown in Figure 4.25:

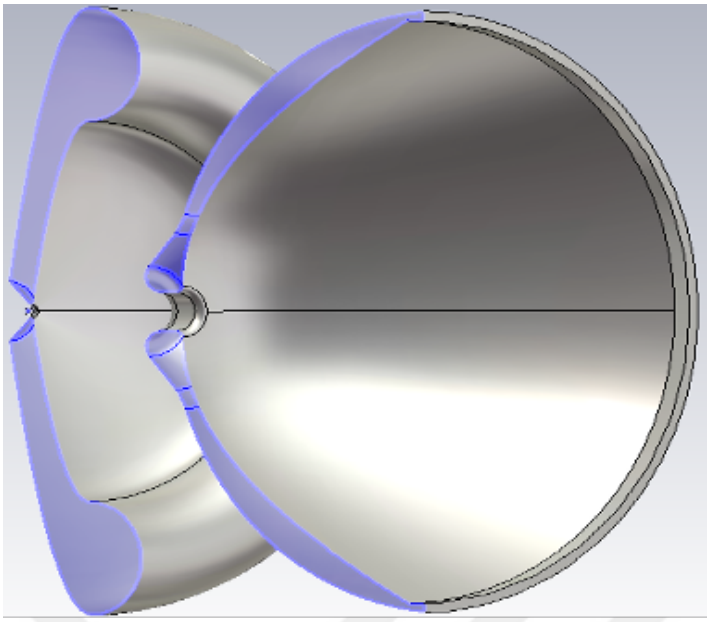


Figure 4.25: Parametrized CST model of focusing and control electrode and anode

Unlike linear geometry, it is replaced with a curve that has a decreasing tangent. A quadratic parabola is shown to be very close to the optimal shape for the focusing electrode curve. With the help of this geometry, a more linear electromagnetic field and a faster acceleration were obtained in the beam path.

In this geometry, as the angle of the focusing electrode increases, thanks to the parabolic geometry, the electric fields formed in front of the cathode do not prevent the beam from coming out. Therefore, the current value does not decrease much. In addition, thanks to the parabolic shape, after the electrons exit the cathode, they encounter a field that prevents them from scattering. Thanks to the decreasing tangent, the beam is prevented from dispersing and its emittance value is reduced in this way.

Although the curve is converted to a parabola, the coefficients of that parabola and the other parameters of the overall electrode shape still must be optimized. In Figure 4.4, $Z_{cath}$ is the cathode distance to electrode aperture, $x_i$ the radius of electrode aperture that can make electrode gap smaller or larger, $r_i$ the electrode tip radius that can be increased or decreased, $\alpha$ the angle that is used for beam current control, $x_o$ the distance of the end of the curve from the z-axis, and $R_o$ the upper electrode tip radius that is used to prevent electric arcing between electrodes.

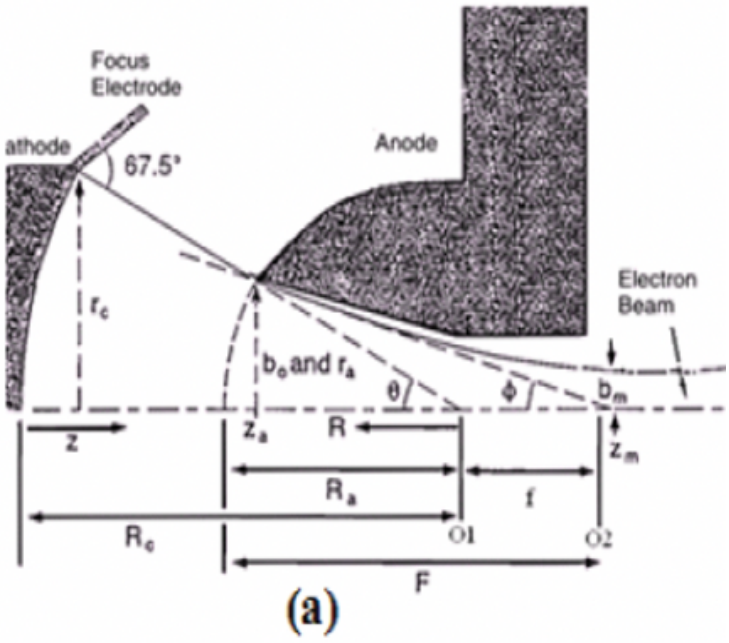



Figure 4.26: Structure of Anode Design [43]

By sweeping the parametric values, the effects of all the mentioned parameters on the design of electron guns are thoroughly investigated in this study, and the findings are given in the following section.

### 4.3 Anode Design

A proper design of anode is another important point for an electron gun. The anode shape must be designed well to fulfill the beam parameters. With the help of the electrostatic field applied by the focusing electrode, the focused electron beam moves towards the anode. After this focus, electrons begin to dissipate again before reaching the anode. After determining the geometry of the focusing and control electrode, the anode geometry must be determined properly in order for the beam to pass through the anode hole without spoiling and falling apart. In order to that, a mathematical modeling and analytical operations should be done well. In Figure 4.26, the design criteria of the anode are shown:

$R_c$ is the radius of the focusing electrode, $R_a$ is the radius of the anode circle, $R$ is the

distance of the anode-cathode centripetal circles. For anode geometry, the value of the angles ($\theta$) is very important at the design stage. These angles play a critical role in the transition from region 2 to region 3 which is shown in Figure 4.3 and allow it to continue on its way without any loss in the beam. The design of the anode geometry is made using Equation 4.1 below. Generally, an anode shape is a conical rose shape with $1.2 - 1.5 \quad b_0$ radius which is the hole radius of the anode shown in Figure 4.26 [43]. In the simulation, this process runs continuously from the second zone to the third zone.

$$\tan\theta = 0.174\sqrt{K}\left(\sqrt{ln\frac{b_0}{b_m}}\right) \tag{4.1}$$

where K is the perveance of the beam, $b_0$ is the radius of the anode aperture and $b_m$ is the beam size.

The angle formula required for the third region is as in Equation 4.1. After the parameters such as required perveance, beam size, etc. are set at the design stage, these values can be calculated numerically by implementing them into the simulation program and angle values can be found for optimum geometry.

## 4.4 Parameter Sweep Results

The proposed fully parametric model is implemented in the CST multi-physics simulation tool as given in Figure 4.25 with an illustrated cross-section.

The parameters of the focusing and control electrode are swept for a range of values in order to find their effects on the current and emittance of the beam. Firstly, the effects of $Z_{cath}$ parameter with changing electrode aperture radius on the beam current and emittance are investigated. The results regarding emittance and beam current are shown respectively in Figure 4.27 and 4.28. As can be seen in these figures, when the cathode distance to electrode aperture is increased, the beam current and emittance are decreased for every electrode aperture radius.

Table 4.2 shows emittance and current values with respect to the radius of the elec-

trode aperture and cathode distance to the electrode aperture.

Table 4.2: Emittance and Current Values By Changing of Cathode Distance to Electrode Aperture ($Z_{cath}$)

| $x_i$ **the radius of electrode aperture (mm)** | **Cathode Distance to Electrode Aperture ($Z_{cath}$) (mm)** | **Current (mA)** | **Emittance (mm*mrad)** |
|---|---|---|---|
| 0.2 | -0.2 | 50.36 | 0.606 |
| 0.2 | -0.3 | 40.57 | 0.473 |
| 0.2 | -0.4 | 32.6 | 0.364 |
| 0.2 | -0.5 | 26.2 | 0.274 |
| 0.25 | -0.2 | 48.96 | 1.734 |
| 0.25 | -0.3 | 48.59 | 0.943 |
| 0.25 | -0.4 | 49.92 | 0.629 |
| 0.25 | -0.5 | 42.12 | 0.4975 |
| 0.35 | -0.2 | 103.8 | 1.1801 |
| 0.35 | -0.3 | 92.2 | 1.1450 |
| 0.35 | -0.4 | 83.6 | 1.116 |
| 0.35 | -0.5 | 75.2 | 1.062 |
| 0.4 | -0.2 | 124.2 | 1.156 |
| 0.4 | -0.3 | 112.4 | 1.146 |
| 0.4 | -0.4 | 101.7 | 1.128 |
| 0.4 | -0.5 | 90.3 | 0.983 |

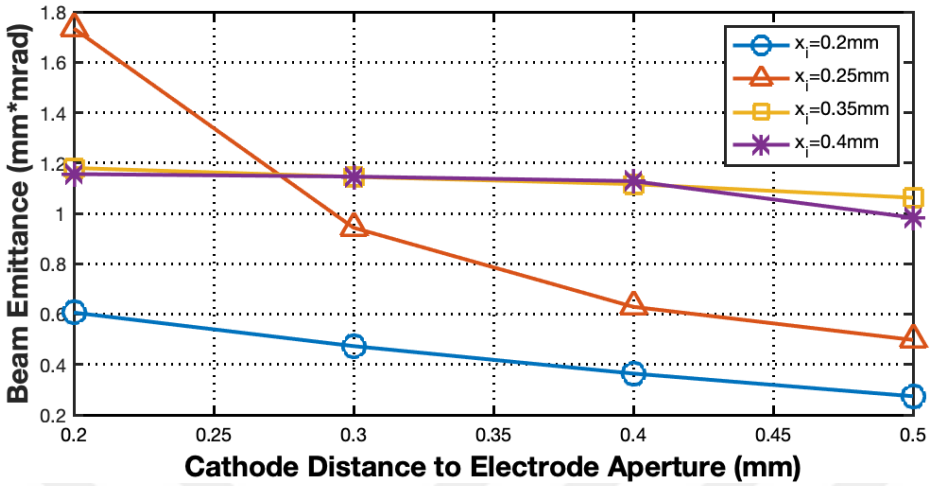



Figure 4.27: Beam current versus cathode distance to electrode aperture distance

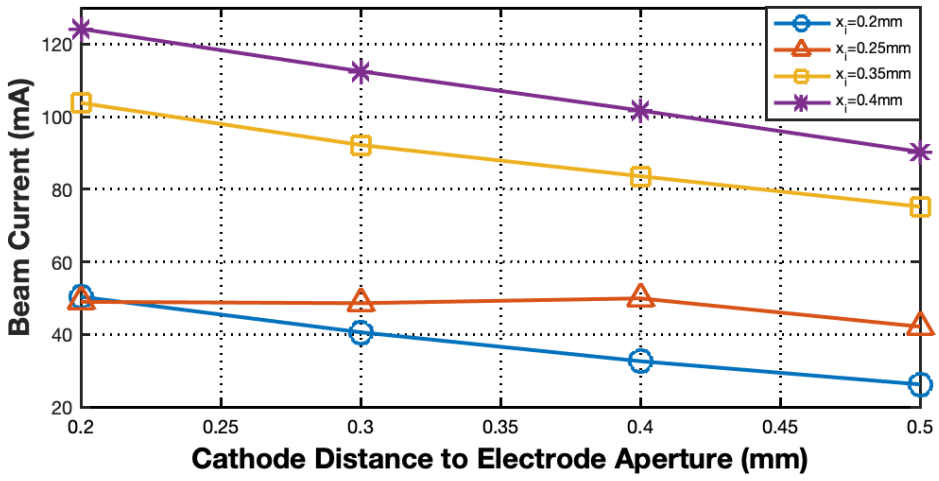



Figure 4.28: Beam current versus cathode distance to electrode aperture distance

Furthermore, the effects of $r_i$ parameter on beam current and emittance are investigated and results are shown in Figure 4.29 and Figure 4.30. As it can be seen from these plots increasing electrode tip radius causes larger emittance and larger beam current for various angles.

Table 4.3 shows emittance and current values with respect to the focusing electrode angle and the electrode tip radius.

Table 4.3: Emittance and Current Values By Changing of Electrode Tip Radius $r_i$

| $\alpha$ **(rad) the angle that is used for beam current control** | **The electrode tip radius** $r_i$ **(mm)** | **Current (mA)** | **Emittance (mm*mrad)** |
|---|---|---|---|
| 0.33 | 0.2 | 78.8 | 2.037 |
| 0.33 | 0.3 | 101.8 | 2.905 |
| 0.33 | 0.4 | 126.7 | 3.547 |
| 0.43 | 0.2 | 67.2 | 1.549 |
| 0.43 | 0.3 | 84.7 | 2.310 |
| 0.43 | 0.4 | 103 | 2.924 |
| 0.53 | 0.2 | 59.4 | 1.205 |
| 0.53 | 0.3 | 73 | 1.794 |
| 0.53 | 0.4 | 87.7 | 2.414 |
| 0.63 | 0.2 | 53.7 | 0.973 |
| 0.63 | 0.3 | 64.4 | 1.441 |
| 0.63 | 0.4 | 76.7 | 1.947 |

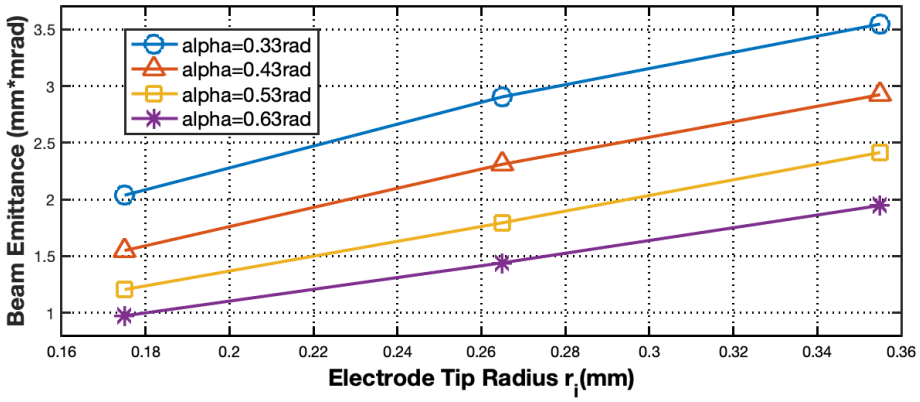



Figure 4.29: Beam emittance versus electrode tip radius result

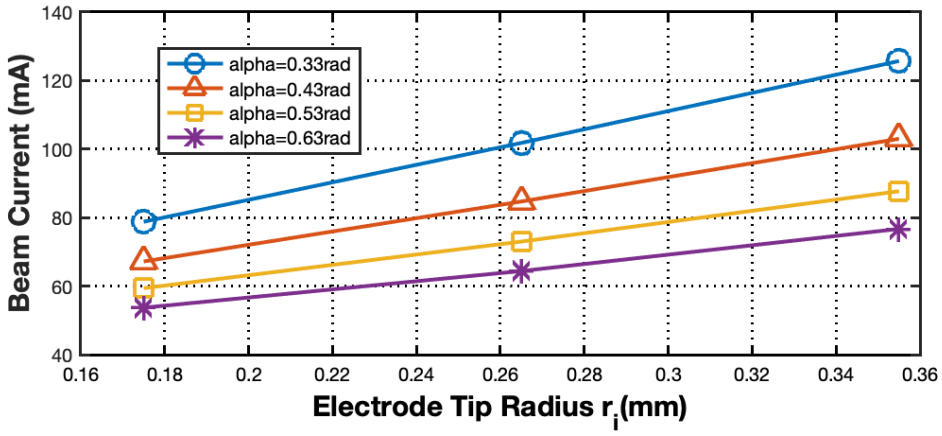



Figure 4.30: Beam current versus electrode tip radius result

Finally, the effects of the $x_o$ parameter on the beam current and emittance are investigated. Corresponding results for beam emittance and beam current are shown in Figure 4.31 and Figure 4.32, respectively.

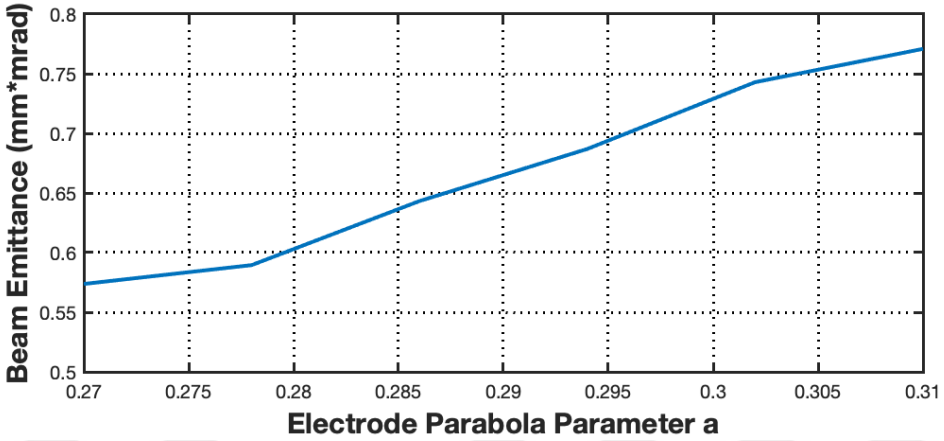



Figure 4.31: Beam emittance versus electrode parabola parameter a

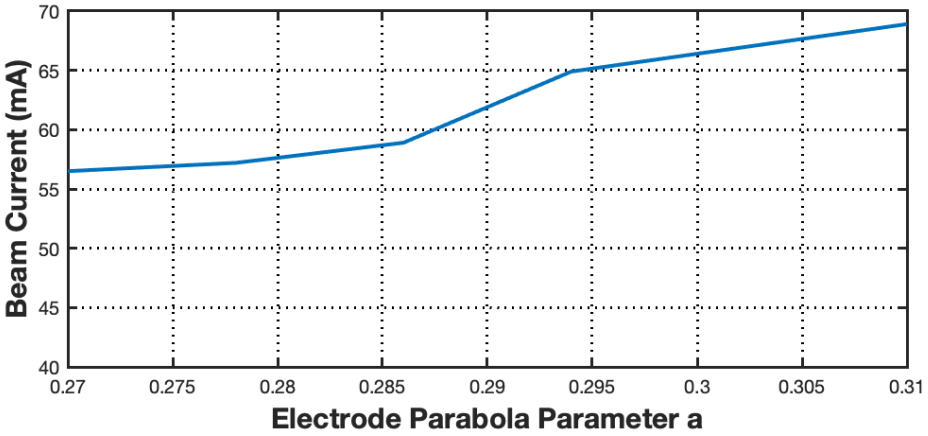



Figure 4.32: Beam current versus electrode parabola parameter a

The distance of the surface curve endpoint, point A in Figure 4.4, from the x-axis can be changed by varying the curve equation parameter a. Therefore, by increasing a value the beam current and emittance are increased. Increasing a means that the parabola bends itself towards the x-axis. It leads to an increase in field strength but decreases the focusing effect of fields. Hence, it increases current and emittance at the same time.

The effects of these parameters are summarized in Table 4.4.

Table 4.4: Effects of Parameters on Beam Current and Beam Emittance

| **Parameter** | **Effect on Beam Current** | **Effect on Beam Emittance** |
|---|---|---|
| $Z_{cath}$ | Inversely Proportional | Inversely Proportional |
| $r_i$ | Proportional | Proportional |
| $a$ | Proportional | Proportional |

In light of the above results, it is understood how and which parameter should be set to obtain the required high current and low emittance value.

Although successful results are obtained, the desired electric field in front of the cathode is still not uniform. According to the above parameter sweep results, the electric field formed in front of the cathode is generally as in Figure 4.33.

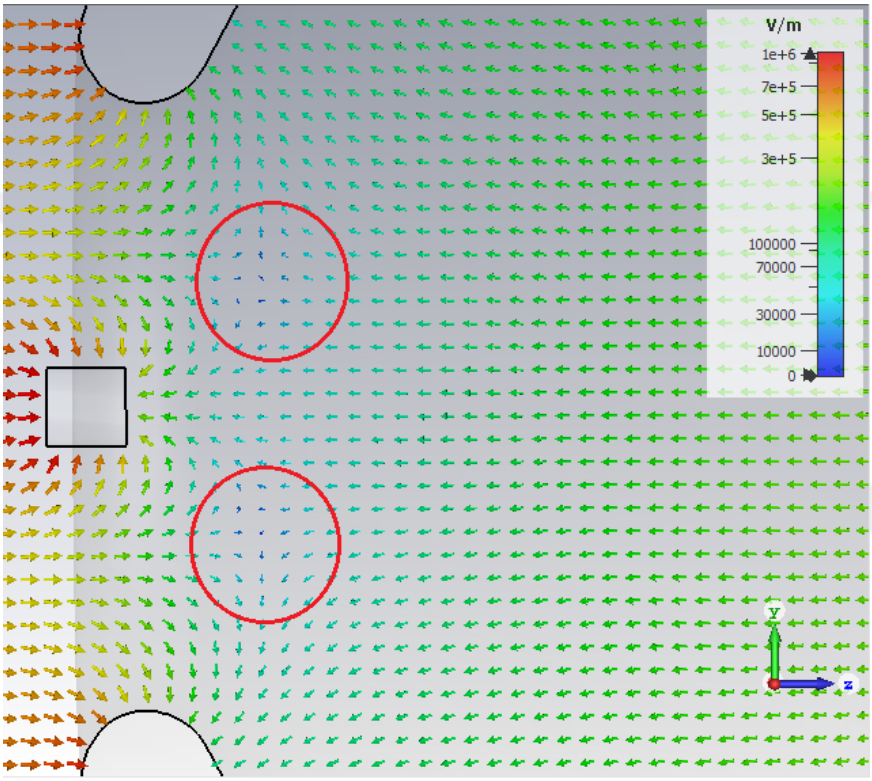



Figure 4.33: Displaying Non-uniform electric field in front of the cathode in parametrized CST model

Circles highlighted in red have a distorting effect on the electron beam in front of the cathode. This affects current and emittance value negatively. As mentioned in the pre-design work section, the expected electric field should be flat and uniform in front of the cathode. This will increase the current value and decrease the emittance value. An Optimization is needed to find this uniform electric field. Since CST makes a 3D solution, an optimization to be done here will take a lot of time. Therefore, parabolic geometry must be transferred to 2D. Thus, the desired electric field and potential curves can be reached much faster. Transferring this geometry to 2D and the optimization part will be done in MATLAB and will be discussed in Chapter 5.

## 4.5 Beam Current Regulation

The proposed gun system is able to regulate the current by changing the voltage of the focusing and control electrode. The maximum current is drawn from the cathode in the case that the electrode and the cathode are in the same potential. However, as the voltage of the electrode is increased with respect to the cathode, the beam current starts to decrease. After some point, the beam current is totally ceased. The variations in the beam current with respect to changing electrode voltages are shown in Figure 4.34. It should be noted that the regulated current values show a slightly exponential decay with linear voltage change and the current has totally vanished around 800V.

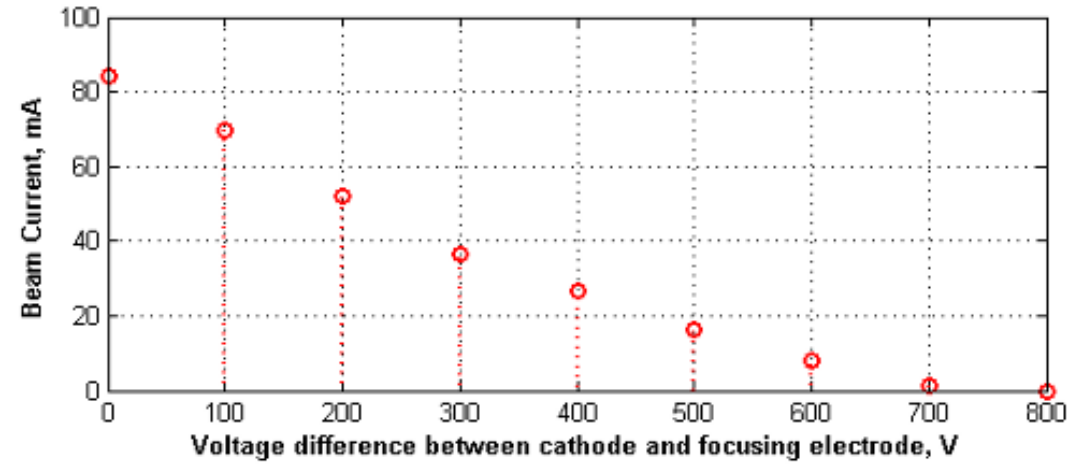



Figure 4.34: Beam current regulation results in CST

# CHAPTER 5

# 2D ELECTRIC FIELD OPTIMIZATION AND DESIGN OF ELECTRON GUN IN MATLAB

## 5.1 Optimized Field Shapes and Analytical Calculations of Potentials

### 5.1.1 What Should Be The Shape of Electric Field and Equipotential Lines?

In the space charge fields section in Chapter 3, the force and electric field formulas that will affect an electron were derived and their figures were shown. Also, as mentioned in the pre-design work, the electric field strength generated in the transverse direction must be very low for electrons to have high current and low emittance values. On the other hand, the electric field strength in the longitudinal direction is expected to be high. The reason for this is to prevent their dispersion and to increase the beam current by increasing the electron density. The expected electric field shape in front of the cathode and for an electron was shown in Figure 3.17.

The lines where the electrical potential is constant along the line are called equipotential lines. A simple representation of equipotential lines is given in Figure 5.1.

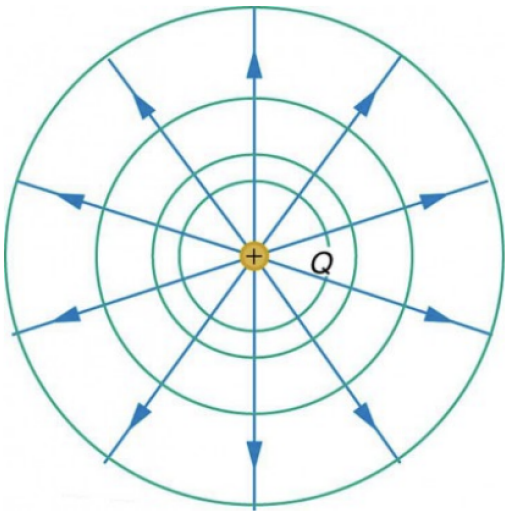



Figure 5.1: View of electric field lines (blue) and equipotential lines (green) [44]

The important point is that potential lines are always perpendicular to electric field lines. No work is done to move any charge along the potential lines because $\Delta V = 0$. Therefore, the work is $W = -q \times \Delta V = 0$ If the force is perpendicular to the motion, the work done on a charge is zero. The force has the same direction as the electric field. Therefore, the motion along an equipotential line must be perpendicular to the electric field. A more accurate expression, the work - electric field relationship is given below:

$$W = Fdcos\theta = qEdcos\theta = 0 \tag{5.1}$$

In Equation 5.1, E and F are shown as magnitudes. The value of the cosine must be 90 degrees for the work done to be zero. In other words, the motion along an equipotential line must be perpendicular to the electric field[44].

The focusing electrode and anode are designed considering the above criteria. The potential lines are expected to be straight in front of the cathode. Since a straight potential line in front of the cathode will create an electric field in the same direction through the beam, the current value will increase. Since there is no electric field component in the transverse direction, the beam will not be dispersed. This will lower the emittance value as well. In addition, the potential curves are expected to follow the designed anode and focusing electrode shape. The importance of this figure is

explained in Chapter 4.

The electric field and potential lines should be calculated analytically for the designed geometry. The values of a static system with certain boundary conditions can be found analytically with the help of the Laplace equation. In Section 5.1.2. finding these values with the help of Laplace will be explained.

### 5.1.2 Numerical Solution for Laplace's Equation Using Finite Difference Method

The Laplace equation is a partial differential equation. The solutions of the Laplace equation are important in many fields of science, such as electromagnetism, astronomy, and fluid dynamics because the solutions specifically explain the behavior of the fluid potential and the electric and gravitational potential. In this study, the potentials between two geometries with certain boundary conditions will be calculated using the finite difference method[45].

The main purpose of static electricity is to find the electric field of a given static charge distribution. In electrostatics, the curl of electric field is zero $\vec{\nabla} \times \vec{E} = 0$. The electric field can be found with the help of Coulomb's law or it can be calculated by taking the gradient of scalar potential:

$$\vec{E} = -\vec{\nabla}\Phi \tag{5.2}$$

From the Maxwell equation divergence of electric field is $\vec{\nabla}.\vec{E} = \frac{-\rho^{'}}{\epsilon_0}$, where $\rho^{'}$ is the charge density, and $\epsilon_0$ is the permittivity of the free space. Combining Equation 5.2 with the divergence of the electric field, it will give:

$$\nabla^2\Phi = \frac{-\rho^{'}}{\epsilon_0} \tag{5.3}$$

Equation 5.3 is called Poisson's equation. If there is no charge density, the right-hand side of the Equation 5.3 will be zero and this equation is known as Laplace's equation:

$$\nabla^2\Phi = 0 \tag{5.4}$$

By solving Laplace's equation for certain boundary conditions on the electric field will give a unique solution for the electric field.

In order to solve Laplace's equation for special geometries, there are specific numerical methods such as finite difference methods, finite elements methods, etc. In this study, finite difference methods are used in order to obtain Laplace's equation solutions[46].

The finite-difference technique converts the differential equations into finite difference equations. This finite difference approach is in algebraic form. In these algebraic equations, it depends on the values at some neighboring points in the solution region. Therefore, the finite difference solution is basically done in the following three steps [45]:

- The solution zone is divided into a grid of nodal points.
- The finite-difference equivalent of the solved differential equation is obtained by an approximation. This equation is in terms of dependent variables at a point.
- The differential equation is solved using the specified boundary or initial conditions.

In Figure 5.2, grids used in the most common 2-D problems are shown:

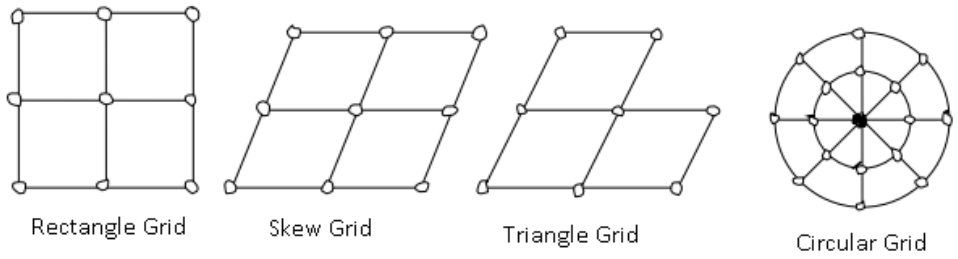



Figure 5.2: Using most common grid types

In this thesis, potential lines depend on two variables (x, y). Therefore, this is an 2-D

condition. In 2-D case Laplace's equation becomes:

$$\nabla^2\Phi = \frac{\partial^2\Phi(x,y)}{\partial x^2} + \frac{\partial^2\Phi(x,y)}{\partial y^2} = 0 \tag{5.5}$$

The electric potential at the boundaries is a fixed value. Thus, the Dirichlet boundary condition plays a role in this study for solving Laplace's equation [47].

Dividing the area of interest (x,y) into a grid with equal spacing h shown in Figure 5.3.

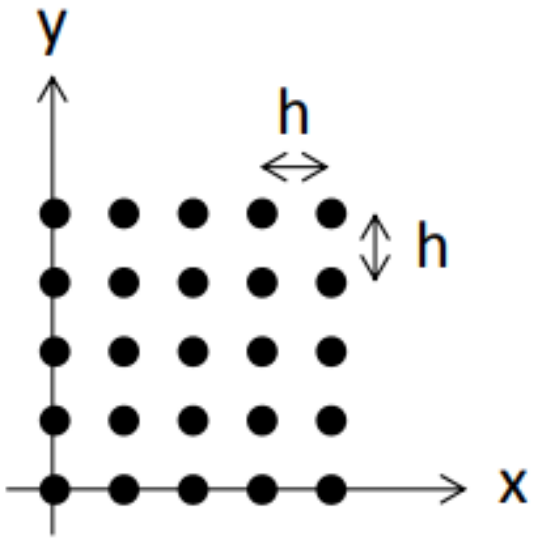



Figure 5.3: View of grids and their gap distance [48]

The discrete form of the Laplace equation gives an approximate solution for the partial derivatives at every grid point (i,j). [47] Their equations are shown below:

$$\left(\frac{\partial^2\Phi(x,y)}{\partial x^2}\right)_{(i,j)} \approx \frac{\Phi_{i+1,j} - 2\Phi_{i,j} + \Phi_{i-1,j}}{h^2} \tag{5.6}$$

$$\left(\frac{\partial^2\Phi(x,y)}{\partial y^2}\right)_{(i,j)} \approx \frac{\Phi_{i,j+1} - 2\Phi_{i,j} + \Phi_{i,j-1}}{h^2} \tag{5.7}$$

Then, by inserting Equations 5.6 and 5.7 into 5.5, Laplace equation and discretized

form is:

$$\left(\frac{\Phi_{i+1,j} - 2\Phi_{i,j} + \Phi_{i-1,j}}{h^2}\right) + \left(\frac{\Phi_{i,j+1} - 2\Phi_{i,j} + \Phi_{i,j-1}}{h^2}\right) \approx 0 \tag{5.8}$$

Thus, $\Phi_{i,j}$ is as follows:

$$\Phi_{i,j} \approx \frac{1}{4}[\Phi_{i+1,j} + \Phi_{i-1,j} + \Phi_{i,j+1} + \Phi_{i,j-1}] \tag{5.9}$$

Illustration of the above equation is shown in Figure 5.4:

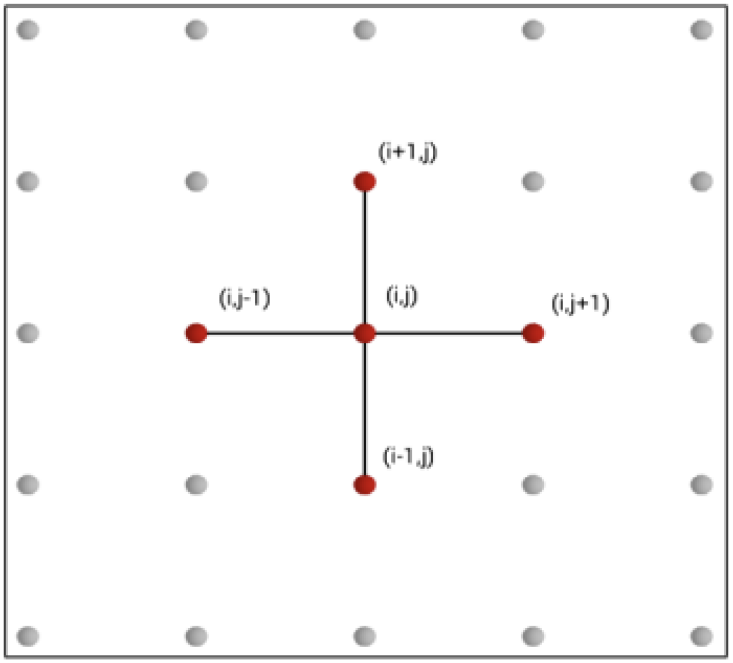



Figure 5.4: The solution of Laplace's Equation on grids [46]

Thanks to this estimation, the potential value of the point $\Phi(i, j)$ depends on the potential values of the four closest points around it as shown in Figure 5.4. In order to calculate $\Phi(i, j)$ numerically, there are two basic methods:

1. Gauss Elimination Matrix Method

It is a method for solving the set of linear equations in the form [A][B] = [C], where [A], [B] and [C] are the matrices. A linear equation will be obtained with different potential values for each grid point. By writing them in matrix form, they can be

solved by the Gauss elimination method. With this method, 2 or more linear equations can be solved simultaneously. However, due to many linear equations, the solving procedure is very slow. Therefore, this method is not preferred for this study[49].

2. Jacobi Iteration Method

In the Jacobi iteration method, an estimated initial value is given to the unknown grid points. Using initial or boundary condition (i.e. $x_1^0 = 0, x_2^0 = 0, ..., x_n^0 = 0$) $x_1^1, x_2^1, ..., x_n^1$ are calculated. Then iteration continues for the next grid points. At the end of each iteration, it is checked whether the error tolerance has been reached as in Equation 5.10. If all the estimations are below this error level, the iteration is stopped.

For every $x_i$ value :

$$|x_i^{k+1} - x_i^k| < \epsilon_{ref} \quad as \quad i = 1, 2, ..., n \tag{5.10}$$

In this study, the Jacobi iteration method is used to calculate all grid points potential. This method is more efficient, faster, and gives better precision with respect to the Gauss elimination method[49].

## 5.2 Obtaining Desired Geometry for Proper Potential Lines and Implementing It in Matlab

In Chapter 4, two different geometries are mentioned. One of them is that the focusing electrode is a linear type. The other is that the same electrode is designed as a parabolic. Studies on CST have shown that the parabolic structure gives better results close to the required design. However, optimizing this geometry with the required field and equipotential lines will take a lot of time in CST because CST makes a 3D solution, so the simulation takes a long time. The geometry designed in this study can be made 2D since it has an axially symmetrical structure. In the parameters specified in Figure 4.4, the optimum E-field and potential lines are found very quickly compared to CST by sweeping these parameters with the geometry prepared on MATLAB. Its results are shown in Section 5.3. The main purpose of MATLAB is to achieve the geometry that meets the requirements by making the optimization

quickly. The structure of the figure drawn on MATLAB is shown in Figure 5.5.

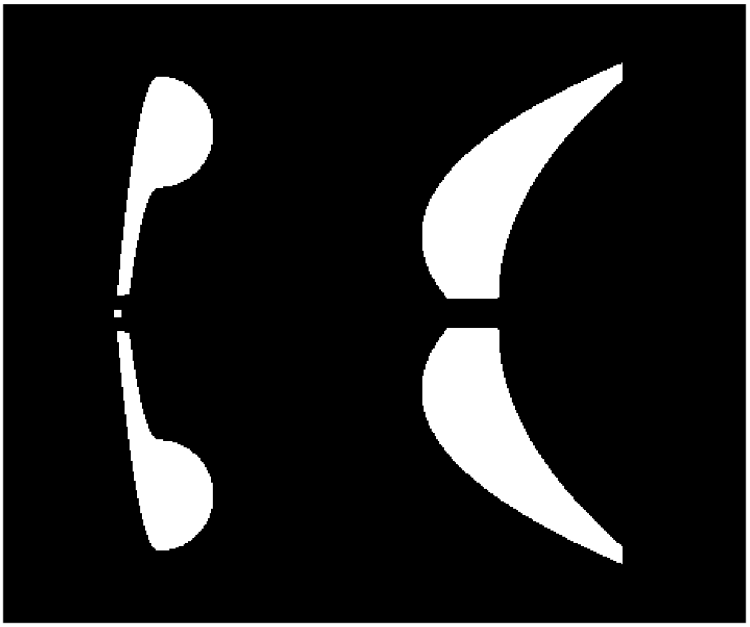


Figure 5.5: Designed geometry in MATLAB

Analytical functions and parameters of the designed geometry are implemented in MATLAB. In addition, the potential equation solved with MATLAB by using the Jacobi Iteration Method. The most suitable electric field and potential lines are found by changing the parameters related to this geometry. It is verified that the requirements are met by applying this optimal result on the CST.

### 5.3 Comparison of MATLAB Results with CST

In Section 5.1.1., it is explained how an electric field is expected in front of the cathode. In addition, what will be the structure of the potential lines is mentioned. The most suitable geometry based on these is shown in Figure 5.5. By solving the Laplace equation using the method described in Section 5.1.2, the electric field and potential lines are found for both -60 kV and -100 kV. The voltage of the focusing electrode is

-60, -100 kV and the anode is at ground voltage.

For -60 kV, the potential line result of MATLAB and CST are given below Figure 5.6 and Figure 5.7 respectively.

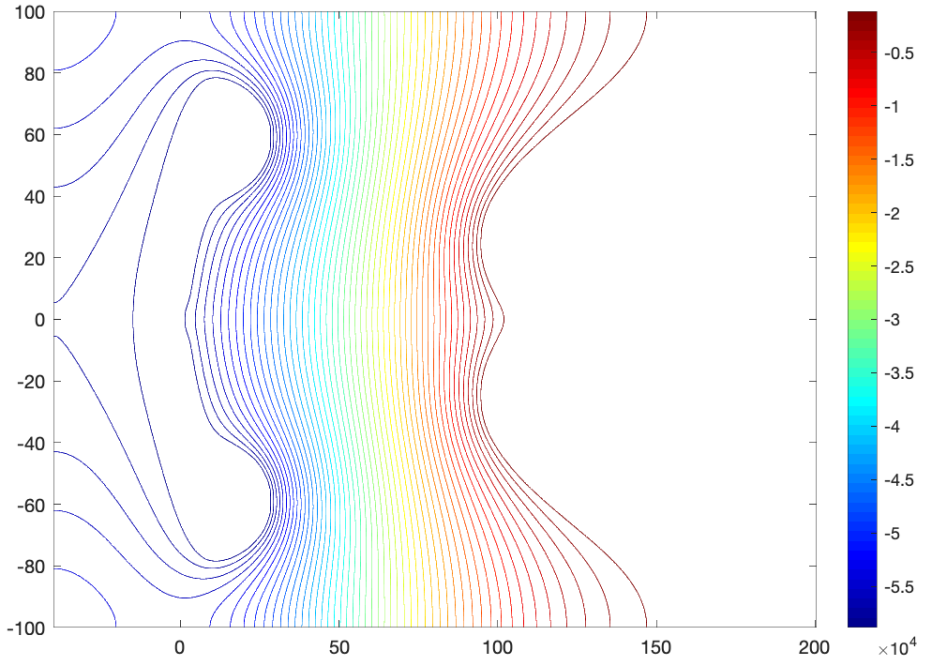



Figure 5.6: The potential curves for -60 kV from MATLAB

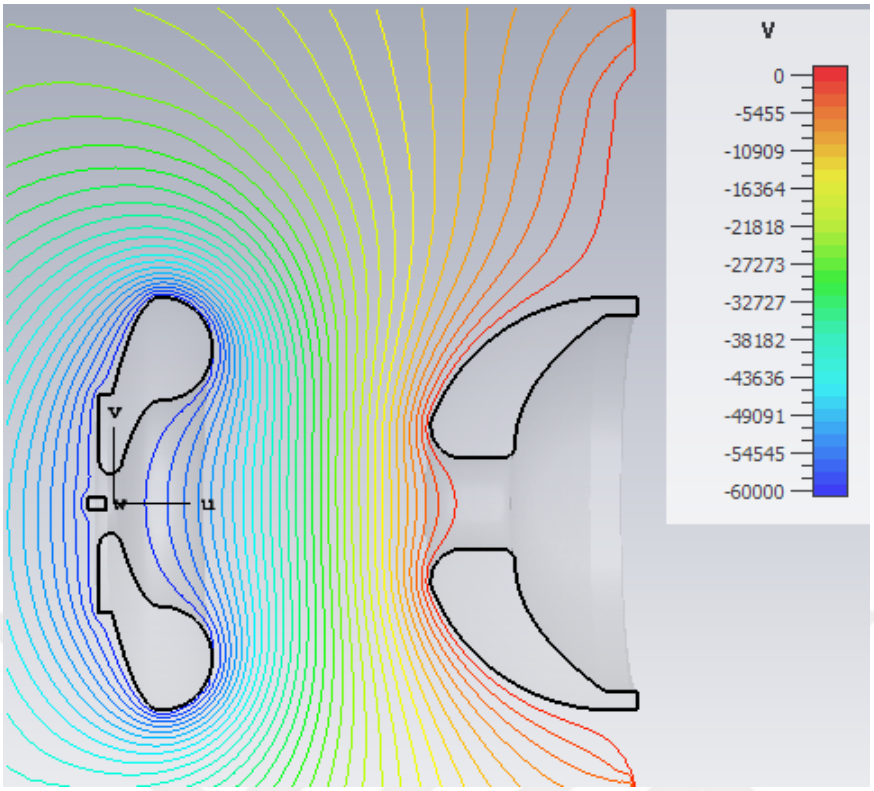



Figure 5.7: The potential curves for -60KV from CST

For -60 kV, the electric field in front of the cathode estimated by using MATLAB and CST are given Figure 5.8 and Figure 5.9 respectively.

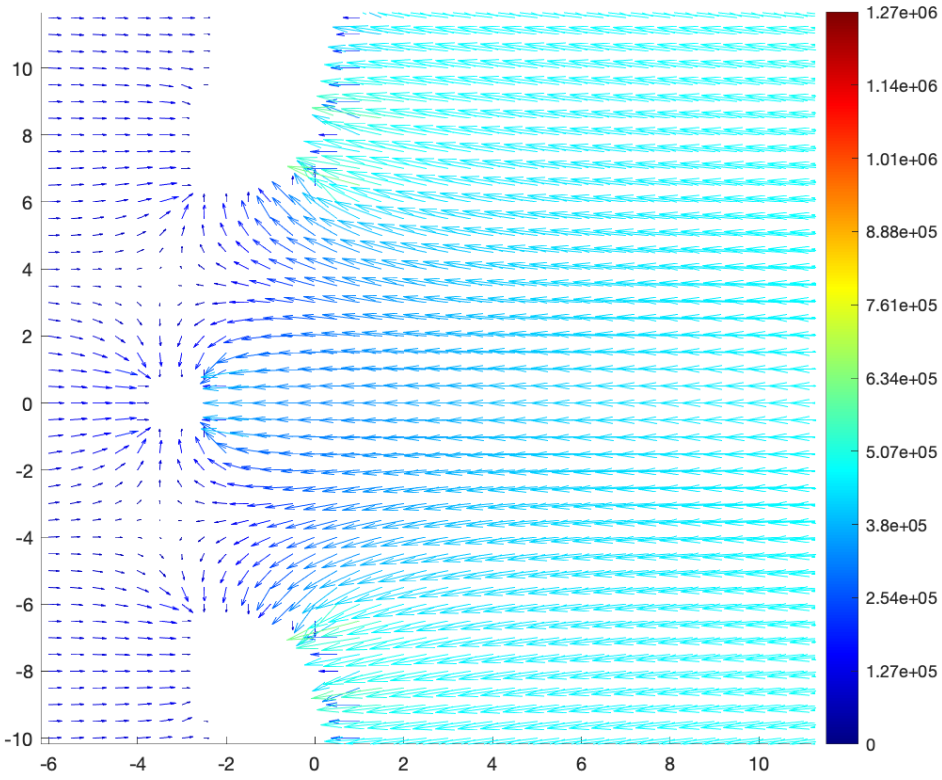



Figure 5.8: Electric Field in front of the Cathode for -60 kV from MATLAB

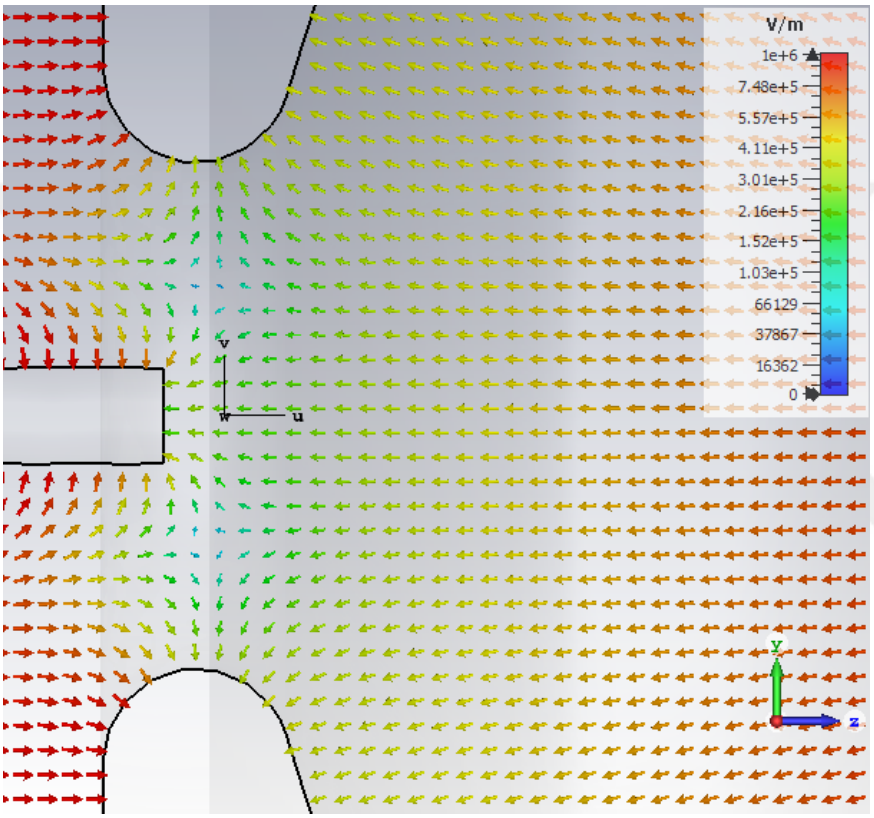



Figure 5.9: Electric Field in front of the Cathode for -60 kV from CST

For -100 kV, the potential curves from MATLAB and CST are given in Figure 5.10 and Figure 5.11 respectively.

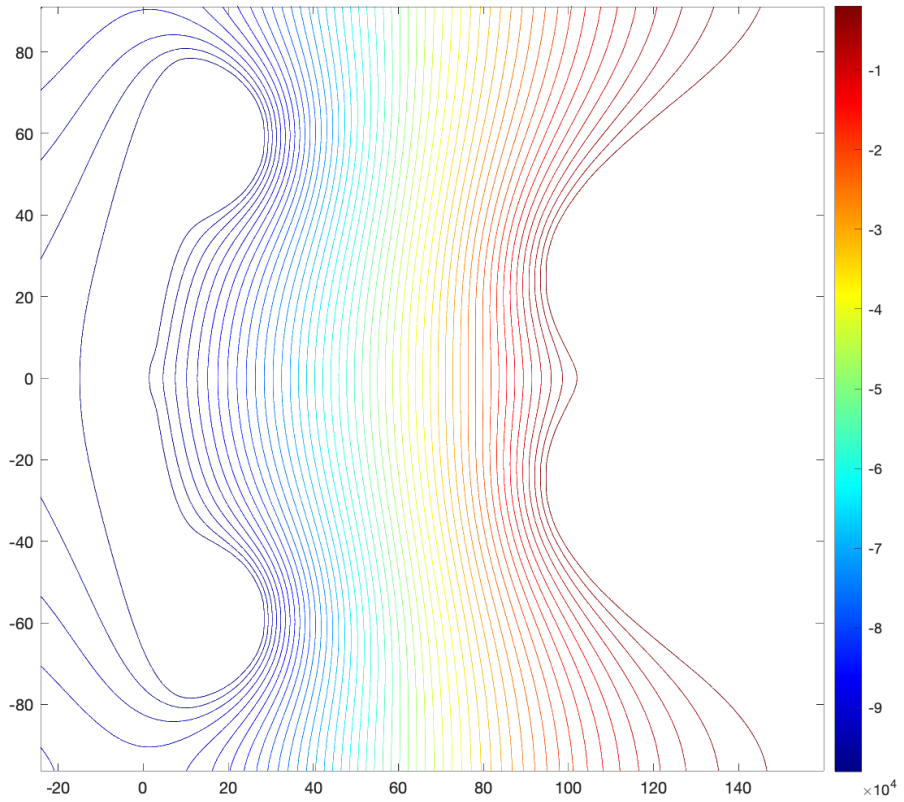



Figure 5.10: Potential curves for -100 kV from MATLAB

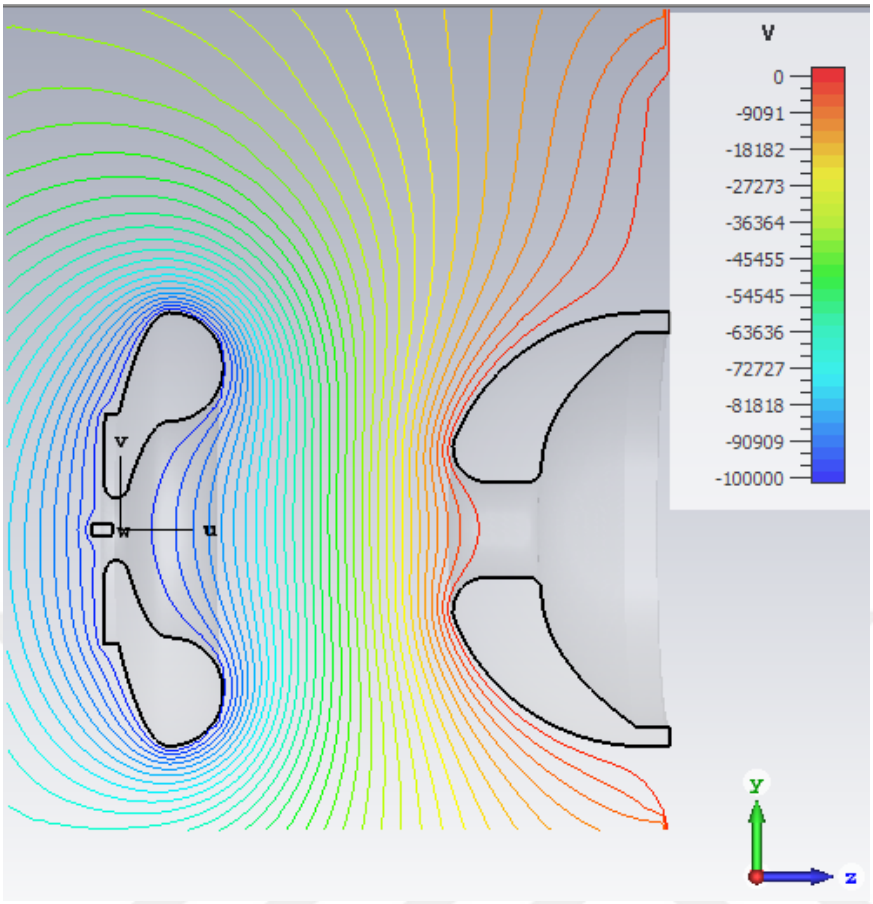



Figure 5.11: Potential curves for -100 kV from CST

For -100 kV, the electric field lines in front of the cathode from MATLAB and CST are given below Figure 5.12 and Figure 5.13 respectively.

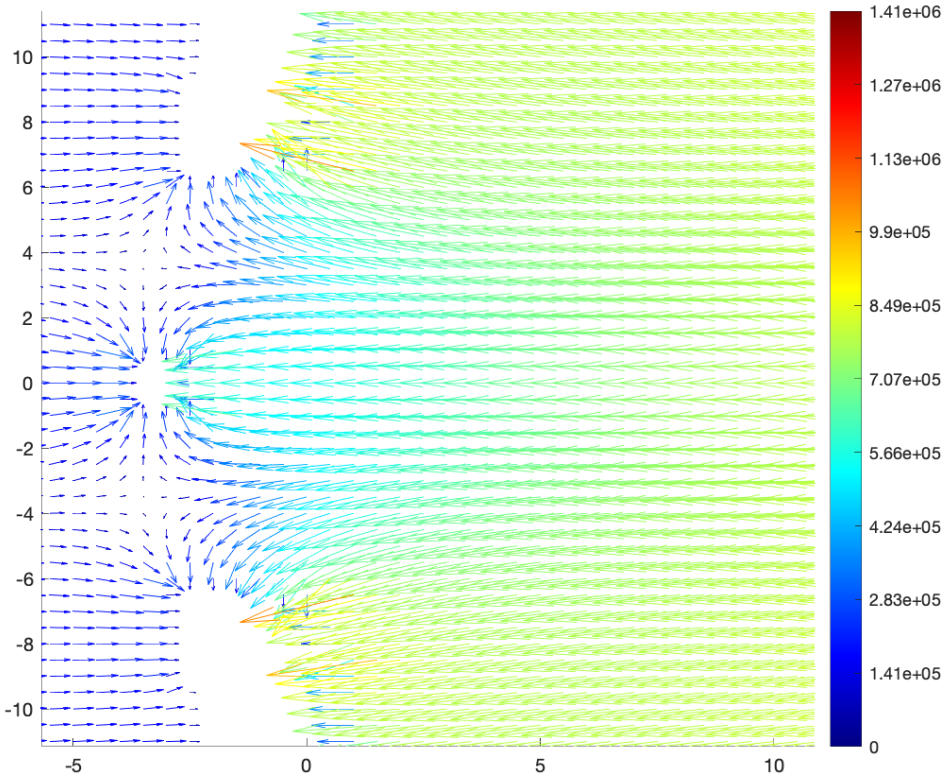



Figure 5.12: Electric field in front of the cathode for -100 kV from MATLAB

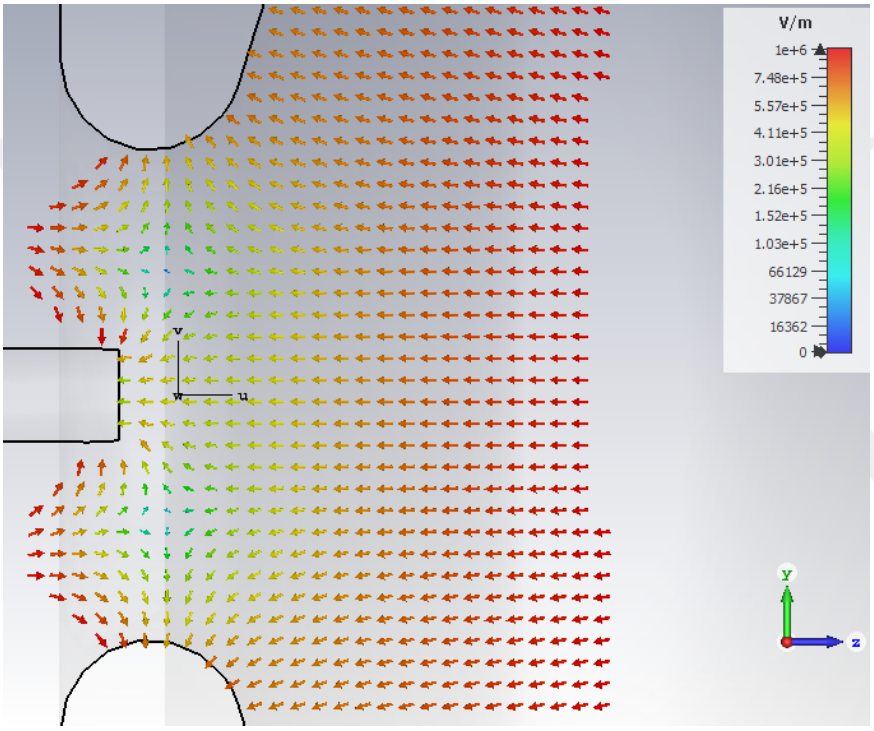



Figure 5.13: Electric field in front of the cathode for -100 kV from CST

As can be seen in the figures, a straight electric field has been obtained in front of the cathode. This indicates that the electric field in the transverse direction is very low. Therefore, the emittance value decreases as the current value increases. In addition, the potential lines are also as expected for both situations. The potential lines with the electric field is shown in Figure 5.14.

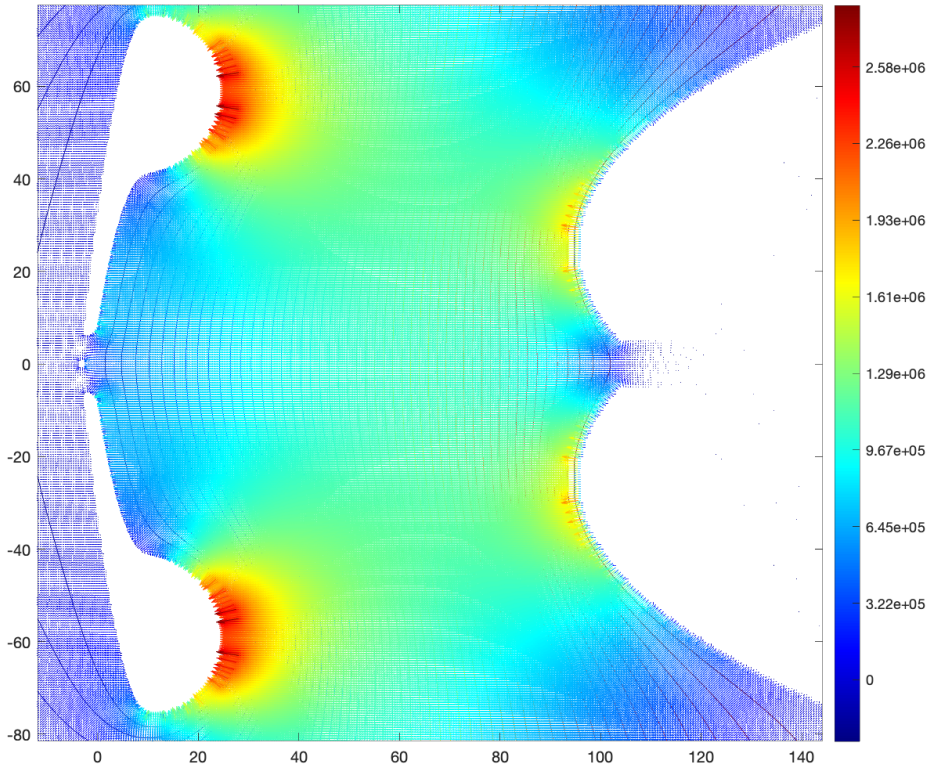



Figure 5.14: Potential Lines with Electric Field Results in MATLAB

As can be seen in Figure 5.14, straight potential lines were obtained around the cathode and towards the anode. This indicates that the electric field must enter perpendicular to the potential lines. Therefore, the electric field components in the transverse direction are minimized. This geometry obtained from MATLAB is also implemented in CST and the following results are obtained.

For -60 kV, the emittance and current graph are obtained from CST given below in Figure 5.15 and Figure 5.16 respectively.

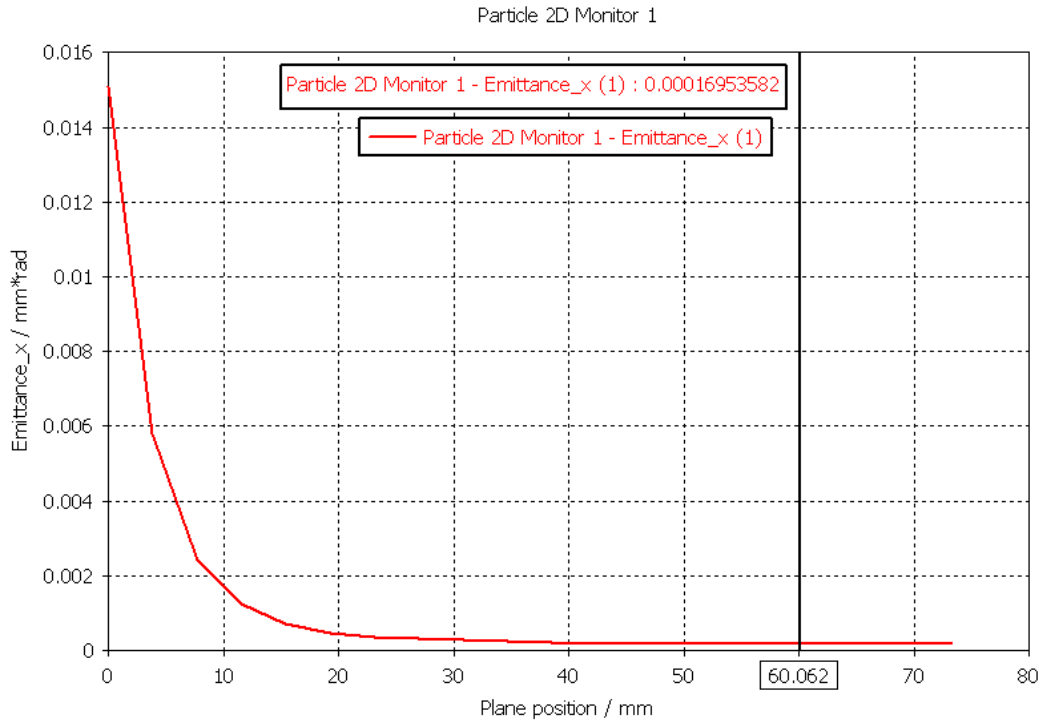



Figure 5.15: Emittance value for -60 kV in CST

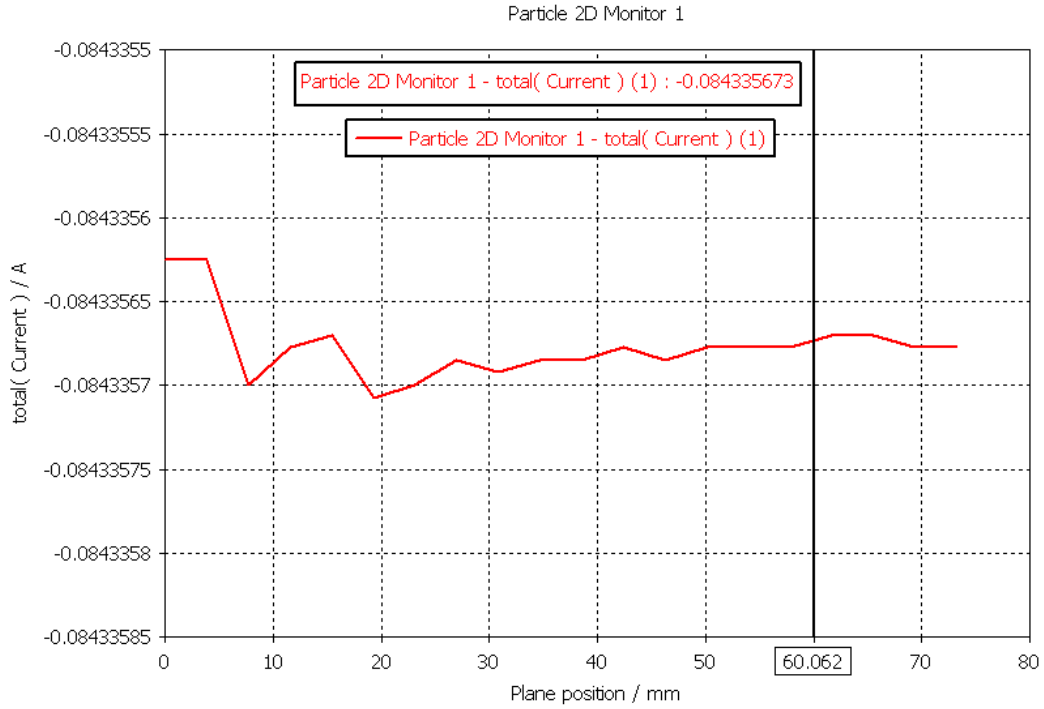



Figure 5.16: Current value for -60 kV in CST

For -100 kV in CST, the emittance and current graph are given in Figure 5.17 and Figure 5.18 respectively.

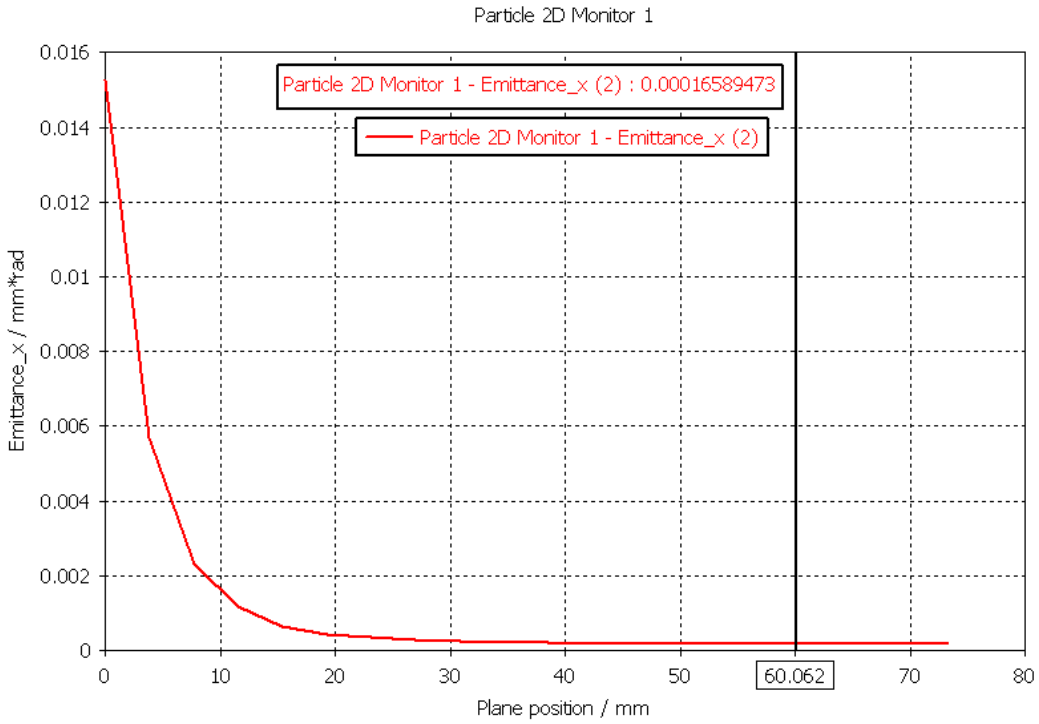



Figure 5.17: Emittance value for -100 kV in CST

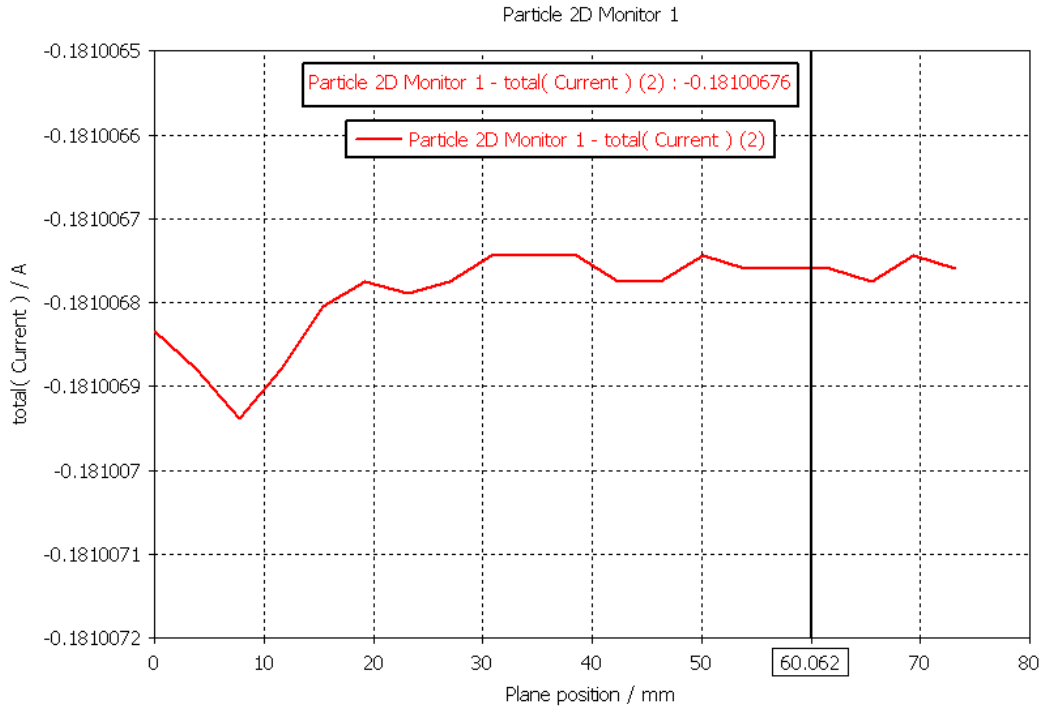



Figure 5.18: Current value for -100 kV in CST

For -60 kV and -100 kV potentials, the 1D graph of the electric field through the beam path is given in Figures 5.19 and 5.20 respectively.

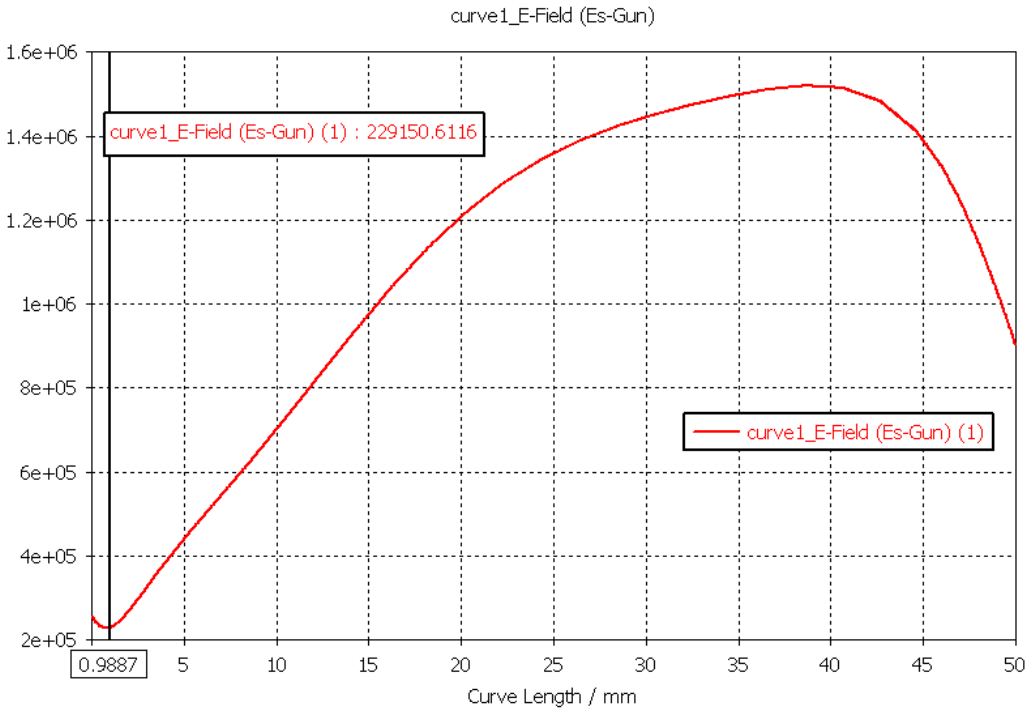



Figure 5.19: Electric field strength for -60 kV in CST

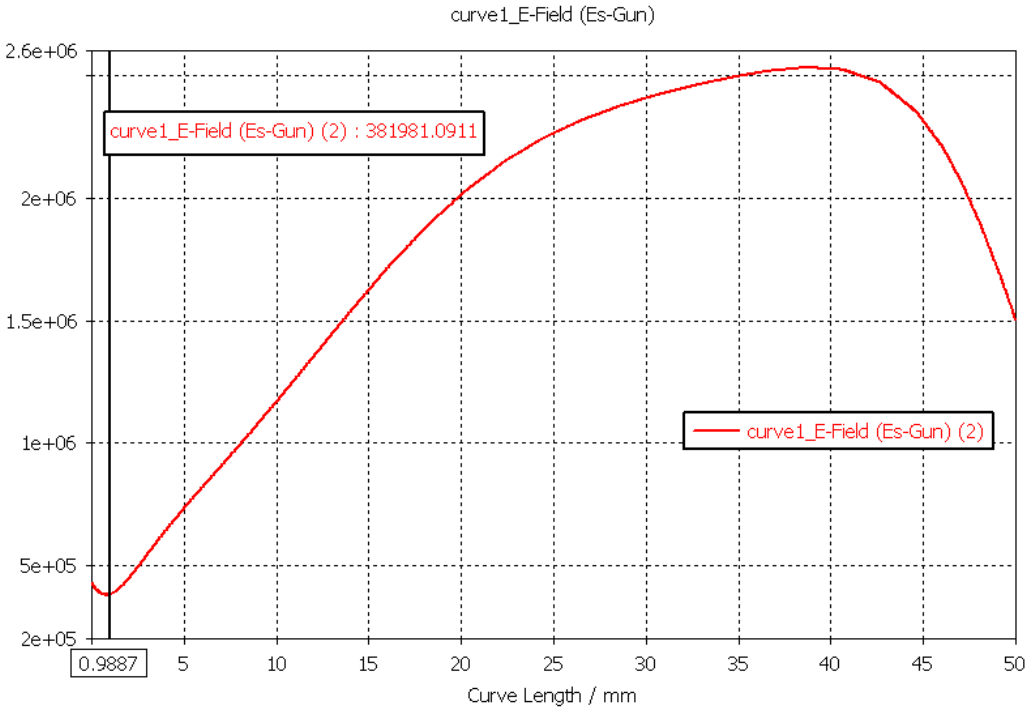



Figure 5.20: Electric field strength for -100 kV in CST

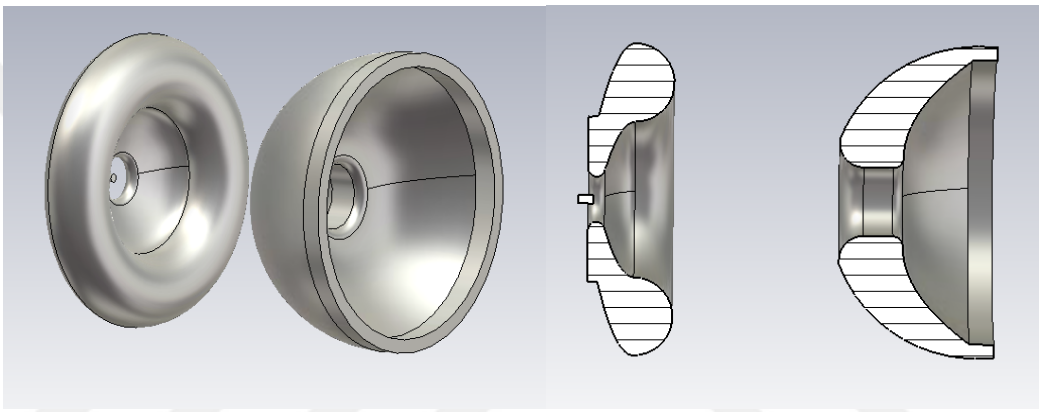
The results are summarized in Table 5.1 below.

Table 5.1: Results of CST Simulation

| Acceleration Voltage (kV) | Current (mA) | Emittance (mm*mrad) | E-Field in Front of Cathode (MV/m) |
|---|---|---|---|
| -60 | 84 | 0.169 | 0.227 |
| -100 | 181 | 0.166 | 0.379 |

As can be interpreted from the table and figures, a low beam emittance which is about 0.16 mm*mrad, and a high beam current which is about 75 to 190 mA are obtained in this study. The electric field values that provide these conditions are also given in Table 5.1.

The design of the electron gun in CST is shown in Figure 5.21:



(a) (b)

Figure 5.21: a) View of optimized design of the electron gun in CST b) the cross-sectional view of optimized design of the electron gun in CST

# CHAPTER 6

# IMPLEMENTATION OF DESIGNED ELECTRON GUN AND TEST RESULTS

After the simulation studies, the designed geometry was manufactured and experimental studies were started. The experiments were carried out in Turkish Accelerator and Radiation Laboratory (TARLA) [50] [51]. The photograph of the produced focusing electrode and anode is shown in Figure 6.1. The test procedure is described in Section 6.1.

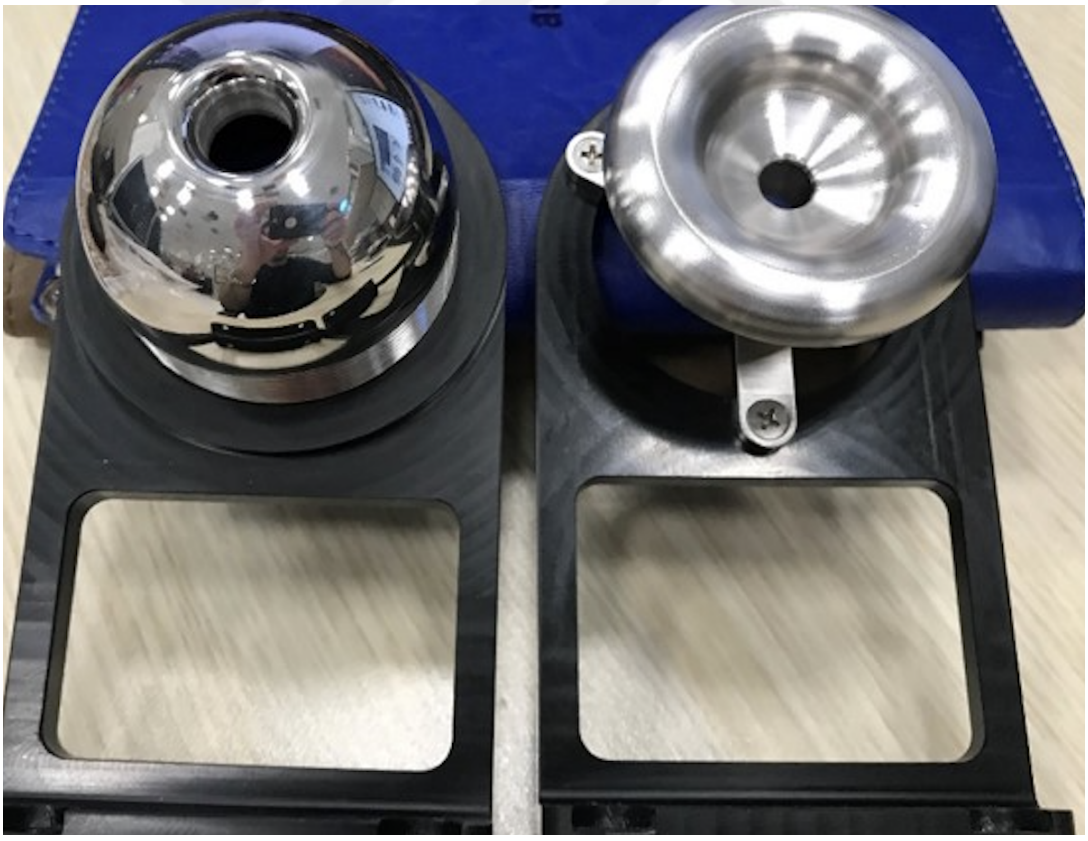


Figure 6.1: Picture of manufactured anode (left) and focusing electrode (Right)

## 6.1 Test Setup and Procedure

One of the most critical points for the test is the electrical connections of the anode and focusing electrode. As explained in the Chapter 3, the focusing electrode and cathode will be at negative high voltage and the anode will be at ground. In addition, the energy required to heat the cathode is supplied by another power source, allowing current to be passed over the used filament, so that the heated filament is ready to emit electrons. Finally, the voltage must be transmitted by another power source to the focusing and control electrode to maintain current control. The block diagram of the system is shown in Figure 6.2:

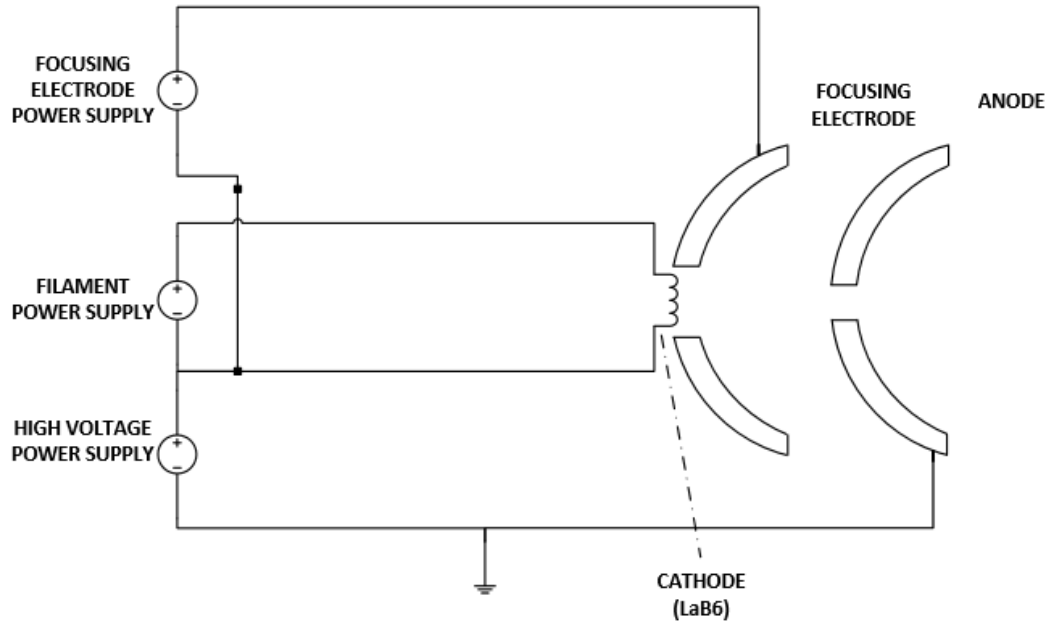



Figure 6.2: System block diagram

The current control can be achieved by changing the voltage of the focusing and control electrode. CST based design results are explained in the beam current regulation. About -60800 V, the beam current is completely cut off, preventing electron output from the cathode. With this method, the required beam current can be obtained. By decreasing the voltage of the focusing and control electrode, the electrons will form a cloud in front of the cathode since they are exposed to an inverted electric field.

The cathode used in the test is a $LaB_6$ cathode which is belongs to KIMBALL PHYSICS

Inc. The current passing over the cathode, the temperature of the heated cathode, and the emission flow plot are given in Figure 6.3.

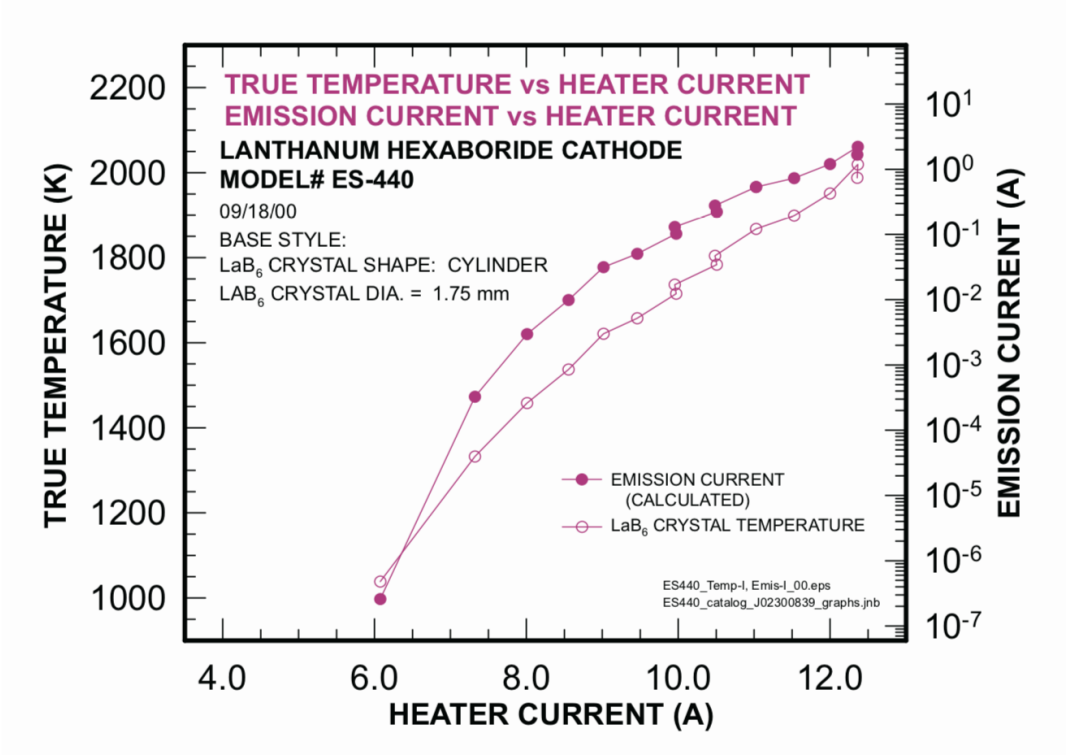



Figure 6.3: Performance characteristics of $LaB_6$ cathode [52]

The photo of the $LaB_6$ cathode is shown in Figure 6.4.



Figure 6.4: Photo of the cathode used in the test

In the cathode datasheet, it is recommended to pass 10A over the cathode. As can be seen from Figure 6.3, when 10A is passed over the cathode, the emission current is around 100 mA. During the test, the current of the cathode was slowly increased and it was finally kept constant at 10 A.

Before performing the test, the voltage of the focusing and control electrode was set to the level of -61000 V to avoid uncontrolled electron removal. Test results are given in Section 6.2.

The manufactured version of the electron gun was shown in Figure 6.1 and the test setup in Turkish Accelerator and Radiation Laboratory (TARLA) is shown in Figures 6.5 and 6.6 respectively.



Figure 6.5: Photo of ceramic structure and focusing electrode placement



Figure 6.6: Photo of the test set-up at Turkish Accelerator and Radiation Laboratory (TARLA) [50] [51]

## 6.2 Test Results

Before starting the test, all electrical connections were made and the system was put into the vacuum. The vacuum level is measured as $8.87 \times 10^{-7}$ mbar.

As mentioned in Section 6.1., the test was performed by keeping the voltage of the control electrode at -61000 V. When the required temperature of the filament was achieved, 10 A current was passed through the filament for a period of time. After waiting long enough, the voltage of the control electrode was set to the same voltage as the accelerator voltage (-60000 V) and the beam current was measured.

The oscilloscope image of the measured current is shown in F igure 6.7.

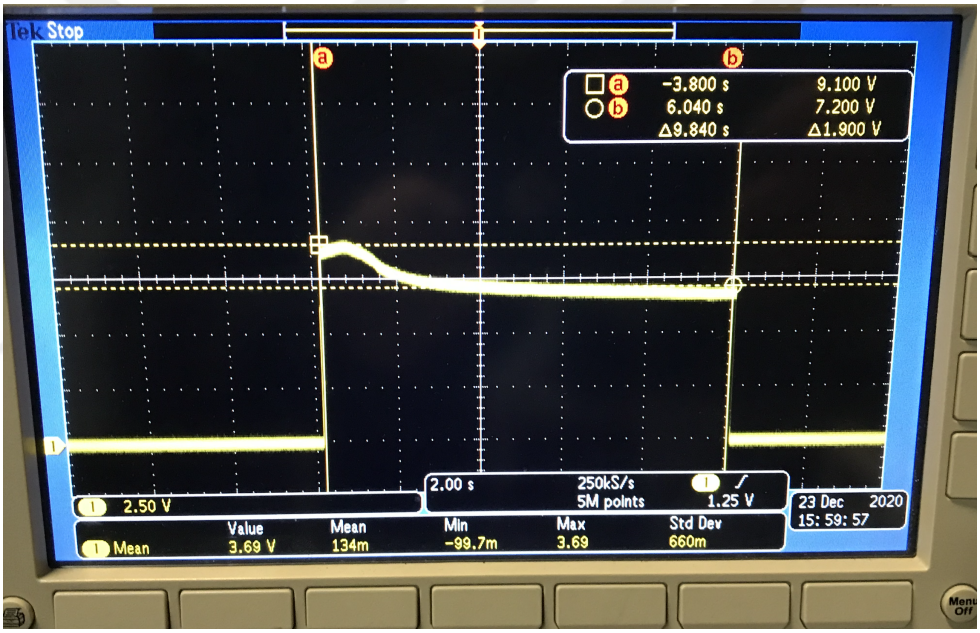



Figure 6.7: Measured current value of the beam, 1V = 10 mA

As can be seen from the picture, the voltage of the focusing electrode is active and it is at -61000 V until -3.8 seconds as seen on the time scale indicated by point a. As of the -3.8 second, the voltage of the focusing electrode was measured as -60000 and the electron beam was extracted from the cathode. A high beam current was obtained when the beam first emerged. The reason for this when the control electrode is active, the beam remaining from the previous operation causes it to accumulate in front of the cathode. When a new beam extraction command is received, the beam current coming

from the cathode combines with the remaining beam from the previous operation, causing a high beam current.

The initial and final versions of the copper table where the electron beam is crashed are shown in Figures 6.8 and 6.9.

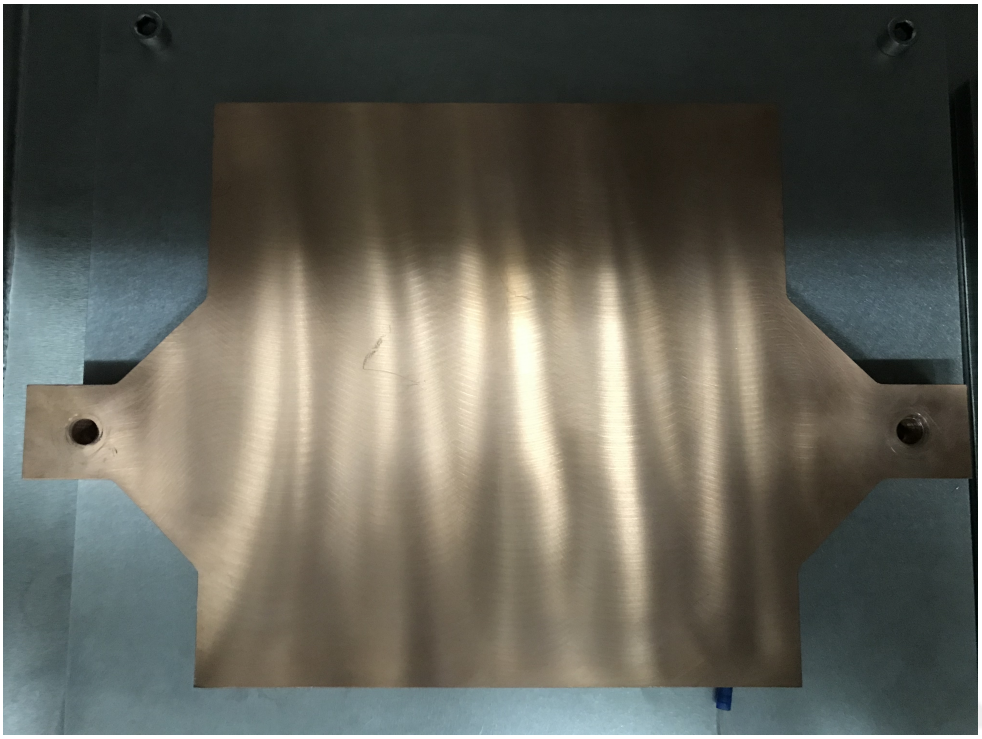


Figure 6.8: Photo of copper table before test



Figure 6.9: Photo of copper table after test. The beam size is measured as 2mm

The diameter of the beam was obtained from Figure 6.9. By using this value emittance is calculated. The distance between where the beam originates and where it strikes is known. The separation between these two points is 790 mm. In addition, the diameter of the cathode is also known as 1.8 mm. The hole diameter measured on the table is approximately 2 mm. This means that the beam could travel this distance without spreading too much. The estimated emittance is given below.

$$\epsilon = 2 \times \sigma_x \times 2 \times \sigma_{vx} \tag{6.1}$$

Here, $2 \times \sigma_x$ is the beam size, and $2 \times \sigma_{vx}$ is the angle of the beam spread. Usually, this angle is smaller than the beam divergence angle. However, in this study an estimation

was made for the worst-case scenario, so this angle was taken equal to the beam divergence angle.

After calculations, emittance is estimated as:

$$\epsilon = 2 \times 2 \times \frac{0.1}{790} = 0.506 \quad mm * mrad \tag{6.2}$$

The beam size is taken as 2 $\sigma$ and angle calculation is shown in Figure 6.10.

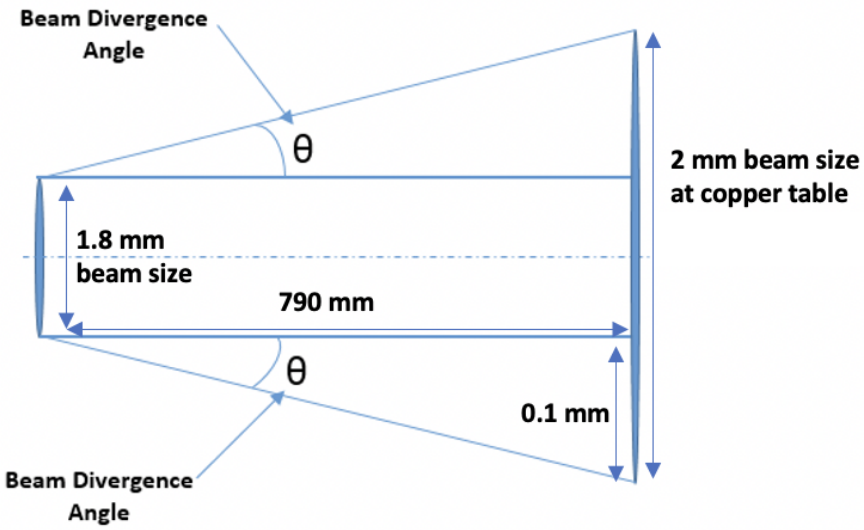



Figure 6.10: Calculation of angle of beam spread

The tangent of the angle $\theta$ will give us $\sigma_{vx}$.

As mentioned above, usually, this angle value is smaller than the beam divergence angle. It is taken like this because a rough calculation is made for emittance. Due to that reason, measured value for emittance is slightly larger than the simulation result. A more sophisticated setup is required for a precise emittance measurement.

The simulation results was verified by experimental tests. The emittance value was also confirmed to be small as predicted.

# CHAPTER 7

# CONCLUSIONS

The aim of this thesis is to design, simulate, and manufacture a DC electron gun that can operate at high power and low emittance. The design and simulation were done with the CST program. In order to obtain the required beam parameters, the optimization of the gun, such as beam current, beam emittance, beam diameter, was done with MATLAB and verified with CST.

The simulation of the electron gun is a complex problem because it solves the motion of electrons in electromagnetic fields for special geometries. Since simulation programs usually perform 3D solutions, it may take time to solve necessary equations and complete the design. For this reason, programs that can perform 2D solutions can be preferred to optimize the electron gun, such as MATLAB, EGUN, etc.

Three important issues have been investigated in this thesis. First, the required geometric structure for low emittance and high power thermionic DC electron gun was determined. The first of these, the linear structure was designed, but its results did not meet the requirements. On the other hand, the second designed structure, parabolic structure, yielded successful results for this study. Secondly, electric field optimizations of the parabolic structure, which gives successful results, were made. In order to do that, the determined parabolic geometry was transferred to MATLAB to make the optimizations faster. Suitable electric field and equipotential lines were found with the help of numerical solution for Laplace's equation using Finite Difference Method in MATLAB. In addition, the geometry found in MATLAB has been validated in CST. According to the results, the geometry that is optimized in MATLAB gave accomplished results that fully met the requirements in CST as well. Finally, the final geometry that was optimized in MATLAB and verified in CST was manufac-

tured.The experiments of the electron gun with these produced materials were carried out in Turkish Accelerator and Radiation Laboratory (TARLA) [51] . The simulations have been verified with the test results obtained. Table 7.1 summarizes the results obtained from the simulation as well as the experiment and the results obtained from the studies conducted by other people.

Table 7.1: Comparison of Simulation and Experiment Results

| | **Emittance (mm*mrad)** | **Current (mA)** | **Acceleration Voltage (kV)** |
|---|---|---|---|
| In This Study (Simulation) | 0.169 | 84 | 60 |
| In This Study (Experiment) | 0.506 | 75 | 60 |
| Other Study [53] | $< 1\ \pi$ | 1000 | 500 |
| Other Study [54] | 1.1 $\pi$ (normalized) | 1000 (peak with 3 $\mu$s) | 500 |

In this thesis, a fully parametric model of the focusing and control electrode in an electron gun is proposed. With the proposed model, the important parameters of the electron gun geometry can be swept for various ranges in CST and its optimization is done with MATLAB. In addition, the trade-off between beam current and beam emittance has been analyzed and presented. It is also shown in this study that the parabolic surface shape is a better solution to obtain maximum beam current and minimum emittance as compared to linear shape. In addition, for a low emittance and high power electron guns, the thermionic cathode is the best solution due to its high current density and low operating temperature features. This electron gun was produced and experimentally verified. Therefore, it is among the most important studies in this field in Turkey. This study was also presented in $13^{th}$ European Conference on Accelerators in Applied Research and Technology (ECAART13). [55]

# REFERENCES


[1] S. Rimjaem, E. Kongmon, M. Rhodes, J. Saisut, and C. Thongbai, "Electron linear accelerator system for natural rubber vulcanization," *Nuclear Instruments and Methods in Physics Research Section B: Beam Interactions with Materials and Atoms*, vol. 406, pp. 233–238, 2017.

[2] M. Hosseinzadeh and A. Sadighzadeh, "Design and numerical simulation of thermionic electron gun," *arXiv preprint arXiv:1509.06363*, 2015.

[3] R.J.Bakish, *Metals*, pp. 38–53. 1986.

[4] J. Fan, Y. Peng, J. Xu, H. Xu, D. Yang, X. Li, and Q. Zhou, "Numerical simulation of beam current control mechanism in the thermionic electron gun," *Vacuum*, vol. 164, pp. 278–285, 2019.

[5] C. Karzmark, C. S. Nunan, and E. Tanabe, *Medical electron accelerators*, p. 67. McGraw-Hill, 1993.

[6] M. Borland, "A high-brightness thermionic microwave electron gun," 1991.

[7] G. Ciovati, "Ac/rf superconductivity," *arXiv preprint arXiv:1501.07398*, 2015.

[8] C. Saisa-ard and S. Rimjaem, "Design and beam dynamic simulation of the thermionic rf electron gun with external resonant cavity for transverse emittance reduction," *Nuclear Instruments and Methods in Physics Research Section A: Accelerators, Spectrometers, Detectors and Associated Equipment*, vol. 940, pp. 243–253, 2019.

[9] E. Al-Dmour, "Fundamentals of vacuum physics and technology," *arXiv preprint arXiv:2006.01464*, 2020.

[10] "Trealization of a mw-level 10.7-ev ( = 115.6 nm) laser by cascaded third harmonic generation of a yb:fiber cpa laser at 1-mhz." `https://www.osapublishing.org/oe/fulltext.cfm?uri=oe-25-12-13517&id=367320`.

[11] H. Wiedemann, *Particle accelerator physics*, p. 310. Springer Nature, 2015.

[12] M. Reiser and P. O'Shea, *Theory and design of charged particle beams*, vol. 312, p. 197. Wiley Online Library, 1994.

[13] H. Wiedemann, *Particle accelerator physics*, p. 290. Springer Nature, 2015.

[14] H. Wiedemann, *Particle accelerator physics*, p. 291. Springer Nature, 2015.

[15] H. Barletta, Spentzouris, "Emittance, uspas notes barletta,spentzouris,harms,"

[16] B. Cheymol, *Development of beam transverse profile and emittance monitors for the CERN LINAC4*. PhD thesis, 2011.

[17] M. Troyon and P. Zinzindohoue, "Energy spread of different electron beams. part i: thermoionic electron beams," *Journal de microscopie et de spectroscopie électroniques*, vol. 12, no. 5, pp. 431–447, 1987.

[18] S. Humphries, *Charged particle beams*. Courier Corporation, 2013.

[19] T. Kalvas, "Beam extraction and transport," *arXiv preprint arXiv:1401.3951*, 2014.

[20] A. Roy, "Electronic emission & electron guns," *Pulsed Power Technology: Pulsed Electron Beams and their Applications*, 2010.

[21] K. L. Jensen, *Introduction to the physics of electron emission*. John Wiley & Sons, 2017.

[22] D. Dowell, S. Lidia, and J. Schmerge, "Lecture 2: Electron emission and cathode emittance," *USPAS course on high brightness electron injectors for 4th generation light sources, UC Santa Cruz*, 2008.

[23] T. Thuillier, "Particle sources." `https://indico.cern.ch/event/850755/contributions/3576010/attachments/1999964/3343261/particle_source_lecture_2020_-_T._Thuillier.pdf`, 2017.

[24] C. N. Ribton, *Development of an electron gun design optimisation methodology*. PhD thesis, Brunel University London, 2017.

[25] W. B. Nottingham, "Thermionic emission," in *Electron-Emission Gas Discharges I/Elektronen-Emission Gasentladungen I*, pp. 1–175, Springer, 1956.

[26] B. L. Morgan, *Advances in Electronics and Electron Physics*. Academic Press, 1988.

[27] J. Lafferty, "Boride cathodes," *Journal of Applied Physics*, vol. 22, no. 3, pp. 299–309, 1951.

[28] H. H. Glascock Jr, "Thorium dispenser cathode for an electron gun," *Journal of Applied Physics*, vol. 37, no. 13, pp. 4995–4995, 1966.

[29] J. Cronin, "Modern dispenser cathodes," *IEE Proceedings I-Solid-State and Electron Devices*, vol. 128, no. 1, pp. 19–32, 1981.

[30] W. Ahmed and M. J. Jackson, *Emerging nanotechnologies for manufacturing*. William Andrew, 2014.

[31] G. N. Fursey, *Field emission in vacuum microelectronics*. Springer Science & Business Media, 2007.

[32] M. Sing, "Introduction to photoemission spectroscopy," *DMFT at*, vol. 25, pp. 14–2.

[33] "Lorentz force in superposition of two magnetic fields." `https://physics.stackexchange.com/questions/465163/lorentz-force-in-superposition-of-two-magnetic-fields`.

[34] K. Schindl, "Space charge," in *Beam Measurement*, pp. 127–151, World Scientific, 1999.

[35] N. Chauvin, "Space-charge effect," *arXiv preprint arXiv:1410.7991*, 2014.

[36] F. Spinazzè, "Theoretical and experimental investigations on the child-langmuir-limited current. studi teorici e sperimentali sulla corrente limite di child-langmuir," 2017.

[37] B. Ragan-Kelley, *Explorations of space-charge limits in parallel-plate diodes and associated techniques for automation*. PhD thesis, UC Berkeley, 2013.

[38] "Wehnelt cylinder." "https://www.scienzemfn.unisalento.it/c/document_library/get_file?folderId=3021404&name=DLFE-199604.pdf"/.

[39] A. Gilmour Jr, *Microwave and Millimeter-Wave Vacuum Electron Devices: Inductive Output Tubes, Klystrons, Traveling-Wave Tubes, Magnetrons, Crossed-Field Amplifiers, and Gyrotrons*. Artech House, 2020.

[40] M. D. Kelisani, S. Doebert, and M. Aslaninejad, "Low emittance design of the electron gun and the focusing channel of the compact linear collider drive beam," *Physical Review Accelerators and Beams*, vol. 20, no. 4, p. 043403, 2017.

[41] Simulia, "Cst studio suite." https://www.3ds.com/products-services/simulia/products/cst-studio-suite/, 2020.

[42] Simulia, "Cst particle studio suite." https://www.3ds.com/products-services/simulia/products/electromagnetic-simulation/particle-dynamics-solutions/, 2020.

[43] S. Ahmadian, F. A. Davani, F. Ghasemi, and M. Shafiee, "A design of thermionic electron gun for traveling wave electron-linac in order to inject beam into booster synchrotron accelerator," 2016.

[44] L. Physics, "Equipotential lines." https://courses.lumenlearning.com/physics/chapter/19-4-equipotential-lines/.

[45] M. N. Sadiku, *Numerical techniques in electromagnetics with MATLAB*. CRC press, 2018.

[46] C. Vendromin, "Numerical solutions of laplace's equation for various physical situations," 2017.

[47] A. K. Mitra, "Finite difference method for the solution of laplace equation," *Department of aerospace engineering Iowa state University*, 2010.

[48] "Numerical solution to laplace equation: Finite difference method." http://www.pa.uky.edu/~plaster/phy611/Laplace_Finite_Difference.pdf.

[49] T. E. Atsue T, "A numerical solution of the 2d laplace's equation for the estimation of electric potential distribution," *The Journal of Scientific and Engineering Research*, 2018.

[50] "Turkish accelerator and radiation laboratory." https://tarla.org.tr/.

[51] A. Aksoy, O. Karsli, A. Aydin, C. Kaya, B. Ketenoglu, D. Ketenoglu, and O. Yavas, "Current status of turkish accelerator and radiation laboratory in ankara: the tarla facility," *Canadian Journal of Physics*, vol. 96, no. 7, pp. 837–842, 2018.

[52] K. Physics, "Lab6 cathode specifications." https://www.kimballphysics.com/cathode-specs-lab6-es-440.

[53] K. Kittimanapun, C. Dhammatong, N. Juntong, W. Phacheerak, M. Phanak, *et al.*, "Low emittance thermionic electron gun at slri," in *9th Int Part Acc Conf (IPAC 2018), Vancouver, BC, Canada*, pp. 4509–4511, 2018.

[54] K. Togawa, T. Shintake, T. Inagaki, K. Onoe, T. Tanaka, H. Baba, and H. Matsumoto, "Ceb 6 electron gun for low-emittance injector," *Physical Review Special Topics-Accelerators and Beams*, vol. 10, no. 2, p. 020703, 2007.

[55] "European conference on accelerators in applied research and technology (ecaart13), m.m.sezer, abstract, p.o-3." https://ecaart13.irb.hr/Programme.